

Magazine of Civil Engineering

ISSN 2712-8172

Online peer-reviewed open-access scientific journal in the field of Civil and Construction Engineering

Founder and Publisher: Peter the Great St. Petersburg Polytechnic University

This journal is registered by the Federal Service for Supervision of Communications, Information Technology, and Mass Media (ROSKOMNADZOR) in 2020. Certificate El No. FS77-77906 issued February 19, 2020.

Periodicity: 8 issues per year

Publication in the journal is open and free for all authors and readers.

Indexing: Scopus, Web of Sceince (ESCI, RSCI), DOAJ, Compendex, Google Academia, Index Copernicus, ProQuest, Ulrich's Serials Analysis System, CNKI

Corresponding address: 29 Polytechnicheskaya st., Saint Petersburg, 195251, Russia

Chief science editor:

D.Sc., Galina L. Kozinetc

Deputy chief science editors: D.Sc., Sergey V. Korniyenko

Executive editor: Ekaterina A. Linnik

Translator, editor: Irina Ye. Lebedeva

Proofreader: Philipp Chrysanthes S. Bastian

DT publishing specialist: Anastasiya A. Kononova

Contacts:

E-mail: mce@spbstu.ru

Web: http://www.engstroy.spbstu.ru

Date of issue: 11.11.2024

© Peter the Great St. Petersburg Polytechnic University. All rights reserved.

© Coverpicture - Polina A. Ivanova

Editorial board:

T. Awwad, PhD, professor, Damascus University, Syrian Arab Republic

A.I. Belostotsky, D.Sc., professor, StaDyO Research & Engineering Centre, Russia

A.I. Borovkov, PhD, professor, Peter the Great St. Petersburg Polytechnic University, Russia

M. Veljkovic, PhD, professor, Delft University of Technology, The Netherlands

R.D. Garg, PhD, professor, Indian Institute of Technology Roorkee (IIT Roorkee), India

M. Garifullin, PhD, postdoctoral researcher, Tampere University, Finland

T. Gries, Dr.-Ing., professor, RWTH Aachen University, Germany

T.A. Datsyuk, D.Sc., professor, Saint-Petersburg State University of Architecture and Civil Engineering, Russia

V.V. Elistratov, D.Sc., professor, Peter the Great St. Petersburg Polytechnic University, Russia

O.N. Zaitsev, D.Sc., professor, Southwest State University, Russia

T. Kärki, Dr.-Ing., professor, Lappeenranta University of Technology, Russia

G.L. Kozinetc, D.Sc., professor, Peter the Great St. Petersburg Polytechnic University, Russia

D.V. Kozlov, D.Sc., professor, National Research Moscow State Civil Engineering University, Russia S.V. Korniyenko, D.Sc., professor, Volgograd State Technical University, Russia

Yu.G. Lazarev, D.Sc., professor, Peter the Great St. Petersburg Polytechnic University, Russia

M.M. Muhammadiev, D.Sc., professor, Tashkent State Technical University, Republic of Uzbekistan H. Pasternak, Dr.-Ing.habil., professor, Brandenburgische Technische Universität, Germany

F. Rögener, Dr.-Ing., professor, Technology Arts Science TH Köln, Germany

V.V. Sergeev, D.Sc., professor, Peter the Great St. Petersburg Polytechnic University, Russia

T.Z. Sultanov, D.Sc., professor, Tashkent Institute of Irrigation and Agricultural Mechanization Engineers, Republic of Uzbekistan

A.M. Sychova, D.Sc., professor, Military Space Academy named after A.F. Mozhaysky, Russia M.G. Tyagunov, D.Sc., professor, National Research University "Moscow Power Engineering Institute", Russia

M.P. Fedorov, D.Sc., professor, Peter the Great St. Petersburg Polytechnic University, Russia

D. Heck, Dr.-Ing., professor, Graz University of Technology, Austria

P. Cao, D.Sc., professor, Jilin University, China A.G. Shashkin, D.Sc., PI Georekonstruktsiya, LLC, Russia

B.M. Yazyev, D.Sc., professor, Don State Technical University, Russia

Contents

Tiraturyan, A.N., Uglova, E.V., Simchuk, E.N., Kadyrov, G.F., Gorskiy, M.Yu. Prediction of temperature distribution in asphalt concrete layers	13101
Kamluk, A.N., Likhomanov, A.O., Govor, E.G., Grachulin, A.V. Mathematical model of foam expansion rate generated in sprinklers	13102
Hoang, M.D., Tran, Q.T., Lee, S.H. Ground granulated blast furnace slag and fly ash concrete	13103
Bokhoeva, L.A., Rogov, V.E., Chermoshentseva, A.S. Antifriction fluoroplastic materials for sliding layers in bridge supports	13104
Al-Kinani, A.M., Fattah, M.Y. Geotechnical characteristics of saline soft soils improved by chemical agents	13105
Chibukhchyan, G., Chibukhchyan, H. Improving the efficiency of cleaning metal pipes of the sewerage system of the city of Yerevan	13106
hernov, V.Yu., Gaisin, I.G., Maltseva, E.M., Nosova, A.N. Strength and thermal conductivity properties of thermowood-cement composition and factors influencing these indicators	13107
Kozinetc, G.L., Badenko, V.L., Sharapov, D., Shonina, E.V. Method of integrated consideration of factors for calculation of anchor system of pontoons	13108



Magazine of Civil Engineering

ISSN 2712-8172

journal homepage: http://engstroy.spbstu.ru/

Research article UDC 625.7/.8

DOI: 10.34910/MCE.131.1



Prediction of temperature distribution in asphalt concrete layers

A.N. Tiraturyan¹ D, E.V. Uglova¹, E.N. Simchuk², G.F. Kadyrov², M.Yu. Gorskiy²

- ¹ Don State Technical University, Rostov-on-Don, Russian Federation
- ² ANO "Scientific Research Institute of Transport and Construction Complex" (NII TSK), Moscow, Russian Federation

⊠ tiraturjanartem@gmail.com

Keywords: asphalt pavements, mechanical properties, durability, temperature, monitoring

Abstract. The paper is devoted to the issues of predicting the temperature distribution in asphalt concrete layers in different periods of the year. Mechanical parameters of asphalt concrete strongly depend on its temperature. The reliability of the temperature dependence used for temperature prediction directly determines the reliability of calculation methods for motorway pavements design. At the same time, it should be noted that many existing models describe the temperature distribution along the depth of the asphalt concrete layer package with a rather large degree of error and are not calibrated for the conditions of the Russian Federation. Methods. The approach proposed by the authors is based on the study of the actual temperature distribution in asphalt concrete pavements by analyzing data from a set of measuring sensors installed at different depths of the asphalt concrete pavement package. The actual temperature distribution was monitored during the annual cycle from March 2023 to April 2024. Results. To approximate the results obtained, a dependence describing the sinusoidal nature of temperature variation on the surface and in the asphalt concrete layers was modified. Modification of the dependence was carried out by introducing an additional empirical parameter characterizing the dependence of the change in the absolute temperature value on the depth. The accuracy of the modified dependence is confirmed by the root mean square error (RMSE) value of up to 10 %. Conclusions. The model modified in the paper can be used at the stage of design and operation of motorways when calculating the temperature conditions of asphalt concrete layers.

Funding: The research was supported by the Russian Science Foundation grant No. 24-29-00110 "Study of the mechanisms of deformation of layered media under the influence of dynamic load and improvement of the method of non-destructive testing of their condition (using the example of highways)". Available online: https://rscf.ru/project/24-29-00110/.

Citation: Tiraturyan, A.N., Uglova, E.V., Simchuk, E.N., Kadyrov, G.F., Gorskiy, M.Yu. Prediction of temperature distribution in asphalt concrete layers. Magazine of Civil Engineering. 2024. 17(7). Article no. 13101. DOI: 10.34910/MCE.131.1

1. Introduction

The mechanical properties of asphalt concrete pavements depend to the greatest extent on temperature. Correct consideration of temperature will significantly increase the reliability of designing asphalt concrete pavements of motorways. At the same time, both prediction of temperature during the year and prediction of its change in the depth of asphalt concrete layers are important. Thus, **the main object** of this research is the temperature distribution along the depth of asphalt concrete pavements during the annual cycle. All the models for accounting for the temperature of functioning of asphalt concrete layers are divided into three groups. The first are the models that relate air temperature and other factors with the

© Tiraturyan, A.N., Uglova, E.V., Simchuk, E.N., Kadyrov, G.F., Gorskiy, M.Yu., 2024. Published by Peter the Great St. Petersburg Polytechnic University.

pavement temperature; the second are the models predicting the pavement temperature in the annual cycle; and the third are the models predicting the temperature variations in the depth of asphalt concrete layers. Many specialists have devoted their works to the problem of investigating the temperature of asphalt concrete layers depending on the ambient temperature. In particular, B.B. Teltayev conducted comprehensive studies of the water-thermal regime of pavements of the highways of the Republic of Kazakhstan [1, 2]. In his works, new results were obtained concerning changes in the nature of temperature distribution along the depth of the pavement in summer and winter periods, and also the possibility of deviation of temperature changes from the quasi-harmonic regime in cold periods of the year was revealed.

At the same time, it is the quasi-harmonic regime of change in air temperature and, consequently, pavement temperature that underlies the modern ideas about temperature modes of asphalt concrete performance. An extensive analysis of existing models describing temperature changes on the surface and in asphalt concrete layers is presented in [3]. In this paper, the models describing the temperature regime of asphalt concrete layers were divided into three groups: based on numerical methods, analytical solutions, and statistical information. At the same time, in a number of works, equations describing temperature changes are divided by time of day [4, 5], for example, into "pave rising" and "pave falling" dependencies. The papers [4, 5] analyse the factors affecting the temperature distribution in road structures in general and in asphalt concrete layers and describe the main factors used in the construction of such models.

Despite the variety of such models, the main interest is undoubtedly represented by the models underlying mechanistic-empirical methods of calculation of road structures [6–9]. The method of predicting the temperature distribution in pavement layers set out in the Mechanistic-Empirical Pavement Design Guide is based on the solution of the heat conduction equation. Models based on this solution are called Climatic-Materials-Structural (CMS) [10, 11] and Cold Regions Research and Engineering Laboratory (CRREL) [12–14] models. The solution of the one-dimensional heat conduction equation is carried out using a finite difference method. The boundary condition at the upper boundary is the air temperature parameters at the pavement surface and at the lower boundary is a node with constant temperature maintained by infinite heat inflow. The CRREL model also predicts the depth of ground freezing and thawing.

In addition to complex analytical methods, a number of regulatory documents and scientific and technical literature contain simpler but no less effective engineering methods that allow taking into account the temperature of asphalt concrete layers. To calculate the pavement temperature as a function of air temperature, the Ladygin equation can be used as follows [15]:

$$T_{as} = 1.3 * T_{air} + 7, (1)$$

where T_{as} is the asphalt surface temperature; T_{air} is the air temperature;

A more complex dependence, taking into account, besides air temperature, solar radiation and albedo of the coating surface, was obtained by Ya.N. Kovalev [16]:

$$T_{as} = \frac{J(1-A)k_w}{\alpha_c} + T_{air},\tag{2}$$

where J is calculated flux of total solar radiation; A is the surface albedo; α_c is the total heat transfer coefficient at the coating-air interface; k_w is the coefficient depending on wind speed.

RDO Asphalt 09 uses a logarithmic law of temperature variation along the depth of asphalt pavements. The proposed relationship is as follows:

$$y = b \ln (0.01x + 1.0) + T, \tag{3}$$

where y is the temperature, °C, on depth x, cm; b is the parameter, depending on T; T is the temperature on surface pavement.

Various dependencies are also used to predict the temperature variation on the pavement surface depending on the air temperature. As noted in [17], the dependence of pavement temperature fluctuations has a cyclic character and can be approximated by a sinusoidal function:

$$X = X_0 + X_m \sin(\omega T);$$

$$\omega = 2\pi/T_0,$$
(4)

where X is the surface temperature; X_0 is the seed temperature value; X_m is maximum amplitude of temperature fluctuation; ω is the cyclic frequency; T_0 is the number of time units in a year (if a day is taken as a time unit, then T_0 = 365); T is a particular point in time (day) from the initial condition of the process.

In particular, the Gaivoronsky formula [18] is one of the special cases of the presented dependence:

$$T_s = T_{air} * \left[1.5 + 0.5 * \cos \frac{\pi * (n-7)}{6} \right],$$
 (5)

where T_s is the surface temperature, °C; T_{air} is the air temperature, °C; n is the ordinal number of the month starting with January.

Thus, we can state a large number of works concerning the temperature of asphalt concrete pavements during the annual cycle. At the same time, the problem of correct choice of dependencies for predicting the temperature of asphalt concrete pavement on the surface and temperature distribution along its depth remains open, which is confirmed by the lack of a unified approach [19–23]. In particular, within the Mechanistic Empirical Design Procedure, which is the most relevant at the moment, the temperature-moisture databases are updated and updated annually, as well as the dependencies used by different regions in their practical activities [24–27]. Moreover, obtaining reliable data on the temperature in asphalt concrete layers and models for its prediction is also of interest to researchers dealing with the problems of asphalt concrete damageability, using the principles of deformation or energy equivalence of continuous and damaged media [28, 29]. Since 2022, air temperature and humidity monitoring stations have been installed in three road-climatic zones of the Russian Federation – II, III, IV.

The objective of the study is to modify an empirical model for predicting the temperature distribution along the depth of asphalt concrete pavements based on field data. In order to achieve this objective, the following tasks are solved:

- equipping the road structure under construction with temperature sensors located at different depths;
- constructing graphs of changes in temperature regimes of asphalt concrete pavements during the annual cycle;
- constructing calculated dependencies of asphalt concrete temperature changes at different depths;
- comparing in-situ and experimental dependencies of temperature changes by depth of asphalt concrete layers;
- modifying dependencies for prediction of temperature changes by depth of asphalt concrete layers providing the greatest correspondence of calculated and experimental data.

2. Methods

An experimental site for studying the temperature and humidity regime of asphalt concrete layers was organized in the III road-climatic zone on the M5 Federal "Ural" highway, the route of which passes through Moscow – Ryazan – Penza – Samara – Ufa – Chelyabinsk, on the section km 286+000 – km 297+000 (Fig. 1). Temperature sensors were installed at different depths in the asphalt concrete layers of the new road structure. The pavement design is presented in Table 1.

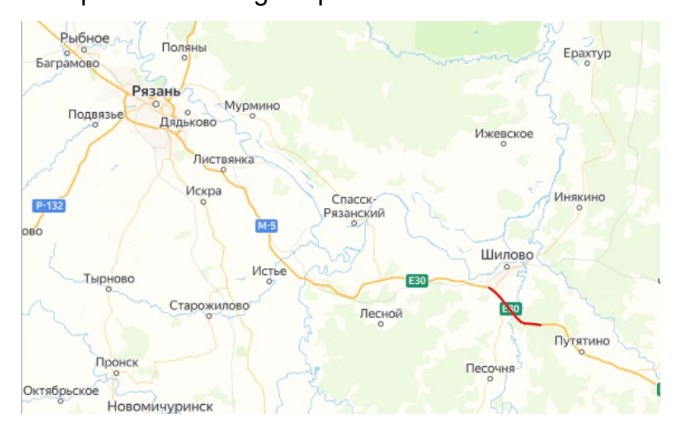


Figure 1. Experimental site.

Table 1. Pavement on monitoring station.

Nº layer		Layer name	Thickness, cm
Asphalt	1	SMA-16	5
surface	2	A22HT (Lower layer of asphalt concrete pavement)	7
	3	A32OT (Upper layer of asphalt concrete pavement)	10
Base	4	Gravel fraction 31.5–63 mm	32
	5	Fine sand with dusty particles content of 5 %	35
Soil	6	Heavy dusty loam	-

Digital temperature transducers – sensors placed in metal sleeves – are used for temperature recording. Each sensor sleeve has a polymer coating to prevent freezing to the borehole walls. Sensors are connected with fire-resistant cable with reduced smoke and gas emission, resistant to chemically aggressive media and retaining its flexibility at operating temperatures down to –60 °C.

Temperature measurement range was from -60 to +85 °C. Instrumental measurement error was ± 0.1 °C over the entire range.

The temperature sensors were installed as follows. After laying the pavement layer, a hole was drilled to the full depth of the finished asphalt concrete layer package, and a groove was made from the hole to the edge of the asphalt concrete layers for laying the cable running from the sensors to the data processing and storage device. After all the necessary holes were made and cleaned, the temperature sensors and data transmission cable were lowered into them. Then they were filled with heated bitumen and sealed with cold asphalt. The scheme of sensor location in the asphalt concrete layers is shown in Fig. 2.

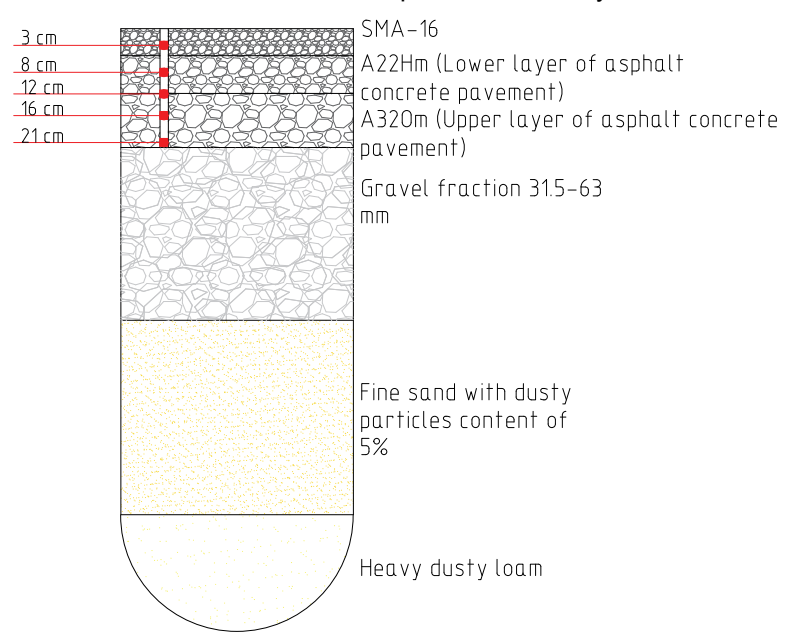


Figure 2. Layout of temperature sensors in the asphalt concrete layers.

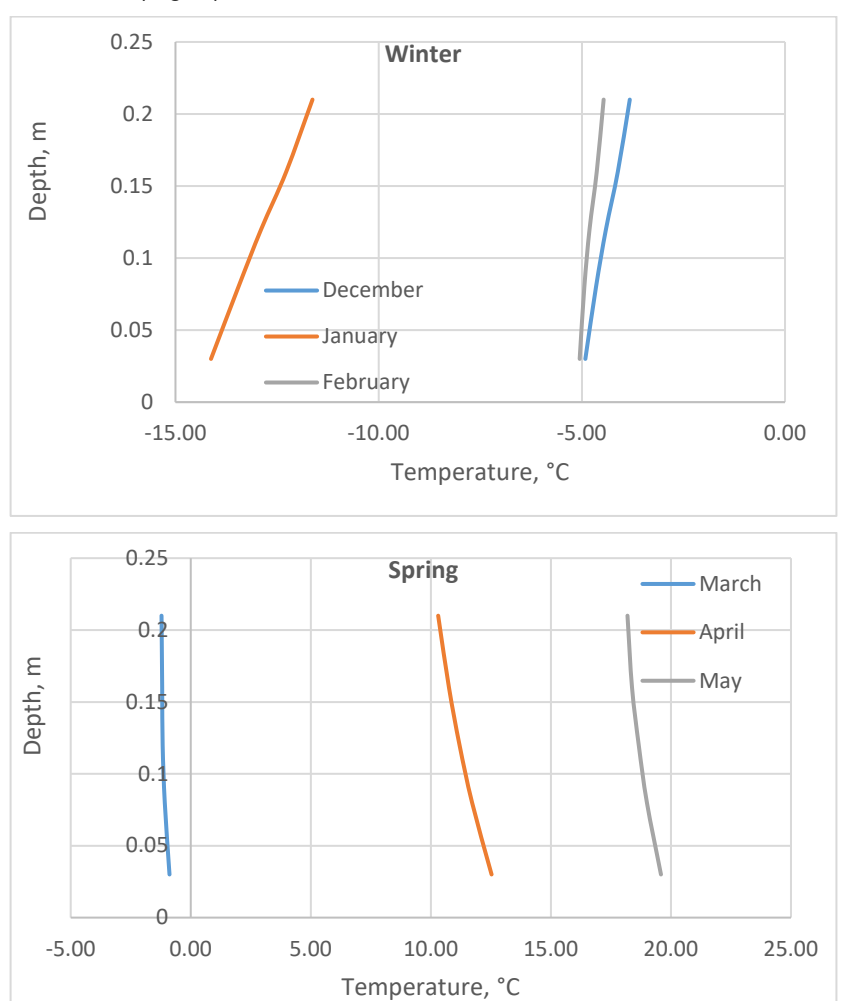
3. Results and Discussion

Temperature monitoring from March 2023 to April 2024, resulted in monthly average air and asphalt pavement layer temperatures (Table 2).

Table 2. Monthly average temperature data.

NA 41	NA	∆ir temnerature °C =	Temperature of asphalt concrete at depth, °C					
Month number	Measuring time	Air temperature, °C	0.03 m	0.08 m	0.12 m	0.16 m	0.21 m	
5	May	14.42	19.58	19.00	18.66	18.38	18.19	
6	June	18.17	24.63	24.17	23.94	23.76	23.67	
7	July	20.55	25.54	25.07	24.83	24.64	24.55	
8	August	20.04	24.64	24.39	24.31	24.26	24.28	
9	September	14.21	16.27	16.25	16.30	16.39	16.52	
10	October	5.53	6.64	6.80	6.97	7.19	7.41	
11	November	0.61	1.55	1.74	1.93	2.15	2.37	
12	December	-2.17	-4.91	-4.65	-4.41	-4.11	-3.82	
1	January	-11.30	-14.13	-13.45	-12.89	-12.27	-11.63	
2	February	-5.79	-5.05	-4.94	-4.81	-4.63	-4.46	
3	March	-2.68	-0.89	-1.08	-1.17	-1.19	-1.22	
4	April	10.68	12.53	11.72	11.19	10.75	10.31	

A graphical representation of the pavement temperature values measured at different depths by seasons is presented below (Fig. 3).



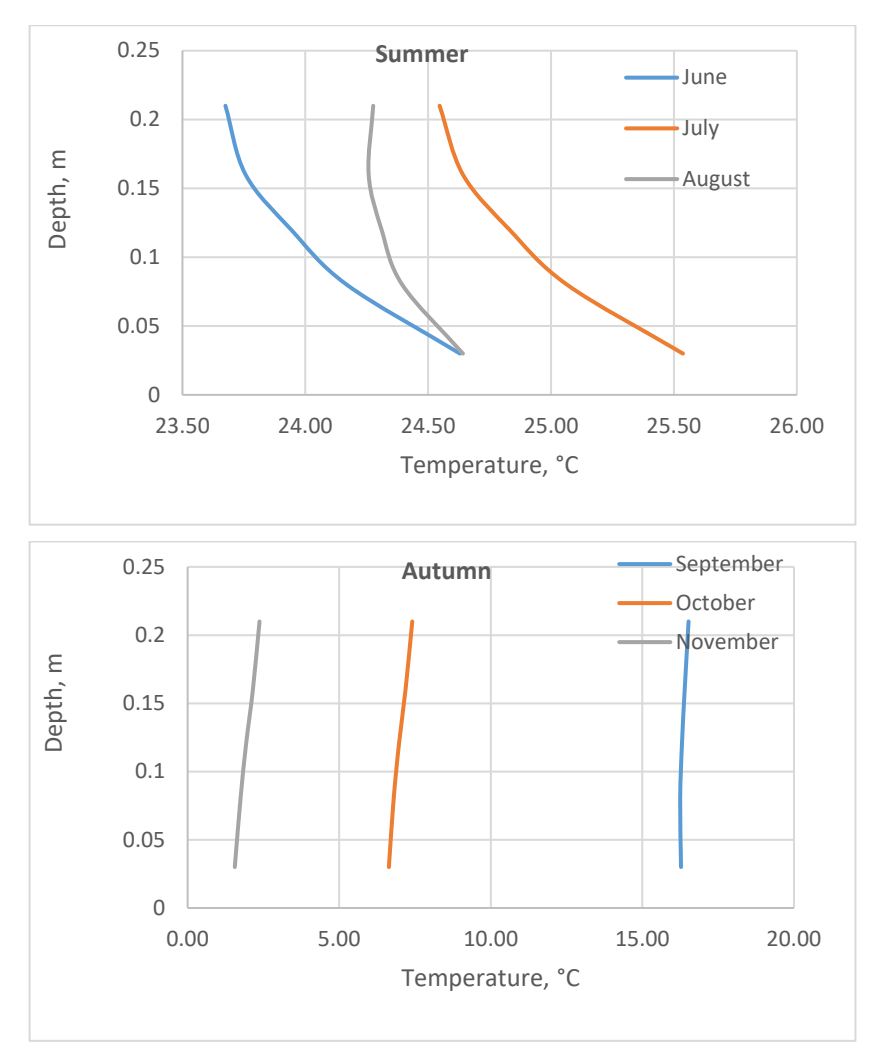


Figure 3. Dependence of changes in average monthly temperatures of asphalt concrete layers at different depths by seasons of the year.

Analyzing this graph, it is necessary to note the changing nature of dependencies characterizing the actual values of temperatures of asphalt concrete pavement layers at different depths. Thus, the dependences of temperature changes in winter, spring, and autumn periods are generally close to the linear form. The dependence characterizing the summer period has a sharply nonlinear, parabolic nature. It can be assumed that the similar dependence for extreme summer temperatures will have even more pronounced nonlinearity (Fig. 4).

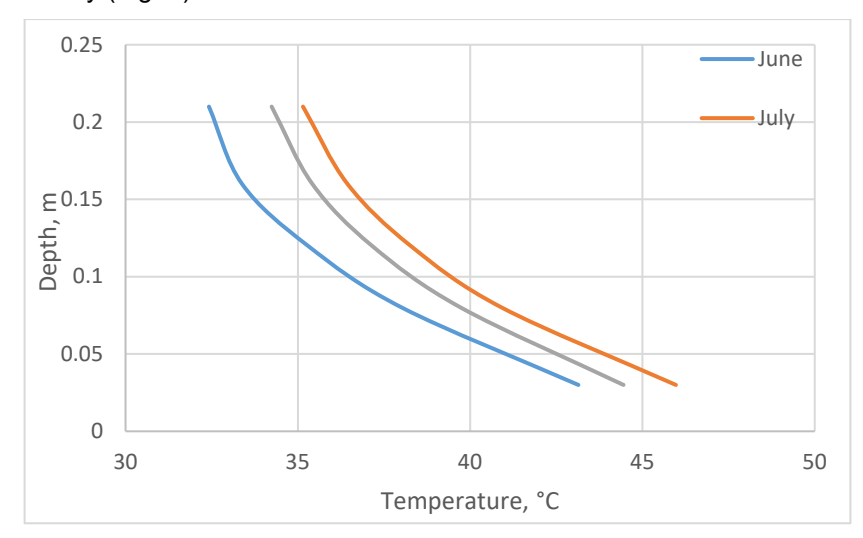


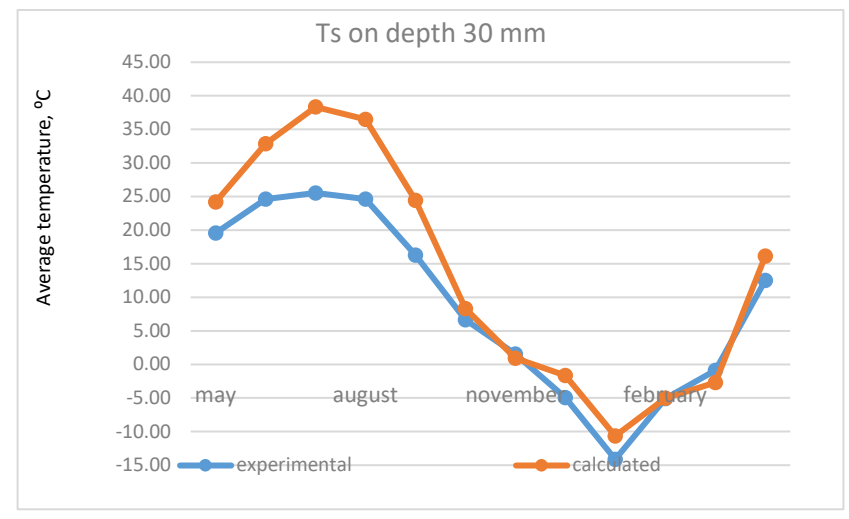
Figure 4. Dependence of changes in extreme temperatures of asphalt concrete layers at different depths in the summer period.

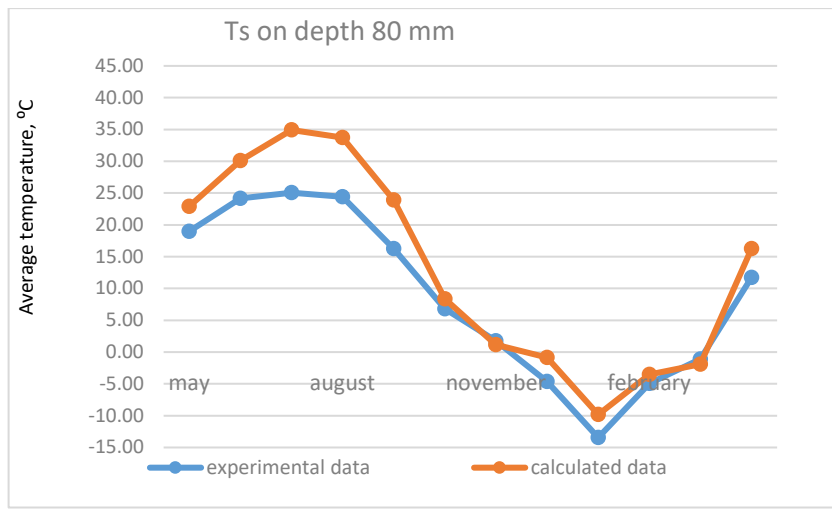
The data obtained were used to verify the formulas presented in the Mechanistic Empirical Guide for determining the temperature of asphalt concrete pavement based on air temperature, as well as for determining the temperature at different depths using formulas (3) and (5). The values of the parameter *b* are given in Table 3, and correspond to the RDO Asphalt 09.

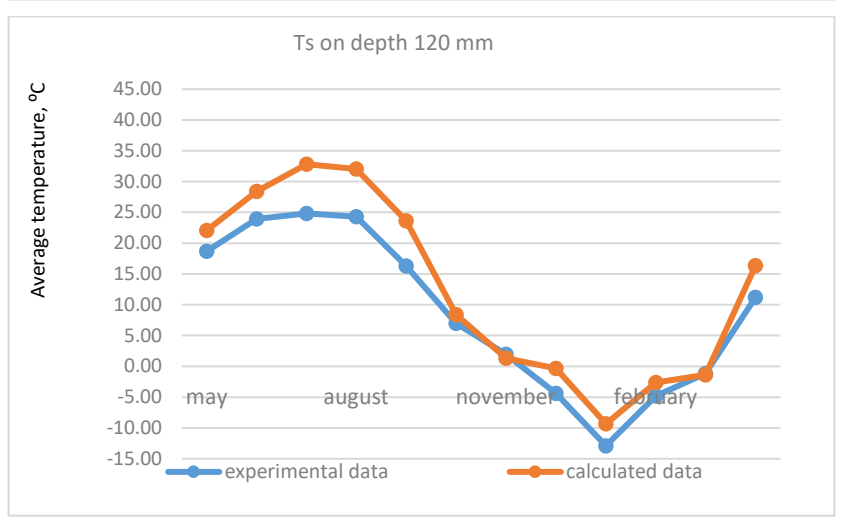
Table 3. Dependence of the parameter b on the surface temperature.

T, °C	<-10	<-5	<0	<5	<10	<15	<20	<25	<30	<35	<40	<45	>45
b	6.5	4.5	2.5	0.7	0.1	0.3	0.4	-1.6	-4.0	-6.2	-8.5	-10.5	-12.0

Based on the calculation results, graphs of calculated and actual temperatures of asphalt concrete pavement at different depths were plotted and compared, the graphs are presented in Fig. 5.







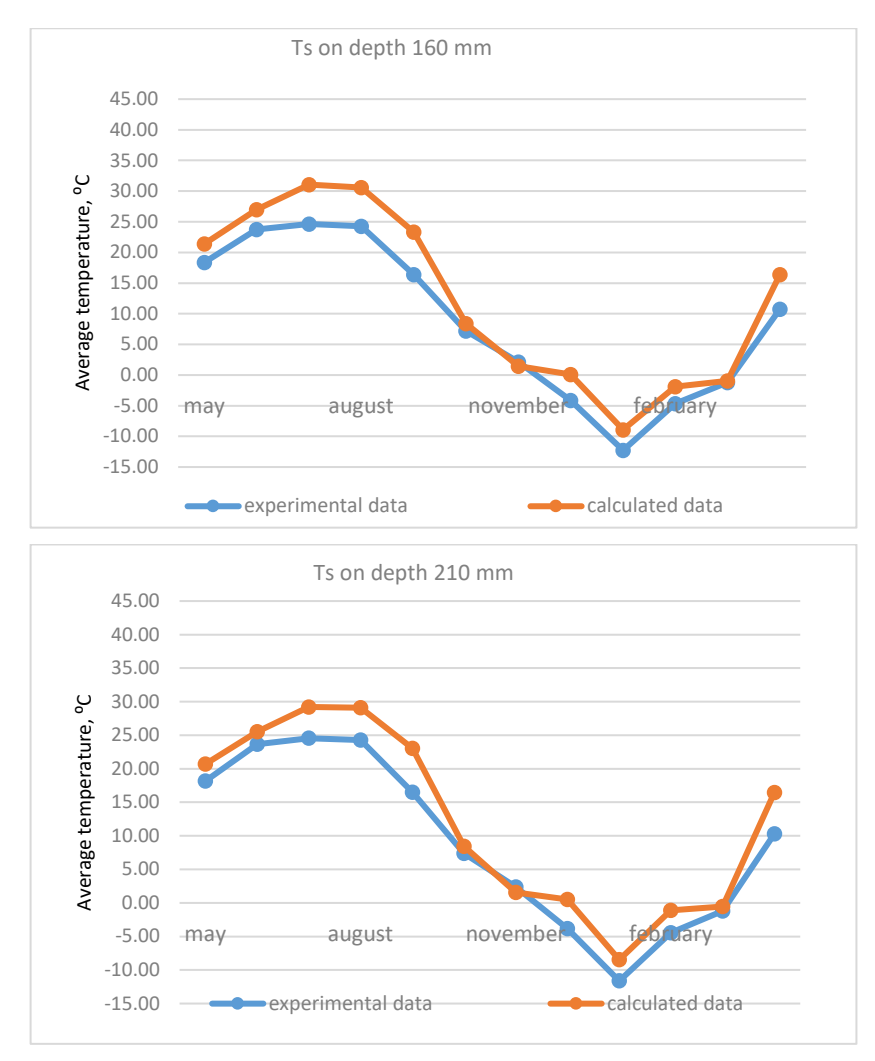


Figure 5. Comparison of calculated asphalt concrete temperature values with actual values at different depths.

To assess the convergence between the calculated and experimental temperatures, the root mean square error (RMSE) was calculated:

$$RMSE = \sqrt{\frac{1}{n} \sum_{i=1}^{n} \left(\frac{t_{calc} - t_{exp}}{t_{exp}} \right)^2},$$
 (6)

where $t_{\rm exp}$ is the experimental temperature value; t_{calc} is the calculated temperature value.

The results of the standard deviation of the error are shown in Table 4.

Table 4. RMSE values.

Sensor depth, m	RMSE, %
0.03	60
0.08	19
0.12	1
0.16	14
0.21	29

As can be seen from the table, the best correspondence between the calculated and experimental data is achieved at a depth of $0.12~\mathrm{m}$. In other cases, the difference between calculated and measured values can reach 60~%.

In order to minimize the RMSE index, the selection of b coefficients for formula (2) was carried out. However, in this case, when approaching the temperature graph for one of the investigated depths, a greater deviation of the calculated temperature from its actual value measured at other depths was observed. To eliminate this problem, dependence (2) was modified to the form:

$$y = b \ln(0.01h + m(h)) + T_s,$$
 (7)

where m(h) is a function that takes into account the variation of the additional empirical parameter mfrom depth in temperature prediction.

Selection of coefficients b in the first approximation was made for the average depth, at which the actual temperature of asphalt concrete is known. The values of this coefficient, at which the graphs of the calculated temperature and the actual measured temperature at a depth of 0.12 m completely coincided with an accuracy of 2 %, are shown in Table 4. Fig. 6 shows the curves of calculated and actual temperature at a depth of 0.12 m from the top of the pavement (Fig. 6, Table 5).

Table 5. Selected values of the dependence of the parameter b on the surface temperature. -2.5 -15 >25 <25 က် 9 5 45 0 2 20 30 35 4

7, °C .55 32 -19.4-2.99-7.6325 25 23 -0.3199 53 Q -15. 83 Ÿ

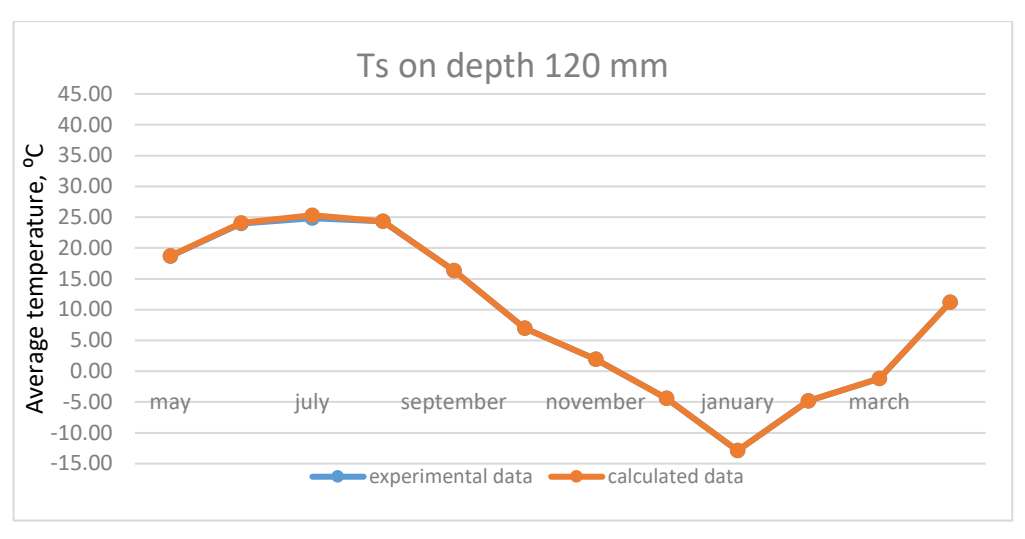


Figure 6. The result of fitting the parameter b for the temperature recorded at 0.12 m depth.

At the next stage, the dependence of the index m on the change of asphalt concrete depth was selected. Thus, having data on asphalt concrete temperatures at the depths of 0.03, 0.08, 0.12, 0.16 and 0.21 m, it was possible to determine the following values of the index m (Table 6).

Table 6. Selected values of dependence of parameter m on asphalt concrete depth.

Depth, cm	<5	<10	<15	<20	<25
m	2	1.5	1	0.5	0

The results of applying the selected dependencies with the selected values of m and b are shown in Figs. 7-10.

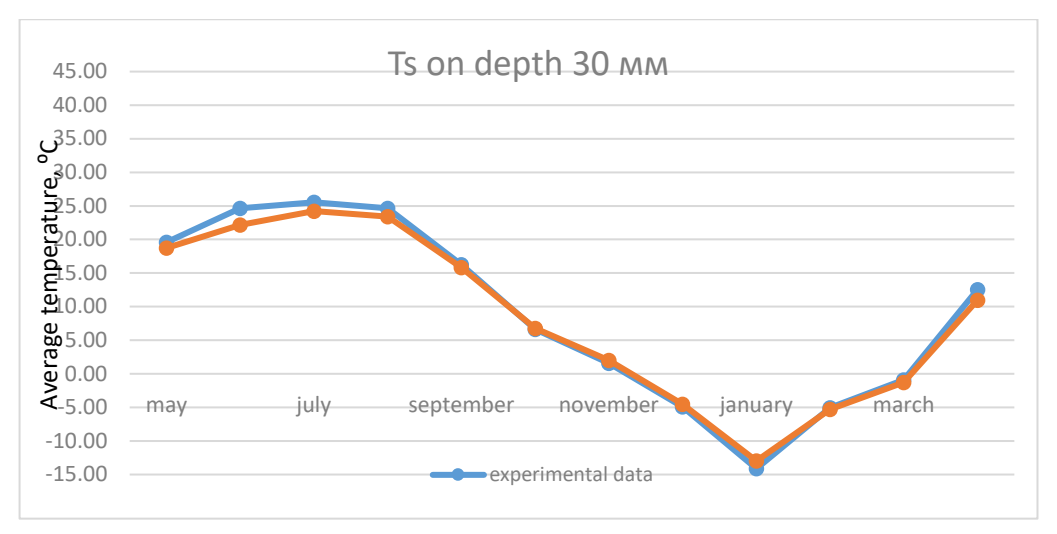


Figure 7. Calculation result using the parameters *b* and *m* for the temperature recorded at a depth of 0.03 m.

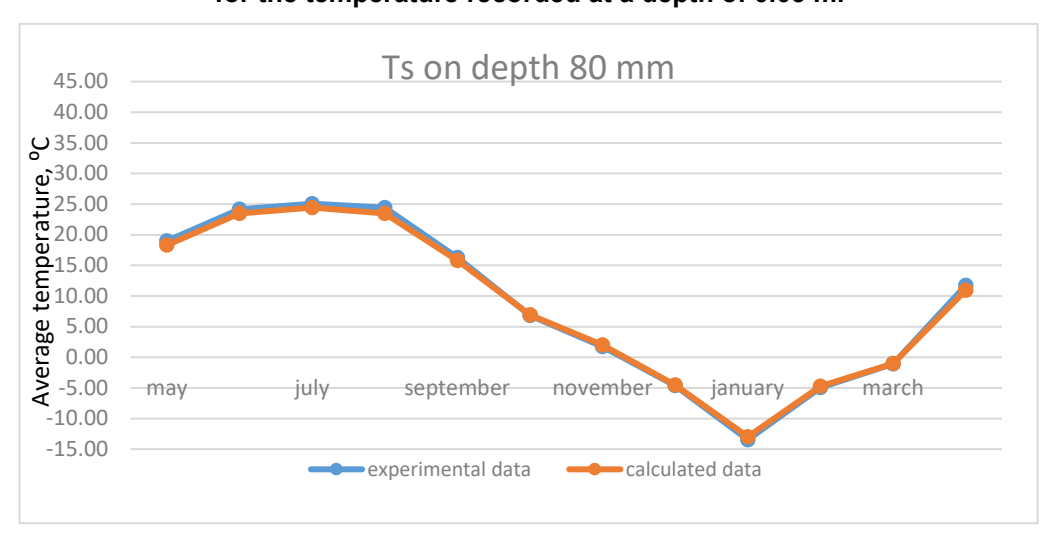


Figure 8. Calculation result using the parameters *b* and *m* for the temperature recorded at a depth of 0.08 m.

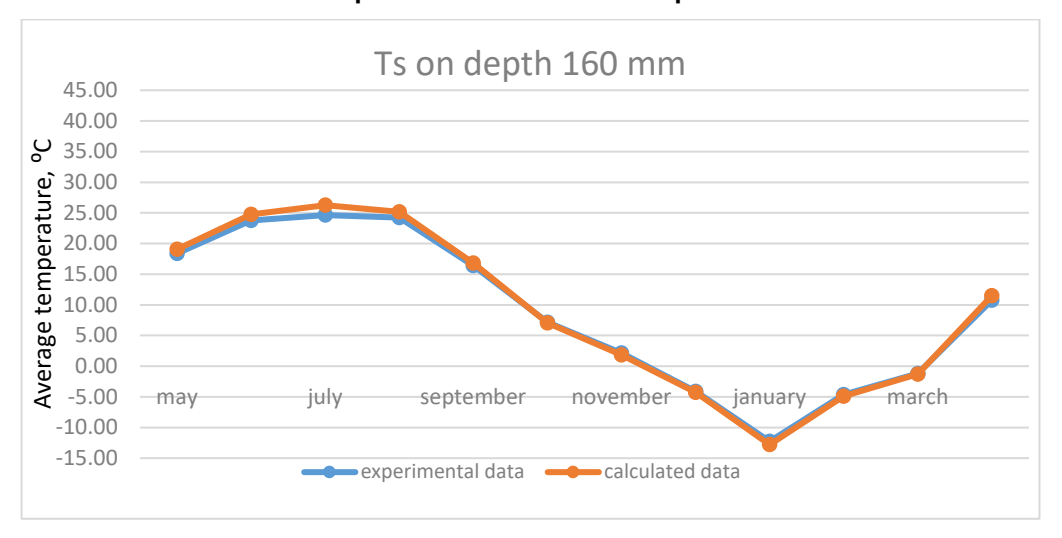


Figure 9. Calculation result using the parameters *b* and *m* for the temperature recorded at the depth of 0.16 m.

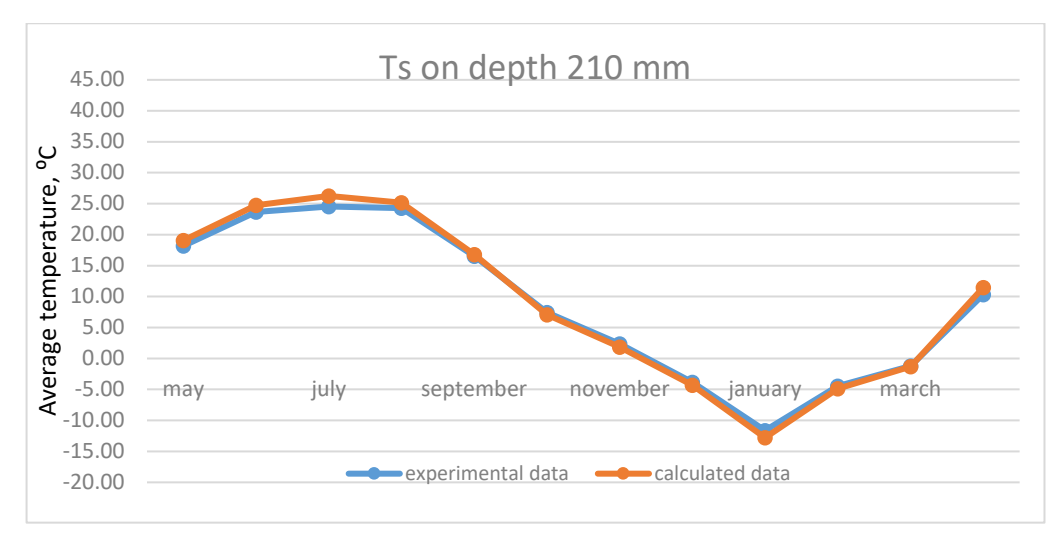


Figure 10. Calculation result using the parameters *b* and *m* for the temperature recorded at a depth of 0.21 m.

The values of the RMSE index based on the results of analyses of dependencies with selected coefficients are shown in Table 7.

Table 7. RMSE values.

Sensor depth, m	RMSE, %
0.03	10
0.08	5
0.12	1
0.16	6
0.21	9

Thus, the choice of the dependence of the parameter b on the pavement temperature and introduction of the function m(h) made it possible to achieve the most accurate results in predicting the variation of design temperatures along the asphalt concrete depth. In the future, it is planned to accumulate more data with different variation of average and median values of monthly air and asphalt concrete temperatures in different road-climatic zones, as well as measurements with a large variation in depth, which will make it possible to correct the obtained dependencies.

However, for the case under consideration it is already obvious that the accuracy of the modified model will significantly exceed the accuracy of the standard RDO Asphalt 09 model and Gaivoronsky model [18], the deviation of which from the field data registered at the survey site will be from 1 to 60 %. Other models, such as the Ladygin model [15] and the Kovalev model [16], will also provide only a fragmentary match between the theoretical curves of temperature change and the experimentally measured data.

The efficiency of implementation of more complex models based on the solution of differential heat conduction equations CMS [10–11] and CRREL [12–14] will also require the development and introduction of a number of empirical coefficients and should be considered only after obtaining a large sample of data for II–IV road-climatic zones. In general, it can be stated that the modified model in this paper has a good level of fit to the experimental data.

4. Conclusion

- The applicability of a set of dependencies for predicting the temperature distribution in asphalt concrete layers and during the annual cycle of pavement operation has been substantiated, providing a good correspondence with the results of experimental observations carried out in the conditions of III road-climatic zone at the monitoring station of temperature and humidity regime of the exploited motorway.
- 2. Modification of the RDO Asphalt 09 dependence for predicting temperature by depth of asphalt concrete pavement package has been performed. The formula is modified by introducing the

- function m(h) characterizing the change of the empirical parameter m from the depth, at which the prediction is carried out.
- 3. The dependence is verified on a set of empirical data on the temperature changes on the pavement surface and in the depth of the asphalt concrete layer package, obtained from a stationary observation point for temperature and humidity regime on the section of the M5 Federal "Ural" highway, the route of which passes through Moscow Ryazan Penza Samara Ufa Chelyabinsk, km 286+000 km 297+000.
- 4. A good correspondence between the calculated results of temperature prediction on the pavement and in asphalt concrete layers and experimental measurements was proved. The RMSE was considered as a criterion of compliance. It was found that when standard dependencies are applied, the maximum RMSE value is 60 %. When using modified formulas, the RMSE will be up to 10 %.

References

- 1. Teltayev, B.B., Liu, J., Suppes, E.A. Distribution of temperature, moisture, stress and strain in the highway. Magazine of Civil Engineering. 2018. 83(7). Pp. 102–113. DOI: 10.18720/MCE.83.10
- 2. Teltayev, B.B, Aitbayev, K.A. Modeling of transient temperature distribution in multilayer asphalt pavement. Geomechanics and Engineering. 2015. 8(2). Pp. 133–152. DOI: 10.12989/gae.2015.8.2.133
- Adwan, I., Milad, A., Memon, Z.A., Widyatmoko, I., Zanuri, N.A., Memon, N.A., Yusoff, N.I.M. Asphalt pavement temperature prediction models: A review. Applied Sciences. 2021. 11(9). Article no. 3794. DOI: 10.3390/app11093794
- Gong, Z., Zhang, L., Wu, J., Xiu, Z., Wang, L., Miao, Y. Review of regulation techniques of asphalt pavement high temperature for climate change adaptation. Journal of Infrastructure Preservation and Resilience. 2022. 3(1). Article no. 9. DOI: 10.1186/s43065-022-00054-5
- 5. Qin, Y., Zhang, X., Tan, K., Wang, J. A review on the influencing factors of pavement surface temperature. Environmental Science and Pollution Research. 2022. 29(45). Pp. 67659–67674. DOI: 10.1007/s11356-022-22295-3
- Hernandez-Fernandez, N., Harvey, J.T., Underwood, B.S., Ossa-Lopez, A. Pavement Fatigue Damage Simulations Using Second-Generation Mechanistic-Empirical Approaches. Transportation Research Record. 2022. 2676(1). Pp. 1–17. DOI: 10.1177/03611981211027152
- 7. El-Ashwah, A.S., El-Badawy, S.M., Gabr, A.R. A Simplified Mechanistic-Empirical Flexible Pavement Design Method for Moderate to Hot Climate Regions. Sustainability. 2021. 13(19). Article no. 10760. DOI: 10.3390/su131910760
- 8. Saliko, D., Ahmed, A., Erlingsson, S. Development and validation of a pavement temperature profile prediction model in a mechanistic-empirical design framework. Transportation Geotechnics. 2023. 40. Article no. 100976. DOI: 10.1016/j.trgeo.2023.100976
- Bayraktarova, K., Eberhardsteiner, L., Zhou, D., Blab, R. Characterisation of the climatic temperature variations in the design of rigid pavements. International Journal of Pavement Engineering. 2022. 23(9). Pp. 3222–3235. DOI: 10.1080/10298436.2021.1887486
- 10. Sutherland Rolim Barbi, P., Tavassoti, P., Tighe, S.L. Climate Change Impacts on Frost and Thaw Considerations: Case Study of Airport Pavement Design in Canada. Applied Sciences. 2023. 13(13). Article no. 7801. DOI: 10.3390/app13137801
- 11. Hasan, M.A., Tarefder, R.A. Development of temperature zone map for mechanistic empirical (ME) pavement design. International Journal of Pavement Research and Technology. 2018. 11(1). Pp. 99–111. DOI: 10.1016/j.ijprt.2017.09.012
- 12. Solatiyan, E., Ibrahim, M.S., Vaillancourt, M., Carter, A. The mechanical performance of reinforced bituminous interfaces with paving fabric under freeze-thaw conditioning. Construction and Building Materials. 2024. 435. Article no. 136809. DOI: 10.1016/j.conbuildmat.2024.136809
- 13. Si, J., Ishikawa, T., Ren, D., Maruyama, K., Ueno, C. Response Prediction of Asphalt Pavement in Cold Region with Thermo-Hydro-Mechanical Coupling Simulation. Sustainability. 2023. 15(18). Article no. 13614. DOI: 10.3390/su151813614
- 14. Knott, J.F., Jacobs, J.M., Sias, J.E., Kirshen, P., Dave, E.V. A Framework for Introducing Climate-Change Adaptation in Pavement Management. Sustainability. 2019. 11(16). Article no. 4382. DOI: 10.3390/su11164382
- 15. Kupriyanov, R.V., Luzgachev, V.A., Zubkov, A.F. Determining the temperature of the asphalt mix during the construction of asphalt concrete non-rigid pavement. Scientific Herald of the Voronezh State University of Architecture and Civil Engineering. Construction and Architecture. 2016. 1(29). Pp. 63–74.
- Shekhovtsova, S.Yu., Vysotskaya, M.A. Influence of carbon primary nano materials in polymer modified binders on the temperature sensitivity of asphalt concrete during operation. IOP Conference Series: Materials Science and Engineering. 2021. 1079(5). Article no. 052030. DOI: 10.1088/1757-899X/1079/5/052030
- 17. Decky, M., Papanova, Z., Juhas, M., Kudelcikova, M. Evaluation of the Effect of Average Annual Temperatures in Slovakia between 1971 and 2020 on Stresses in Rigid Pavements. Land. 2022. 11(6). Article no. 764. DOI: 10.3390/land11060764
- 18. Korochkin, A.V. Teoriia rascheta zhestkoi dorozhnoi odezhdy s asfal'tobetonnym pokrytiem [Calculation theory for rigid asphalt concrete pavements]. Moscow: MADI, 2017. 148 p.
- 19. Lekea, A., Steyn, W.J.vdM. Performance of Pavement Temperature Prediction Models. Applied Sciences. 2023. 13(7). Article no. 4164. DOI: 10.3390/app13074164
- Ntramah, S., Tutu, K.A., Tuffour, Y.A., Adams, C.A., Adanu, E.K. Evaluation of Selected Empirical Models for Asphalt Pavement Temperature Prediction in a Tropical Climate: The Case of Ghana. Sustainability. 2023. 15(22). Article no. 15846. DOI: 10.3390/su152215846
- 21. Zhu, S., Lyu, Y., Wang, H., Zhou, L., Zhu, C., Dong, F., Fan, Y., Wu, H., Zhang, L., Liu, D., Yang, T., Kong, D. Pavement Temperature Forecasts Based on Model Output Statistics: Experiments for Highways in Jiangsu, China. Remote Sensing. 2023. 15(16). Article no. 3956. DOI: 10.3390/rs15163956
- 22. Feng, L., Tian, H., Yuan, X., Miao, L., Lin, M. Variation Characteristics of Pavement Temperature in Winter and Its Nowcasting for Xianyang Airport Expressway, China. Atmosphere. 2023. 14(2). Article no. 361. DOI: 10.3390/atmos14020361

- 23. Lee, H., Kwon, H.-G., Ahn, S., Yang, H., Yi, C. Estimation of Perceived Temperature of Road Workers Using Radiation and Meteorological Observation Data. Remote Sensing. 2023. 15(4). Article no. 1065. DOI: 10.3390/rs15041065
- 24. Barriera, M., Pouget, S., Lebental, B., Van Rompu, J. In Situ Pavement Monitoring: A Review. Infrastructures. 2020. 5(2). Article no. 18. DOI: 10.3390/infrastructures5020018
- 25. Miao, Y., Sheng, J., Ye, J. An Assessment of the Impact of Temperature Rise Due to Climate Change on Asphalt Pavement in China. Sustainability. 2022. 14(15). Article no. 9044. DOI: 10.3390/su14159044
- 26. Mokoena, R., Mturi, G., Maritz, J., Mateyisi, M., Klein, P. African Case Studies: Developing Pavement Temperature Maps for Performance-Graded Asphalt Bitumen Selection. Sustainability. 2022. 14(3). Article no. 1048. DOI: 10.3390/su14031048
- Llopis-Castelló, D., García-Segura, T., Montalbán-Domingo, L., Sanz-Benlloch, A., Pellicer, E. Influence of Pavement Structure, Traffic, and Weather on Urban Flexible Pavement Deterioration. Sustainability. 2020. 12(22). Article no. 9717. DOI: 10.3390/su12229717
- 28. Aleksandrova, N.P., Aleksandrov, A.S., Semenova, T.V., Chusov, V.V. Experimental investigation of damage accumulation in asphalt-concrete coatings. News of Higher Educational Institutions. Construction. 2019. 4(724). Pp. 114–127. DOI: 10.32683/0536-1052-2019-724-4-114-127
- 29. Aleksandrov, A.S., Aleksandrova, N.P., Semenova, T.V. Application of the principle of energy equivalence of continuous and damaged bodies to calculation of asphalt concrete coatings by strength and plasticity criteria. News of Higher Educational Institutions. Construction. 2018. 3(711). Pp. 79–88.

Information about the authors:

Artem Tiraturyan, Doctor of Technical Sciences ORCID: https://orcid.org/0000-0001-5912-1235

E-mail: tiraturjanartem@gmail.com

Evgenia Uglova, Doctor of Technical Sciences

E-mail: uglova.ev@yandex.ru

Evgeniy Simchuk, PhD in Economics

E-mail: niitsk@niitsk.ru

Georgiy Kadyrov,

E-mail: georgijk39@gmail.com

Mihail Gorskiy,

E-mail: miha-gorsky@mail.ru

Received: 18.07.2024. Approved after reviewing: 13.10.2024. Accepted: 23.10.2024.



Magazine of Civil Engineering

ISSN 2712-8172

journal homepage: http://engstroy.spbstu.ru/

Research article

UDC 614.844.5:614.844.2 DOI: 10.34910/MCE.131.2



Mathematical model of foam expansion rate generated in sprinklers



A.N. Kamluk 🗓 . A.O. Likhomanov 🖾 🕒 . E.G. Govor 🕒 . A.V. Grachulin 🗓







University of Civil Protection of the Ministry of Emergency Situations of the Republic of Belarus, Minsk, Republic of Belarus

Keywords: automatic foam extinguishing system, sprinkler, nozzle, foam, foam expansion, fluid dynamics

Abstract. Foam solution discharge is always accompanied by changes in the operating pressure due to different pressure losses along the pipeline in automatic foam extinguishing systems. Changes in the operating pressure affect the process of a liquid jet fragmentation into droplets and the formation of foam films. Therefore, to increase the accuracy of calculations when designing automatic foam extinguishing systems, it is worthwhile to evaluate the main characteristics of the foam in terms of fire extinguishing efficiency, in particular, its expansion. For this purpose, the generalization of the experimental data using the theory of similarity and taking into consideration the hydrodynamic features of the deflector type sprinkler operation and the properties of foam solution was carried out to develop a novel simplified mathematical model. This model allows to predict the foam expansion depending on the geometric parameters of the sprinkler elements and the empirical coefficient, which takes into account the peculiarities of the chemical composition of the foam concentrate. This new model predictions of foam expansion show good agreement with the experimentally measured foam expansion. The average error in foam expansion was less than 9 %.

Citation: Kamluk, A.N., Likhomanov, A.O., Govor, E.G., Grachulin, A.V. Mathematical model of foam expansion rate generated in sprinklers. Magazine of Civil Engineering. 2024. 17(7). Article no. 13102. DOI: 10.34910/MCE.131.2

1. Introduction

The object of current research is air-mechanical foam, which is used to extinguish fires in automatic foam extinguishing systems (AFES). The AFES are one of the main parts of fire protection systems for chemical, oil refining, metallurgical, and energy enterprises [1-3]. The AFES are intended to automatically discharge the extinguishing agent without human involvement to the protected area to localize or eliminate fire at the initial stage with minimal damage, as well as to prevent re-ignition of the combustible substance by creating the foam cushion. Air-mechanical foam, which is used as fire extinguishing agent in the AFES, is the aggregate of air-filled bubbles formed by mechanical mixing an aqueous solution of a suitable foam concentrate and air in the foam sprinklers and foam generators. One of the main classification characteristics of air-mechanical foam in terms of fire extinguishing efficiency is its expansion. Foam expansion is a ratio of the volume of foam to the volume of the foam solution from which it was made [4, 5]. Foam is usually classified into three main groups based on the conditions of application (extinguishing method, type of combustible material, type of foam concentrate, etc.): low-expansion (with expansion in the range from 1 to 20), medium-expansion (with expansion in the range from 21 to 200), and high-expansion

¹ McGree, T. U.S. Experience with Sprinklers [Online]. URL: https://www.nfpa.org/News-and-Research/Data-research-andtools/Suppression/US-Experience-with-Sprinklers (date of application: 01.07.2024).

[©] Kamluk, A.N., Likhomanov, A.O., Govor, E.G., Grachulin, A.V., 2024. Published by Peter the Great St. Petersburg Polytechnic University.

(with expansion greater than 200) [5, 6]. Low-expansion foam is intended mainly for putting out fire over its entire area. Such foam has greater penetration ability, better spreads on the protected area, and cools burning surfaces more effectively than other types of foam [7, 8]. It is common knowledge that the higher the expansion of foam (in the range from 1 to 20), the greater its extinguishing efficiency would be [4, 9].

In the AFES, low-expansion foam is usually generated using deflector type sprinklers [6]. Foam solution discharge is always accompanied by changes in the operating pressure due to different pressure losses along the pipeline. Changes in the operating pressure affect the process of a liquid jet fragmentation into droplets and the formation of foam films [10, 11]. Therefore, to increase the accuracy of calculations when designing the AFES, it is worthwhile to evaluate the main characteristics of foam in terms of fire extinguishing efficiency, in particular, its expansion. In this case, both the geometry of the sprinkler and the hydrodynamics of foam solution flow must be taken into consideration.

Previous studies of the influence of sprinkler geometry were associated, as a rule, with optimizing the water flux distribution and uniformity, which is formed by the fire sprinkler head. In [12], the author tried to resolve the initial spray structure of fire sprinklers with a volume-of-fluid modeling. He studied the initial spray formation process of commercial fire sprinklers with a large-eddy simulation and a volume-of-fluid model. Then he determined factors affecting water flux distribution of fire sprinklers and effect of water flux uniformity on fire suppression characteristics and optimized the fire sprinkler head design using a microgenetic algorithm to produce a uniform distribution of droplet size and water flux [13, 14]. The final optimized design showed that the section angle of the fire sprinkler head should be larger, the tines should be more protruding, and the slots should be more concave to improve the water flux distribution. However, the author noted that caution should be exercised when applying these results to conditions other than those used in this study.

Previously, many studies were carried out to develop models for predicting the distribution of water flux and quite accurate and adequate models were obtained [15–19]. However, all studies carried out to date by other authors have focused on water. Foam is a dispersed system with a gas dispersed phase and a liquid dispersion medium. The water and foam spray simulations differ significantly from each other. To predict the expansion of foam, we have studied its dependence on the geometric parameters of the deflector type sprinkler in [11, 20]. As a result, we developed the regression model as a polynomial to predict the foam expansion K depending on the sprinkler frame arm length L (mm), the outer deflector diameter D (mm), the tine inclination angle α (deg), and the deflector working surface coefficient K_{ς} (%):

$$K = 50.7 - 1.012L + 0.00412L^{2} - 1.117K_{s} + 0.00686K_{s}^{2} - 0.129D + \\ + 0.00077D^{2} + 0.0625\alpha - 0.00087\alpha^{2} + 0.02769LK_{s} - 0.0001715LK_{s}^{2} - \\ - 0.0001194L^{2}K_{s} + 0.000000747L^{2}K_{s}^{2} + 0.00107LD - 0.0000067LD^{2} + \\ + 0.00073K_{s}D - 0.000005K_{s}D^{2}.$$
 (1)

The developed regression model has high accuracy (the coefficient of determination R^2 is equal to 0.97). This model can be successfully implemented for engineering new sprinklers for the protection of buildings and structures of different types. However, the developed model is just a regression equation, which is why it is not interpretable. The field of its application is limited by the conditions of experiments and measurements based on which it was developed. In particular, it concerns the hydrodynamic parameters of the flow of foam solution, which are governed by the geometry of the flow path of the sprinkler nozzle and the properties of the foam solution.

For this reason, the main goal of current research is to develop a simplified mathematical model with variables in a dimensionless form, which would provide a possibility to evaluate the effect of the geometric parameters of the frame arm and the deflector of the sprinkler, the hydrodynamic parameters of the jet and the properties of the foam solution on the foam expansion.

2. Methods

2.1. Hydrodynamic Parameters of the Jet

A jet is formed when liquid is delivered through a hole of some diameter into an open space. As it moves, it directly interacts with the environment. Due to the mutual action of the inertia forces, the surface tension, the viscous friction, and the aerodynamic forces, perturbations (i.e. waves) appear on the outer longitudinal boundary of the jet. The integrity of the jet brakes when the amplitude of oscillations increases to a certain critical value. After that, the jet gets the gradual fragmentation resulting in the formation of small structures (i.e. ligaments) and droplets [21, 22].

It is known that liquid jets break up in several regimes: the laminar or turbulent Rayleigh regime, the downstream transition regime, the turbulent surface breakup regime, and the atomization regime (Fig. 1) [23]. Each of the regimes is characterized by certain combinations of the acting forces and differs from each other by the hydrodynamics and the structure of the jet if the operating parameters are changed (e.g. pressure). To summarize the experimental data, the dimensionless quantities like the Reynolds number (Re), the Weber number (We), and the Ohnesorge number (Oh) are generally used in the studies of liquid jets break up process (Fig. 2). These numbers represent the relation between the inertia forces, the viscous friction forces, and the surface tension [25]:

$$Re = (uD_h)/v; We = (\rho D_h u^2)/\sigma_s; Oh = \eta/\sqrt{\sigma_s \rho D_h},$$
 (2)

where u is a characteristic jet velocity, m·s⁻¹; D_h is a hydraulic diameter, m; v is a kinematic viscosity of the foam solution, m²·s⁻¹; η is a dynamic viscosity of the foam solution, Pa·s; σ_s is a surface tension coefficient, N·m⁻¹, and ρ is a density of the foam solution, kg·m⁻³.

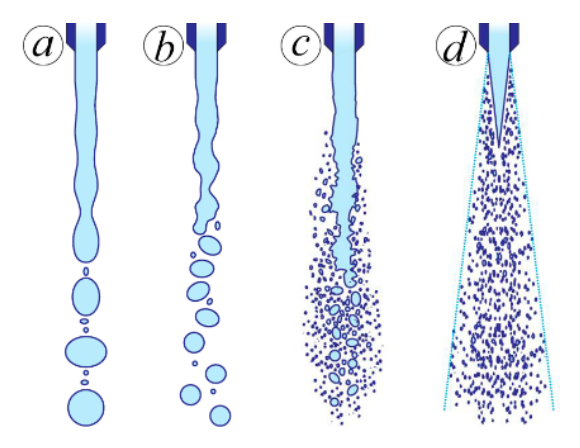


Figure 1. Schematic view of the jet breakup process regimes (a is the laminar Rayleigh, b is the downstream transition, c is the turbulent surface breakup, and d is the atomization regime) [23].

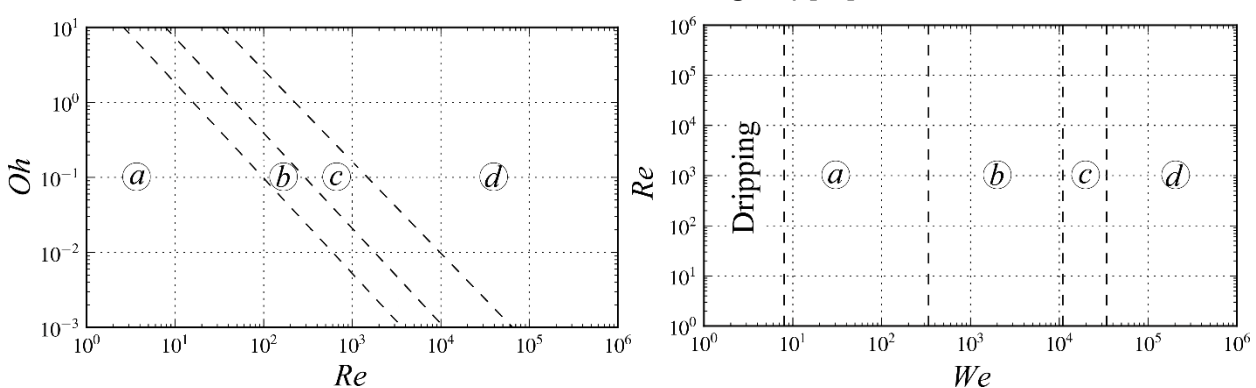


Figure 2. Diagrams that are used to determine the jet breakup process regime (a is the laminar Rayleigh, b is the downstream transition, c is the turbulent surface breakup, and d is the atomization regime) [25].

When it comes to deflector type sprinklers, the breakup process of liquid jet usually occurs in the turbulent surface breakup or atomization regimes (Fig. 2, positions c and d), since the outflow of the foaming solution occurs through the nozzle flow path of a fairly small diameter (from 8 to 25 mm) at a very high velocity (usually significantly more than 10 m/s). In that case, the inertia forces, the viscous friction forces, and aerodynamic forces have the greatest influence on the jet breakup process [24]. Taking into account the fact that the foam solution contains surfactants that change the surface tension of the liquid but do not affect its kinematic and dynamic viscosity, it is appropriate to use the Weber number to summarize the experimental data. It has been well studied that the length of waves formed on the jet surface after leaving the orifice of the sprinkle nozzle is inversely proportional to the Weber number, and their amplitude, on the contrary, is directly proportional to it [22, 26]. When the Weber number increases, a more intense breakup process of the jet into small structures and droplets is observed. Moreover, that, in its turn, can affect the foam generation process in the sprinkler.

2.2. Foam Solution Properties

According to (2), the dimensionless quantities used to determine the physical similarity of turbulent flows include a number of variables that characterize the physical and chemical properties of the fluid, which are density, surface tension coefficient, dynamic and kinematic viscosities. Accordingly, by varying the values of these parameters, the character of fluid flow (average velocity, geometry, and structure of the jet) also changes. Working foam solutions made of commercially produced foam concentrates have almost identical physical and chemical properties, values of which fluctuate in narrow ranges under normal ambient conditions: ρ = 1000–1020 kg·m⁻³, σ_s = 0.029–0.032 N·m⁻¹, η = (9.0–9.4)·10⁻⁴ Pa·s, and $v = (0.89-1.00) \cdot 10^{-6} \text{ m}^2 \cdot \text{s}^{-1}$. It follows that at the same operating pressure of the foam solution before the nozzle of the sprinkler with the same geometric parameters of the flow path, the character of the flow of liquid before not reaching the frame arm and the deflector of the sprinkler is generally identical despite the use of different types and brands of foam concentrates. Nevertheless, foam expansion actually differs for various types and brands of foam concentrates if geometrically identical sprinklers are used as it was shown in the experimental study [27]. Therefore, one can assume that the foam expansion depends on the chemical composition of the foam concentrate and, consequently, on the type and nature of the chemical reactions occurring during the foam generation process. It should be noted that the influence of the nature of reagents in the composition of modern foam concentrates, as well as their concentration in the working foam solution on the parameters of the foam generation process is poorly studied. In particular, it is due to the lack of data on the chemical composition of the foam concentrates on the market.

To take into consideration composition peculiarities of foam concentrate in the simplified mathematical model for the determining foam expansion, an empirical coefficient $\gamma_{e.r}$ can be implemented. This coefficient can be determined experimentally and calculated as a ratio of the foam expansion for the foam concentrate under study $(K_{e.r})$ to the foam expansion for some reference foam concentrate (K_{st}) . For example, on the territory of the Republic of Belarus, one of the most popular foam concentrate of type S (in sense that it is a synthetic hydrocarbon foam concentrate without fluorinated surfactants) is PO-6RZ (" Π O-6P3" in Russian). Therefore, in our study, we implemented PO-6RZ as the reference foam concentrate. The coefficient $\gamma_{e.r}$ is assigned a value of 1 for it.

In [27], the experimental determining of the main characteristics of foam, in particular its expansion, was carried out using 13 deflector type sprinklers with different geometric parameters of its elements and 3 different foam concentrates. After some straightforward transformations of the experimental data obtained in [27], we plotted the dependences of the foam expansion for type S foam concentrate Syntek-6NS ("Синтек-6HC" in Russian) and type WA foam concentrate OPS-0.4 ("ОПС-0.4" in Russian) on the foam expansion for the reference foam concentrate PO-6RZ (Fig. 3). As it follows from Fig. 3, the dependences are linear. It allow us to determine the values of the coefficient $\gamma_{e,r}$ for the foam concentrates under study: 0.92 for Syntek-6NS and 0.68 for OPS-0.4, respectively.

It must be emphasized that in the previous studies [11, 20, 25, 27], an aqueous solution with the manufacturer's recommended concentration of the foam concentrate in it (6% for PO-6RZ and Syntek-6NS, 1 % for OPS-0.4) was used.

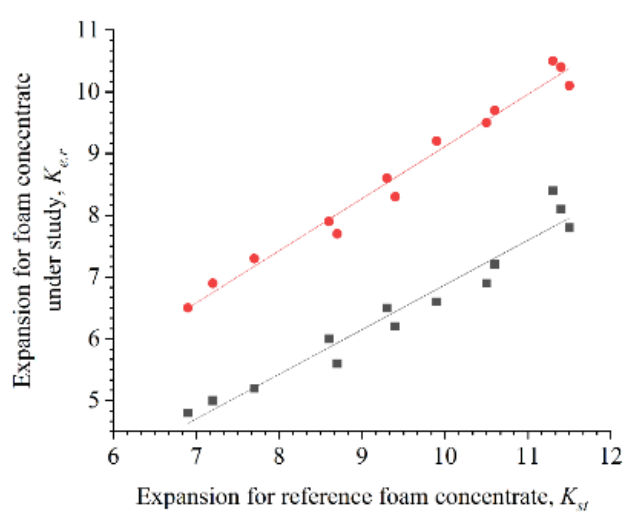


Figure 3. The dependence of foam expansion for foam concentrates Syntek-6NS (circles) and OPS-0.4 (squares) on foam expansion for the reference foam concentrate PO-6RZ (based on [27]).

2.3. Geometric Parameters of the Sprinkler

Geometric parameters of the elements of the deflector type sprinkler are presented in Fig. 4.

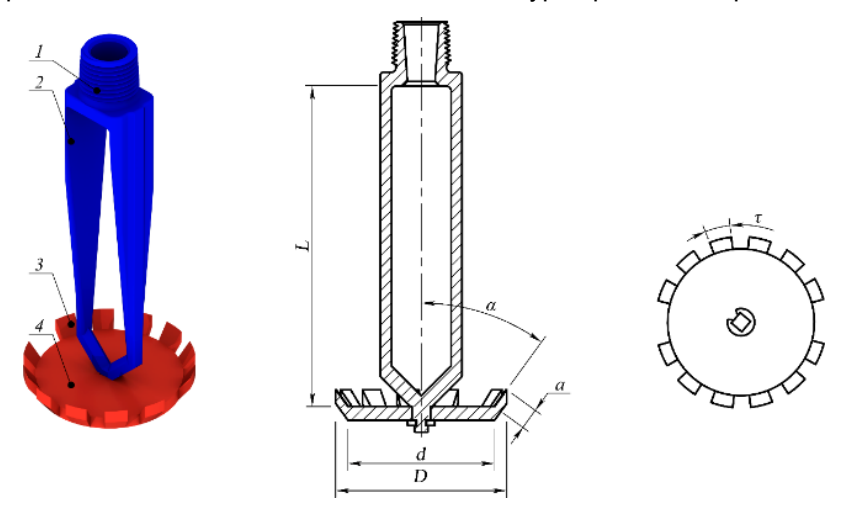


Figure 4. Main elements of the deflector type sprinkler and its geometric parameters (1 is the nozzle; 2 is the frame arm; 3 is the tine; 4 is the deflector;

D is the outer deflector diameter; a is the tine length; d is the inner deflector diameter; τ is the deflector tine spacing angle; α is the tine inclination angle; L is the frame arm length) [27].

To account for individual geometric parameters, such as the inner deflector diameter d and the deflector tine spacing angle τ , the deflector working surface coefficient K_s is used [27]:

$$K_{s} = \frac{360d^{2} \sin \alpha + \left(D^{2} - d^{2}\right) \sum \tau}{360\left(d^{2} \sin \alpha + D^{2} - d^{2}\right)} \cdot 100\% =$$

$$= \frac{360d^{2} \sin \alpha + \left(\left[d + \left(D_{y} - d\right) \sin \alpha\right]^{2} - d^{2}\right) \sum \tau}{360\left(d^{2} \sin \alpha + \left[d + \left(D_{y} - d\right) \sin \alpha\right]^{2} - d^{2}\right)} \cdot 100\%,$$
(3)

where $D_v = d + 2a$.

To make a decision about the geometric parameters of the sprinkler frame arm and deflector for inclusion in a simplified mathematical model, the results of the dispersion analysis of experimental data obtained in [28] (Fig. 5) were used. As seen in Fig. 5a, among the individual factors (the first 8 rows of the table), the deflector working surface coefficient K_s ("Coefficient $K_s(L)$ ") characterizes most of the variability of foam expansion (the sum of squares of deviations "SS" is equal to 19.56, which is about 27 % of the total sum of squares of deviations "Total SS"). The deflector working surface coefficient K_s is followed by the frame arm length ("Length L(L)" and "Length L(Q)" in Fig. 5a), the outer deflector diameter ("Diameter D(L)" and "Diameter D(Q)" in Fig. 5a), and the tine inclination angle ("Inclination $\alpha(L)$ " and "Inclination $\alpha(Q)$ " in Fig. 5a) when it comes to influence on the foam expansion. It should be noted that the tine inclination angle α describes a very small part of the variability of the foam expansion (2 % of the total sum of squares of deviations). In addition, according to the table of factor effects estimation in Fig. 5b, the tine inclination angle practically does not affect the value of the foam expansion (ΔK is no more than 0.3). Therefore, this factor can be neglected.

	ANOVA; Var.:Expansion K; R-sqr=,97145;									
	4 3-level fact	4 3-level factors, 1 Blocks, 81 Runs;								
		DV: Expansion K								
Factor	SS	df	MS	F	р					
(1) Length L(L)	5,47157	1	5,47157	169,3029	0,00000					
Length L(Q)	7,13405	1	7,13405	220,7439	0,00000					
(2) Coefficient K₅(L)	19,56444	1	19,56444	605,3686	0,00000					
Coefficient K₅(Q)	0,15635	1	0,15635	4,8380	0,03145					
(3) Diameter D(L)	2,61717	1	2,61717	80,9812	0,00000					
Diameter D(Q)	2,14352	1	2,14352	66,3254	0,00000					
(4) Inclination α(L)	1,23005	1	1,23005	38,0604	0,00000					
Inclination α(Q)	0,69751	1	0,69751	21,5826	0,00001					
1L by 2L	15,47111	1	15,47111	478,7116	0,00000					
1L by 2Q	5,50298	1	5,50298	170,2747	0,00000					
1Q by 2L	0,25411	1	0,25411	7,8627	0,00667					
1Q by 2Q	0,73069	1	0,73069	22,6091	0,00001					
1L by 3L	16,38001	1	16,38001	506,8350	0,00000					
1L by 3Q	4,96141	1	4,96141	153,5173	0,00000					
2L by 3L	0,26488	1	0,26488	8,1959	0,00566					
2L by 3Q	0,42603	1	0,42603	13,1823	0,00056					
Error	2,06837	64	0,03232							
Total SS	72,44401	80								

		Effect Estimates; Var.:Expansion K; R-sqr=,97145; 4 3-level factors, 1 Blocks, 81 Runs; MS Residual=,0323182								
		DV: Expansion K								
	Effect	Std.Err.	t(64)	р	-95,%	+95,%				
Factor					Cnf.Limt	Cnf.Lim				
Mean/Interc.	8,732330	0,021422	407,6324	0,000000	8,689534	8,77512				
(1) Length L(L)	0,658253	0,050590	13,0116	0,000000	0,557189	0,75931				
Length L(Q)	0,694519	0,046745	14,8575	0,000000	0,601134	0,78790				
(2) Coefficient K₅(L)	1,253015	0,050927	24,6042	0,000000	1,151277	1,35475				
Coefficient K₅(Q)	0,102222	0,046474	2,1995	0,031459	0,009379	0,19506				
(3) Diameter D(L)	-0,465572	0,051736	-8,9990	0,000000	-0,568927	-0,36221				
Diameter D(Q)	0,368674	0,045269	8,1440	0,000000	0,278239	0,45911				
(4) Inclination α(L)	0,301852	0,048928	6,1693	0,000000	0,204107	0,39959				
Inclination α(Q)	0,196852	0,042373	4,6457	0,000017	0,112202	0,28150				
1L by 2L	1,311111	0,059924	21,8795	0,000000	1,191399	1,43082				
1L by 2Q	0,716667	0,054921	13,0489	0,000000	0,606948	0,82638				
1Q by 2L	0,155926	0,055607	2,8041	0,006673	0,044837	0,26701				
1Q by 2Q	0,242333	0,050965	4,7549	0,000012	0,140519	0,34414				
1L by 3L	1,259032	0,055925	22,5130	0,000000	1,147310	1,37075				
1L by 3Q	0,606304	0,048934	12,3902	0,000000	0,508547	0,70406				
2L by 3L	0,162103	0,056623	2,8628	0,005669	0,048986	0,27522				
2L by 3Q	0,179886	0,049545	3,6307	0,000563	0,080908	0,27886				

Figure 5. ANOVA analysis of variance (a) and estimation of factor effects (b) carried out using STATISTICA software (SS is the sum of squares of deviations, df is the number of degrees of freedom, MS is the mean squares of deviations (MS = SS/df), F is the F-test (MSfactor/MSerror), p is the statistical significance level (p-value), Error is the error of the experiment, Total SS is the total sum of squares of deviations) [28].

Thus, the simplified mathematical model for determining the foam expansion can be represented in dimensionless form as follows:

$$K = B_e \gamma_{e,r} K_s^c \left(L/D \right)^g \left(D/D_{\text{max}} \right)^q W e^z, \tag{4}$$

where B_e is the empirical coefficient; c, g, q, z are the powers of the equation variables; $D_{\rm max}$ is the largest diameter of the sprinkler deflector and equal to 100 mm. The dimensionless parameter $\left(L/D\right)$ represents the relative length of the sprinkler frame arm, and the $\left(D/D_{\rm max}\right)$ is the scaling factor.

3. Results and Discussion

The search for the values of c, g, q, and z from (4) was performed by taking the natural logarithm of this equation and comparing it with the obtained experimental dependences of the foam expansion K on the included variables. The values of powers are taken equal to the slope of regression lines for the corresponding dependencies. For the dependences $\ln\left(K\right) = f\left(\ln\left(K_s\right)\right)$ and $\ln\left(K\right) = f\left(\ln\left(D/D_{\max}\right)\right)$, the slopes are: c = 0.5 and q = -0.05 (Fig. 6, 7). The dependence

 $\ln(K) = f\left(\ln(L/D)\right)$ is non-linear and the regression line is a curve with a maximum in the range $L/D = 3.0 \pm 0.3$ (Fig. 8). For this reason, we decided to divide the dependence $\ln(K) = f\left(\ln(L/D)\right)$ into two linear sections with slope coefficient g equal to 0.10 at $L/D \le 3.0$ (Fig. 8, position 1) and -0.03 at $3.0 < L/D \le 7.5$ (Fig. 8, position 2).

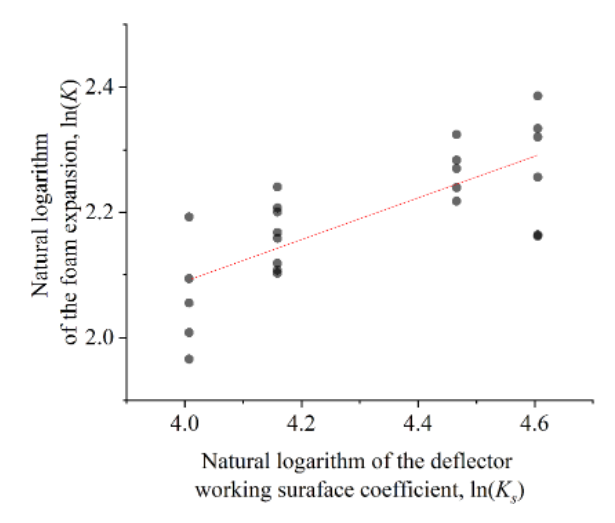


Figure 6. Dependence of the natural logarithms of the foam expansion and the deflector working surface coefficient.

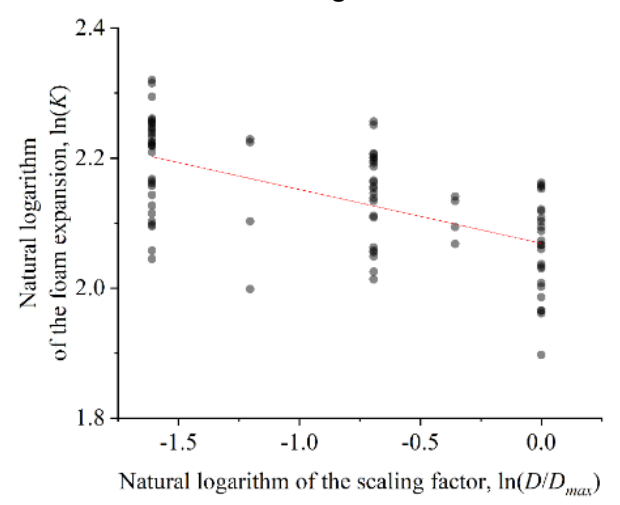


Figure 7. Dependence of the natural logarithms of the foam expansion and the outer deflector diameter of the sprinkler reduced to its largest diameter.

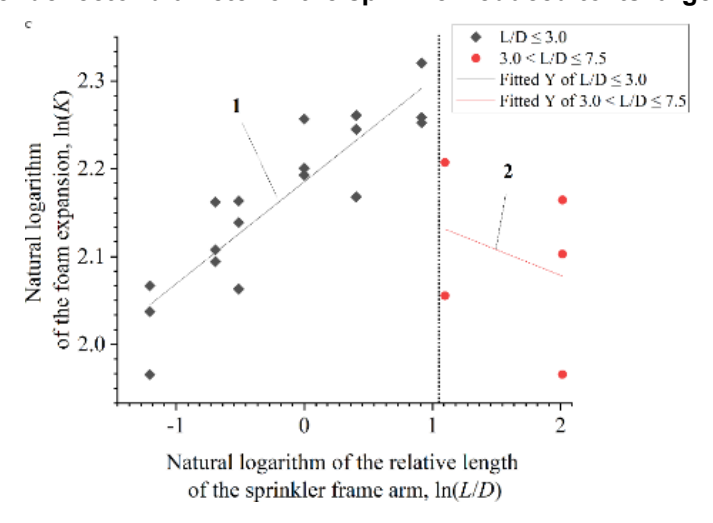


Figure 8. Dependence of the natural logarithms of the foam expansion and the relative length of the sprinkler frame arm (the slope of the fitted curves 1 and 2 are 0.10 and -0.03, respectively).

Five full factorial experiments were carried out to determine the dependence of the foam expansion on the Weber number. During experiments, five sprinklers with different dimensions of the nozzle flow path were used to change the character of the fluid flow. The design of the full factorial experiments included p=4 factors $(L,\,K_s,\,D,\,\alpha)$ that varied on n=3 value levels (since the dependencies of foam expansion on each factor are nonlinear as follows from [11]). Each full factorial experiment consisted of 81 series of experiments ($N=p^n=3^4=81$). The design of full factorial experiments was similar to that described in detail in [11]. Fig. 9 shows the appearance and dimensions of the flow path of the sprinkler nozzle. The values of the Weber number at the orifice of the nozzle are also indicated. The operating pressure of the working foam solution with the manufacturer's recommended concentration of the foam concentrate before the sprinkler nozzle was 0.1 MPa and remained constant.



Figure 9. Appearance and dimensions of the flow path of the sprinkler nozzles (A is the diameter of the nozzle inlet; B is the length of the nozzle flow path; C is the diameter of the nozzle orifice; We is the Weber number at the nozzle orifice at operating pressure 0.1 MPa).

Fig. 10 shows the dependences of the natural logarithm of the foam expansion and the natural logarithm of the Weber number for 5 different configurations of the frame arm and deflector of the sprinkler (for the remaining 76 configurations, the character of the dependences is similar). Taking into account that in the studied range of changing the distance from the orifice of the nozzle to the deflector of the sprinkler (from 30 to 150 mm) the average jet velocity remains almost constant [29, 30], the Weber number was calculated for the liquid jet at the orifice of the sprinkler nozzle. Based on the obtained results, the average slope of the regression line of the dependence $\ln\left(K\right) = f\left(\ln\left(We\right)\right)$ is equal to z=0.32. It should be emphasized that the Weber number growth causes an increase in the foam expansion as observed in Fig. 10. It can be explained by the growth of hydrodynamic pressure on the frame arm and deflector of the sprinkler that adds to the process of formation of a new surface and, accordingly, increases the number of forming foam films and bubbles.

The new simplified mathematical model (4) predictions of foam expansion show good agreement with the experimentally measured foam expansion. There was an average error in foam expansion of less than 9 % and the largest error of less than 20 % for all cases when the empirical coefficient Be = 0.026 was used.

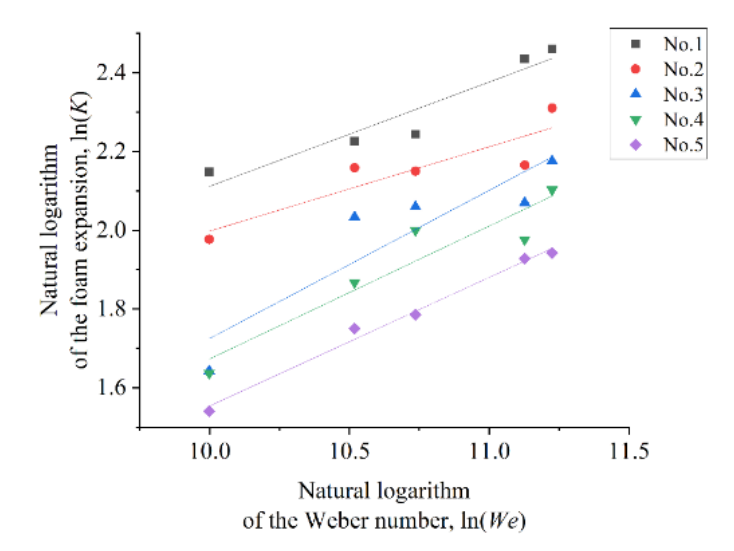


Figure 10. Dependence of the natural logarithms of the foam expansion and the Weber number with fitted curves (configurations of the frame arm and deflector geometric parameters: No. 1 – K_s = 87%, L = 114 mm, D = 63 mm; No. 2 – K_s = 100%, L = 50 mm, D = 20 mm; No. 3 – K_s = 55%, L = 50 mm, D = 50 mm; No. 4 – K_s = 64%, L = 100 mm, D = 30 mm; No. 5 – K_s = 64%, L = 30 mm, D = 100 mm).

Thus, the final form of the empirical equation for determining the foam expansion is as follows:

$$K = 0.026\gamma_{e,r}K_s^{0.5} (L/D)^g (D/D_{\text{max}})^{-0.05} We^{0.32},$$
(5)

where $\gamma_{e.r}$ is equal to 1 for the foam concentrate PO-6RZ, 0.92 for Syntec-6NS and 0.68 for OPS-0.4; g is equal to 0.10 at $L/D \le$ 3.0 and -0.03 at 3.0 $< L/D \le$ 7.5.

The boundary conditions of the developed model (4) are as follows: K_s is from 55 to 100 %, L is from 30 to 150 mm, D is from 20 to 100 mm, We is from 22·10³ to 75·10³, $D_{\rm max}$ is equal to 100.

4. Conclusions

A novel simplified mathematical model (5) for predicting expansion of foam generated in the deflector type sprinklers in automatic foam extinguishing systems was developed. The predictions of this new foam expansion model are in good agreement with the experimentally measured values. The average foam expansion error was less than 9 %.

The developed model can be used as an express method to predict the foam expansion in sprinklers taking into account the dimensions of the frame arm and deflector of the sprinkler, jet hydrodynamics and the properties of the applied foam concentrate of type S or WA. If the applied foam concentrate differs from those mentioned in this article, the corresponding coefficient $\gamma_{e,r}$ must be substituted into the model (5).

The coefficient γ_{er} can be determined experimentally according to the method described in details in [27].

Further studies will be devoted to establish the physical nature and the dependence of the coefficient $\gamma_{e.r}$ on the physical properties of the foam concentrate, as well as its chemical composition. It will provide a way to make the developed model (5) applicable for any foam concentrate. In addition, at the moment, the dependence of foam expansion on other dimensionless parameters, for example, on the ratio of the parameters K_s (the deflector working surface coefficient) and L (the frame arm length), are poorly understood. This dimensionless parameter is likely to have a high correlation with foam expansion and may be fundamentally important. In addition, in future studies, solutions of single surfactants that are generally used to prepare foaming solutions for extinguishing fires (for example, an aqueous solution of sodium lauryl sulfate or similar commonly used surfactant) will be taken as a reference foaming agent. This will make it possible to increase the reproducibility of the results by other authors.

Moreover, further research should focus on developing models to predict two other very important characteristics of the foam in terms of firefighting, such as its dispersion and stability. Dispersion is a value inverse to the average diameter of bubbles in the foam volume, and stability is a value defined as the time

of destruction of a certain part of foam volume. The ability to predict the main characteristics of the foam will make it possible to evaluate more objectively the level of fire protection of buildings and structures by automatic foam extinguishing systems.

References

- 1. Chen, T., Fu, X.-C., Bao, Z.-M., Xia, J.-J., Wang, R.-J. Experimental study on the extinguishing efficiency of compressed air foam sprinkler system on oil pool fire. Procedia Engineering. 2018. 211. Pp. 94–103. DOI: 10.1016/j.proeng.2017.12.142
- 2. Shafiq, I., Hussain, M., Shafique, S. et al. A comprehensive numerical design of firefighting systems for onshore petroleum installations. Korean Journal of Chemical Engineering. 2021. 38. Pp. 1768–1780. DOI: 10.1007/s11814-021-0820-6
- Till, R.C., Coon, J.W. Foam Systems. Fire Protection. Springer. Cham, 2019. Pp. 147–157. DOI: 10.1007/978-3-319-90844-1_11
- 4. Dlugogorski, B.Z., Kennedy, E.M., Schaefer, T.H., Vitali, J. What properties matter in fire-fighting foams? Proceedings of the 2nd National Research Institute of Fire and Disaster Symposium Science, Technology and Standards for Fire Suppression Systems. Tokyo, 2002. Pp. 57–76.
- 5. International Organization for Standardization (ISO). Fire extinguishing media Foam concentrates. Part 3: Specification for low-expansion foam concentrates for top application to water-miscible liquids. ISO 7203-3:2019. Geneva, 2019. 39 p.
- 6. Kamliuk, A.N., Likhomanov, A.O., Grachulin, A.V. Pennye orositeli dlia avtomaticheskikh ustanovok pozharotusheniia [Foam sprinklers for automatic extinguishing systems]. Minsk: UGZ, 2023. 244 p.
- 7. Korol'chenko, D.A., Sharovarnikov, A.F., Degaev, E.N. Fire extinguishing effectiveness of low multiplicity foam. Science Review. 2015. 8. Pp. 114–120.
- 8. Hil', E.I., Voevoda, S.S., Sharovarnikov, A.F., Makarova, I.P. Experimental determination of minimum discharge intensity and optimum rate of foaming agent input during suppression of oil products flame. Fire Safety. 2015. 4. Pp. 76–81.
- Laundess, A.J., Rayson, M.S., Dlugogorski, B.Z., Kennedy, E.M. Small-Scale Test Protocol for Firefighting Foams DEF(AUST)5706: Effect of Bubble Size Distribution and Expansion Ratio. Fire Technology. 2011. 47. Pp. 149–162. DOI: 10.1007/s10694-009-0136-2
- Myers, T.M., Marshall, A.W. A description of the initial fire sprinkler spray. Fire Safety Journal. 2016. 84. Pp. 1–7. DOI: 10.1016/j.firesaf.2016.05.004
- 11. Kamluk, A., Likhomanov, A. Increasing foam expansion rate by means of changing the sprinkler geometry. Fire Safety Journal. 2019. 109. Article no. 102862. DOI: 10.1016/j.firesaf.2019.102862
- Kim, T. Resolving the initial spray structure of fire sprinklers with a volume-of-fluid modeling. Fire Safety Journal. 2016. 133. Article no. 103641. DOI: 10.1016/j.firesaf.2022.103641
- 13. Kim, T. Factors affecting water flux distribution of fire sprinklers and effect of water flux uniformity on fire suppression characteristics. Fire Safety Journal. 2023. 138. Article no. 103804. DOI: 10.1016/j.firesaf.2023.103804
- 14. Kim, T. Optimization of fire sprinkler design for uniform water flux distribution using a micro-genetic algorithm. Fire Safety Journal. 2024. 144. Article no. 104090. DOI: 10.1016/j.firesaf.2024.104090
- 15. Myers, T., Trouve, A., Marshall, A. Predicting sprinkler spray dispersion in FireFOAM. Fire Safety Journal. 2018. 100. Pp. 93–102. DOI: 10.1016/j.firesaf.2018.07.008
- Myers, T., Marshall, A., Baum, H.R. A Free-Surface Model of a Jet Impinging On a Sprinkler Head. Fire Safety Science. 2014.
 11. Pp. 1184–1195. DOI: 10.3801/IAFSS.FSS.11-1184
- 17. Link, E.D., Jordan, S.J., Myers, T.M., Sunderland, P.B., Marshall, A.W. Spray dispersion measurements of a sprinkler array. Proceedings of the Combustion Institute. 2017. 36(2). Pp. 3305–3311. DOI: 10.1016/j.proci.2016.06.056
- 18. Valencia, A., Marshall, A.W. A universal lookup table for determining sprinkler spray patterns. Fire Safety Journal. 2021.126. Article no. 103432. DOI: 10.1016/j.firesaf.2021.103432
- Ren, N., Wang, Y. Modeling of Sprinkler skipping for the suppression of large-scale rack-storage fires. Fire Safety Journal. 2023. 141. Article no. 103953. DOI: 10.1016/j.firesaf.2023.103953
- Kamluk, A., Likhomanov, A., Grachulin, A. Field testing and extinguishing efficiency comparison of the optimized for higher expansion rates deflector type sprinkler with other foam and foam-water sprinklers. Fire Safety Journal. 2020. 116. Article no. 103177. DOI: 10.1016/j.firesaf.2020.103177
- 21. Tafreshi, H.V., Pourdeyhimi, B. The effects of nozzle geometry on waterjet breakup at high Reynolds numbers. Experiments in Fluids. 2003. 35. Pp. 364–371. DOI: 10.1007/s00348-003-0685-y
- Jie, H., Jingjing, W., Xiumei, L., Beibei, L., Wei, L., Ming, G., Yongwei, X., Zonghang, C., Jichao, M. Investigation on Surface Wave Characteristic of Water Jet. Mathematical Problems in Engineering. 2019. 2019. Article no. 4047956. DOI: 10.1155/2019/4047956
- 23. Lin, S.P., Reitz, R.D. Drop and spray formation from a liquid jet. Annual Review of Fluid Mechanics. 1998. 30. Pp. 85–105. DOI: 10.1146/annurev.fluid.30.1.85
- 24. Trettel, B. Reevaluating the jet breakup regime diagram. Atomization and Sprays. 2020. 30(7). Pp. 517–556. DOI: 10.1615/AtomizSpr.2020033171
- Likhomanov, A.O., Kamlyuk, A.N. The breakup length of axisymmetric turbulent jet in the foam deflector type sprinkler for automatic extinguishing systems. Journal of Civil Protection. 2021. 5(2). Pp. 159–173. DOI: 10.33408/2519-237X.2021.5-2.159
- 26. Eggers, J., Villermaux, E. Physics of liquid jets. Reports on Progress in Physics. 2008. 71(3). Article no. 036601. DOI: 10.1088/0034-4885/71/3/036601
- Likhomanov, A.O., Govor, E.G., Kamlyuk, A.N. On the relationship between the sprinkler geometric parameters, stability and expansion rate of the generated foam. Journal of Civil Protection. 2021. 5(2). Pp. 174-185. DOI: 10.33408/2519-237X.2021.5-2.174
- 28. Likhamanau, A., Kamluk, A. Mathematical model for predicting foam expansion rate depending on the geometrical parameters of deflector type sprinkler. Nauchnye i obrazovatelnye problemy grazhdanskoi zashchity [Scientific and educational problems of civil protection]. 2019. 41(2). Pp. 27–38.
- 29. Kotousov, L.S. Measurement of the water jet velocity at the outlet of nozzles with different profiles. Technical Physics. 2005. 50. Pp. 1112–1118. DOI: 10.1134/1.2051447

30. Kotousov, L.S. Measurement of the water jet velocity at the outlet of nozzles with different profiles. Technical Physics. 2006. 51. Pp. 289. DOI: 10.1134/S1063784206020265

Information about the authors:

Andrei Kamluk, PhD in Physics and Mathematics ORCID: https://orcid.org/0000-0002-9347-0778

E-mail: kan@ucp.by

Alexey Likhomanov, PhD in Technical Sciences ORCID: https://orcid.org/0000-0002-9374-1486

E-mail: alexlikh20@gmail.com

Eduard Govor,

ORCID: https://orcid.org/0000-0002-4040-3264

E-mail: govor-098@mail.ru

Alexander Grachulin, PhD in Technical Sciences ORCID: https://orcid.org/0000-0003-3832-8258

E-mail: grachulin_a@mail.ru

Received: 09.07.2024. Approved: 13.10.2024. Accepted: 21.10.2024.



Magazine of Civil Engineering

ISSN 2712-8172

journal homepage: http://engstroy.spbstu.ru/

Research article UDC 691.327

DOI: 10.34910/MCE.131.3



Ground granulated blast furnace slag and fly ash concrete

- ¹ Vietnam Institute for Building Science and Technology, Hanoi, Vietnam
- ² Research and Development Institute Lotte E&C, Seoul, Korea
- ⊠ hmduc@yahoo.com

Keywords: ground granulated blast furnace slag (GGBFS), fly ash, concrete, slump, compressive strength

Abstract. Utilization of ground granulated blast furnace slag (GGBFS) and fly ash (FA) to resolve the problem of increasing discharged and total accumulated industrial waste has attracted public concern. This article presents the research results on the effect of the replacement of up to 60 wt.% cement with GGBFS and FA, separately and in combination. It shows that mineral admixtures improve the workability of concrete mixture and reduce the required water-reducing admixture to reach a defined slump, prolonging the setting time of fresh concrete. The compressive strength of concrete with GGBFS at an early age decreases while increasing at 60 days and 90 days with the GGBFS content from 20 wt.% to 40 wt.%. The compressive strength of concrete with FA well develops at a later age, but it decreases at all ages as the FA replacement ratio increases. Cement replacement with a combined mineral admixture of 20 wt.% GGBFS and 20 wt.% FA does not significantly change the compressive strength at 28 days and later. Based on test results, the efficiency factor of mineral admixtures was calculated to use for selecting the proportion of concrete.

Citation: Hoang, M.D., Tran, Q.T., Lee, S.H. Ground granulated blast furnace slag and fly ash concrete. Magazine of Civil Engineering. 2024. 17(7). Article no. 13103. DOI: 10.34910/MCE.131.3

1. Introduction

The development of the economy and industries in Vietnam inevitably causes environmental problems due to the discharging of large amounts of waste. According to the latest estimates, up to now, Vietnam has 30 coal-fired thermal power plants in operation, discharging about 16 million tons of ash and slag annually. The total amount of ash and slag accumulated over the years is about 100 million tons, of which, by the end of 2021, 48.4 million tons have been treated and reused. Blast furnace slag waste from steel production also reaches about 4.3 million tons per year. In that context, the utilization of industrial wastes, including fly ash (FA) and ground granulated blast furnace slag (GGBFS), is an inevitable development trend of building material production in general and concrete production in particular.

Industrial wastes, such as FA and GGBFS, have been used in concrete to replace aggregate, cement, or both. Studies on the separate use of FA [1–8], GGBFS [9–14], or a combination of the two above admixtures [15–23] in concrete all over the world show that with the appropriate replacement ratio, the mineral admixtures improve the properties of fresh and hardened concrete, especially the durability of concrete in some aggressive environments. When added to concrete, the active mineral admixture, on the one hand, has the filling effect and makes the structure denser, and on the other hand, reacts with Ca(OH)₂ to create binding minerals. The combining effect of the two above processes depends on many factors, such as the composition, properties, and amount of the admixture, the using ratio, the cement content, and other factors. The optimum admixture's content is usually determined based on actual test results with specific material.

Y. Cho et al. [3] study the influence of the 25 wt.% replacement of cement by 16 types of FA on the compressive strength of cement mortar. The results show that chemical parameters based on the

amorphous chemical composition of FA have higher correlations with the compressive strength of the FA cement mortars than the chemical parameters based on crystalline components. The chemical parameters correlate with the 91-day strength better than the 28-day strength of FA cement mortars, as the pozzolanic reaction progressed further after 91 days. A. Oner et al. [2] investigate the strength development of concrete containing FA and the optimum use of FA in concrete. This study showed that strength increases with increasing amounts of FA up to an optimum value, beyond which it starts to decrease with further addition of FA. The optimum value of FA for the four test groups is about 40 wt.% of cement. The FA to cement ratio is an important factor determining the efficiency of FA. C. Luan et al. [4] study the effect of fly ashes, including low-calcium and high-calcium, on C-S-H structure, hydration products, hydration heat, and compressive strength of UHPC. The results showed that FA reduced the early-age compressive strength, but it increased middle- and late-age compressive strength, reduced the drying shrinkage and chloride impermeability coefficient of UHPC, and the effect of high-calcium FA was better than that of low-calcium FA.

Concerning GGBFS, A. Oner et al. [9] show the improvement of the 7-day to 365-day compressive strength with the increasing GGBS content. After an optimum point, at around 55 wt.% of the total binder content, further increasing GGBFS content does not improve the compressive strength. It is caused by the unreacted GGBFS acting as a filler material in the paste. S.C. Pal et al. [10] conclude that the reactivity of GGBFS depends on the source of slag, type of raw material, method, and cooling rate. The hydraulic index strongly correlates with the SiO₂, CaO, MgO, Al₂O₃, glass content, and Blaine's fineness of GGBFS at both 7 days and 28 days. S.C. Pal also develops the equations to determine the reactivity of slag based on the physical and chemical properties of slag. This equation accounts for the variations of the slag characteristics, which predict the hydraulic index and the strength performance of slag at 7 days and 28 days.

The combined utilization of FA and GGBFS has also been attracting the attention of researchers. The study of A. Szczesniak et al. [15] shows that adding FA to slag cement concrete in amounts of up to 33 wt.% by weight of cement is beneficial. The FA addition of 33 wt.% compared with the addition of 25 wt.% by the weight of cement in concrete based on CEM IIIA 42.5 cement does not significantly affect compressive strength and, in the case of concrete based on CEM IIIA 32.5 cement, even causes an increase in this strength. The possibility of using the k-value at XD1-3 exposure conditions for CEM IIIA cement classes should be carefully considered. A. Phul et al. [21] investigate the effect of cement replacement with up to 30 wt.% mineral admixtures, including GGBFS and FA, in concrete with a constant water-to-cement ratio of 0.47 and show that the workability of concrete increases initially with increasing replacement percentage up to an optimum limit but then decreases partially. The cement replacement with 20 wt.% GGBFS and 10 wt.% FA gives the highest compressive strength. The study of Z. Qu et al. [22] shows the reduction of the early-age mechanical properties of concrete with various FA and GGBFS at different cement replacement levels up to 40 wt.%. But at 28 days, the compressive strength of FA concrete is not lower, while GGBFS concrete is higher than that of reference concrete. C.U. Juang et al. [16] investigate the cement replacement by FA and GGBFS as long-term 40 wt.%, 50 wt.%, and 60 wt.%. The results showed that at high volumes of replacement, increasing GGBFS by 10% can increase the strength by 37 %. R. Rivera et al. [17] carried out the full factorial design for the 2 days, 7 days, and 28 days compressive strength of mortar with 25 wt.% and 40 wt.% of GGBFS and/or FA. The finer the GGBFS, the better the performance of ternary cement was achieved. It shows the more effective synergistic effect of the finer GGBFS due to a more adequate particle size distribution. This study also develops a relationship between compressive strength, fineness, GGBFS content, and FA content for each age.

When studying mineral additives, researchers pay great attention to quantifying the effectiveness of mineral additives. To evaluate the influence of mineral admixture on concrete strength, many researchers use the efficiency factor of additive k-value. The efficiency factor k-value represents the cement substitution capacity of mineral admixtures in equation (1), which correlates the compressive strength of concrete with the ratio of water to the binder.

$$f_C = b \times \left(\frac{1}{W/(C + k \times P)}\right) - a,\tag{1}$$

where f_C is the compressive strength of concrete; C, W, and P are the cement, water, and mineral admixture contents; a and b are the regression coefficients; k is the efficiency factor of mineral admixture.

The efficiency factor k-value is standardized in the European standard EN 206 "Concrete – Specification, performance, production, and conformity" as a k-factor concept. Based on the research in

Europe, EN 206 also recommends k-values for some admixtures. However, studies show that, in practice, there is a certain fluctuation of this value.

L. Wang et al. [24] consider the threshold value of the effective replacement ratio as the turning point of the strength curve with the replacement ratio. The threshold value of the effective replacement ratio by FA decreased with increasing curing temperature, whereas the reaction efficiency of FA increased with increasing curing temperature. The reaction efficiency of FA can be described more intuitively and quantitatively. G.K. Babu et al. [25] established the "overall cementing efficiency" (k) of FA through a "general efficiency factor" (k_e) , dependent on the age, and a "percentage efficiency factor" (k_p) , dependent on the replacement percentage. Meanwhile, K. Hwang et al. [5] develop an estimation equation for compressive strength development. The equation can express coefficient α , which indicates the activity of FA as a binder, in the form of a function of age, FA content, and Blaine-specific surface area of FA. Further, the coefficient α can be a product of α_1 , which takes account of the effect of FA to cement ratio, and α_2 , which expresses the effect of the specific surface area by Blaine.

M.S. Magalhães et al. [26] investigate the effect of the FA fineness and content, the water content, and the concrete age on the k-value. The results indicate that the k-values of Brazilian FA are higher than the one recommended by EN 206. Furthermore, the k-value depends on FA content and decreases when the content in the mixture increases. Water-to-binder ratio and hydration time significantly influence the k-value, too. The results also indicate an improvement in the k-value and relationship between compressive strength, Young's modulus, and the FA amount in the mixture with an increase in FA fineness.

Until now, EN 206 still does not specify the k-value of GGBFS due to its variation. R. Härdtl [27] confirms the broad range of performance of GGBFS from different sources and the strong influence of the interaction with Portland cement, which requires a conservative approach when defining the limits of a prescriptive k-value for GGBFS. In a recent study, B. Boukhatem et al. [28] used an artificial neural network to predict the efficiency factor of GGBFS in concrete based on published test results. He developed a mathematical model for predicting the value of GGBFS in terms of percentage replacement (from 0 % to 80 %) and concrete age (from 2 days to 90 days).

The utilization of GGBFS and FA in concrete has been studied and implemented for many years in Vietnam and has achieved encouraging results. However, the current technical documents in Vietnam still do not have specific guidance on evaluating the effectiveness of using mineral additives in concrete. The efficiency factor of Vietnamese mineral admixtures depends on its original, type, replacement ratio, the age of the concrete, and other factors and can be determined experimentally. This paper presents the results of research on the effects of partial replacement of cement with local mineral admixtures, including FA, GGBFS, and a combination of FA and GGBFS, on the properties of fresh concrete as well as the compressive strength of concrete.

2. Materials and Method

In this study, we used PC40 Portland cement from But Son Cement Plant with a specific gravity of 3.11 g/cm³, a standard consistency of 29.0 %, and initial and final setting times of 135 min and 195 min. The compressive strength of cement at 3 days and 7 days is 34.2 MPa and 51.9 MPa, respectively.

Fine aggregate is the Lo River yellow sand with a bulk specific gravity (dry) of 2.62 g/cm³, a bulk density of 1480 kg/m³, the mass of particles coarser than 5 mm of 2.2 wt.%, clay silt and dust content of 0.6 wt.%, and a fineness modulus of 2.6. The coarse aggregate used in the study is crushed stone from Hoa Binh with a bulk specific gravity (dry) of 2.72 g/cm³, a bulk density of 1420 kg/m³, clay silt and dust content of 0.3 wt.%, and a maximum particle size of 20 mm. The grading of the aggregate fulfills the standard requirements.

SilkRoad SPR1500, a high-range water-reducing chemical admixture based on polycarboxylate, has a 17.6 % water reduction ability, and the properties meet the requirements for type F admixture.

We use coal FA from the Pha Lai Thermal Power Plant. FA after treatment (floated) has a total content of SiO2+Al2O3+Fe2O3 of 88.52 wt.%, SO3 content of 0.14 wt.%, dissolved alkali content of 0.63 wt.%, chloride content of 0.01 wt.%, loss on ignition of 1.15 wt.%, specific gravity of 2.23 g/cm³, mass of particles on sieve 0.045 mm of 22 %. FA has a required water content of 98.3 % and a strength activity index of 92.7 % at 28 days.

We also use the GGBFS S95 of Hoa Phat Hai Duong Steel Factory with a specific gravity of 2.89 g/cm³, a specific surface area of 5120 cm²/g, a strength index at the age of 7 days of 76.2 %, 28 days of 101.4 %, a consistency ratio of 97.5 %, MgO content of 7.88 wt.%, SO3 content of 0.37 wt.%, a chloride content of 0.02 wt.%, and a loss on ignition of 0.45 wt.%.

We mix the concrete mixture in a free-falling laboratory mixer and determine the properties of fresh concrete. We cast the cylindrical test specimens with a diameter of 150 mm and a height of 300 mm in a series, each consisting of 3 cylinders. We cure the standard specimens in the laboratory until the testing ages. Testing to determine the properties of fresh and hardened concrete was carried out according to active national standards.

3. Results and Discussions

We study the effect of GGBFS and FA on the properties of fresh and hardened concrete in the mixtures with a constant content of cementitious materials. We used mineral admixtures, including GGBFS, FA, and GGBFS+FA, to partially replace cement by weight at the ratios of 20 wt.%, 40 wt.%, and 60 wt.% of the total content of cementitious materials. When using a mixture of GGBFS+FA, the replacement ratio of each admixture is 20 wt.% and 40 wt.%. To maintain a constant cementitious materials-to-water ratio and water content, we selected the appropriate dosage of high-range water-reducing chemical admixture so that the slump of the fresh concrete varied from 150 mm to 200 mm. Table 1 shows the actual concrete proportions.

			Material's	conte	nt for 1r	Parameters					
N 0	ID	Cem.	GGBFS	FA	Fine agg.	Coarse agg.	Water	Adm., (%)	W/CM	GGBFS/CM, %	FA/CM, %
1	S0.F0	357	0	0	829	1062	178	1.0	0.51	0	0
2	S2.F0	286	71	0	825	1063	179	0.9	0.51	20	0
3	S4.F0	215	143	0	823	1065	179	0.7	0.51	40	0
4	S6.F0	142	214	0	815	1060	178	0.6	0.51	60	0
5	S0.F2	287	0	71	810	1063	179	8.0	0.51	0	20
6	S0.F4	217	0	144	795	1070	181	0.6	0.51	0	40
7	S0.F6	146	0	220	783	1080	182	0.0	0.50	0	60
8	S2.F2	216	72	72	809	1067	179	0.5	0.50	20	20
9	S2.F4	146	72	145	794	1073	181	0.4	0.50	20	40
10	S4.F2	144	143	72	803	1064	179	0.5	0.50	40	20

Table 1. Proportion of fresh concrete.

The test results for fresh concrete including, density, slump, air content, and setting time are presented in Table 2.

		Density,			Setting time, min		
No	ID	kg/m³	Slump, mm	Air content, %	Initial	Final	
1	S0.F0	2434	150	2.0	455	585	
2	S2.F0	2432	180	1.9	480	615	
3	S4.F0	2435	160	1.8	505	635	
4	S6.F0	2419	160	1.9	620	745	
5	S0.F2	2418	160	2.2	505	640	
6	S0.F4	2416	200	2.3	650	820	
7	S0.F6	2420	180	1.8	810	985	
8	S2.F2	2425	150	2.4	515	665	
9	S2.F4	2420	190	2.1	720	935	
10	S4.F2	2413	160	2.5	675	805	

Table 2. Properties of fresh concrete.

The experimental results in Table 2 show that, as there is an increase in the cement replacement ratio of mineral admixtures, the dosage of water-reducing admixture needed for the concrete mixture to reach the same slump decreases. It proves that both GGBFS and FA improve the slump of the concrete mixture, in which FA was able to improve the slump more than GGBFS. The spherical shape of FA particles and increasing binder volume when replacing cement are the reasons for this phenomenon.

Although the specific gravity of GGBFS and FA is less than that of cement, with a total cementitious materials content of about 360 kg/m³, replacing cement with GGBFS, FA, or GGBFS+FA at a ratio up to 60 wt.% does not significantly change the density of the concrete. The air content of concrete with mineral

admixtures varies from 1.8 % to 2.5 % compared to 2.0 % of the concrete without it. The variation of air content is within the statistical error.

Partial cement replacement with a mineral admixture prolongs the setting time of fresh concrete, both initial and final. The initial setting time increases from 455 minutes of reference concrete to 620 minutes and 810 minutes of concrete with GGBFS and FA, respectively. The final setting time increases from 585 min to 745 min and 985 min for concrete using GGBFS and FA, respectively. Thus, FA increases the setting time of fresh concrete more than GGBFS. Increasing the setting time of concrete using GGBFS+FA has an intermediate value compared with concrete using FA or GGBFS separately.

Table 3 shows the compressive strength of concrete at 3 days of age to 90 of days age and the ratio of compressive strength at the different ages to those of the 28 days of the same proportion. Fig. 1 to Fig. 4 visualizes the effect of the cement replacement ratio of mineral admixtures on concrete compressive strength.

Na	ID	Compressive	strength, MPa a	t the age, days /	Ratio to the 28 da	ays strength, %
No	ID	3	7	28	60	90
1	S0.F0	29.0 / 64	38.9 / 85	45.6 / 100	49.3 / 108	51.3 / 112
2	S2.F0	24.6 / 57	35.2 / 82	43.0 / 100	50.9 / 118	54.3 / 126
3	S4.F0	20.0 / 50	28.3 / 70	40.3 / 100	49.5 / 123	53.5 / 133
4	S6.F0	15.2 / 40	25.4 / 68	37.6 / 100	44.3 / 118	47.0 / 125
5	S0.F2	22.4 / 58	29.7 / 77	38.5 / 100	45.4 / 118	50.1 / 130
6	S0.F4	16.3 / 50	22.5 / 69	32.7 / 100	40.3 / 123	45.5 / 139
7	S0.F6	7.9 / 40	13.1 / 66	20.0 / 100	25.9 / 130	28.0 / 140
8	S2.F2	14.9 / 38	25.3 / 64	39.7 / 100	48.3 / 122	49.5 / 125
9	S2.F4	10.5 / 31	20.4 / 60	33.8 / 100	37.1 / 110	40.8 / 121
10	S4.F2	10.4 / 30	20.1 / 58	34.7 / 100	38.3 / 100	42.6 / 123

Table 3. Compressive strength of concrete.

Research results show that, at the age of up to 28 days, partly replacing cement with mineral admixtures, including GGBFS, FA, and GGBFS+FA, reduces the compressive strength of concrete. However, this trend changes significantly at longer ages. At 60 days and 90 days, with the GGBFS replacement ratio up to 40 wt.%, the strength of concrete hardly decreased but somehow improved. However, when combined with FA, the strength can be unchanged only at the GGBFS replacement ratio of up to 20 wt.%. With an FA replacement ratio of 40 wt.%, the addition of GGBFS results in a significant decrease in the strength of the concrete at any age.

Unlike GGBFS, partly replacing cement with FA causes the strength of concrete to decrease at all replacement ratios at all ages. The strength reduction rate increases rapidly at a high FA ratio. The use of FA in combination with GGBFS did not change this trend. This effect can be explained by the fact that, unlike GGBFS, the FA admixture has low activity, so using it instead of cement, especially at a high ratio, while the water content and cementitious materials to water ratio remain unchanged, decreases the hydration products as well as the CSH minerals and causes strength reduction.

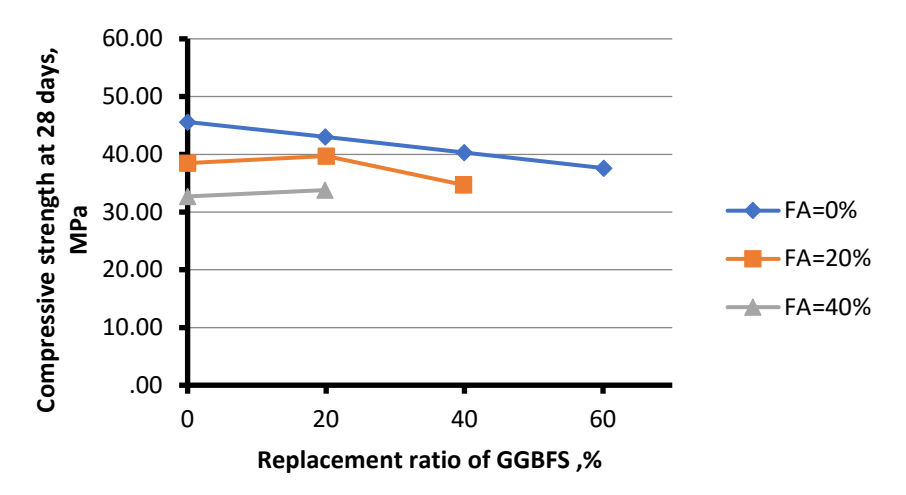


Figure 1. Effect of GGBFS on the compressive strength of concrete at 28 days.

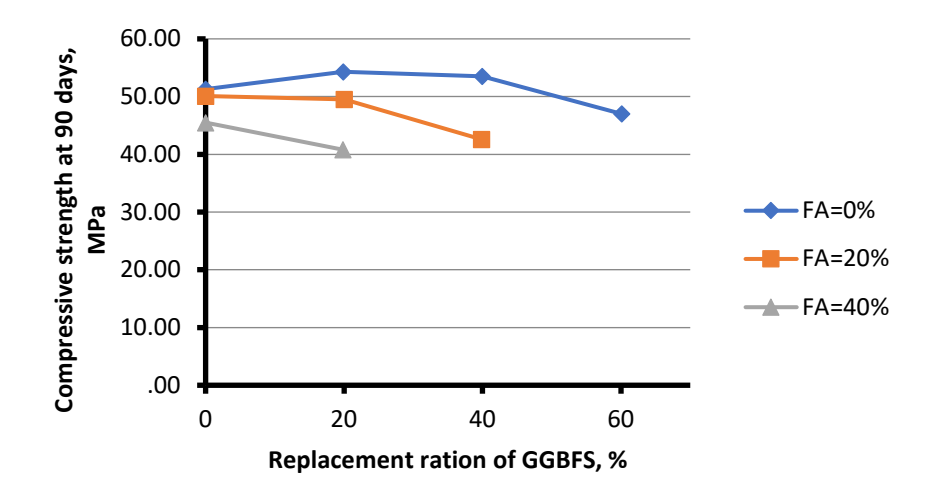


Figure 2. Effect of GGBFS on the compressive strength of concrete at 90 days.

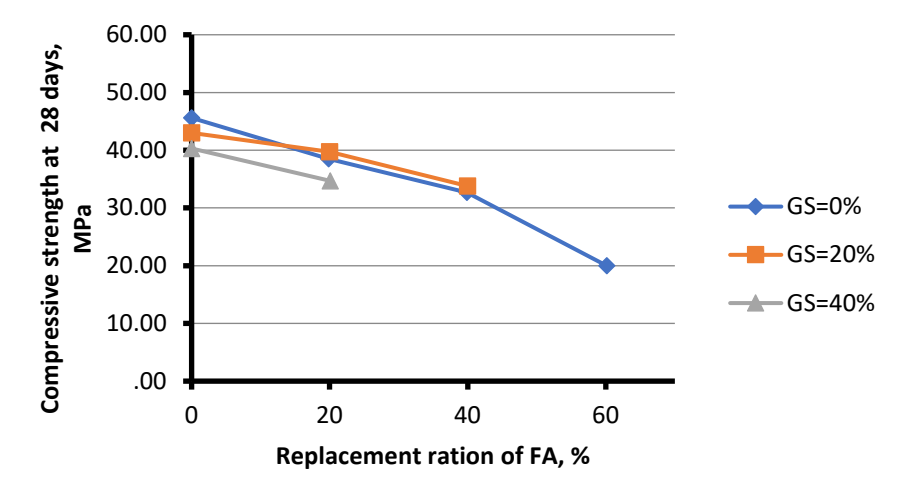


Figure 3. Effect of FA on the compressive strength of concrete at 28 days.

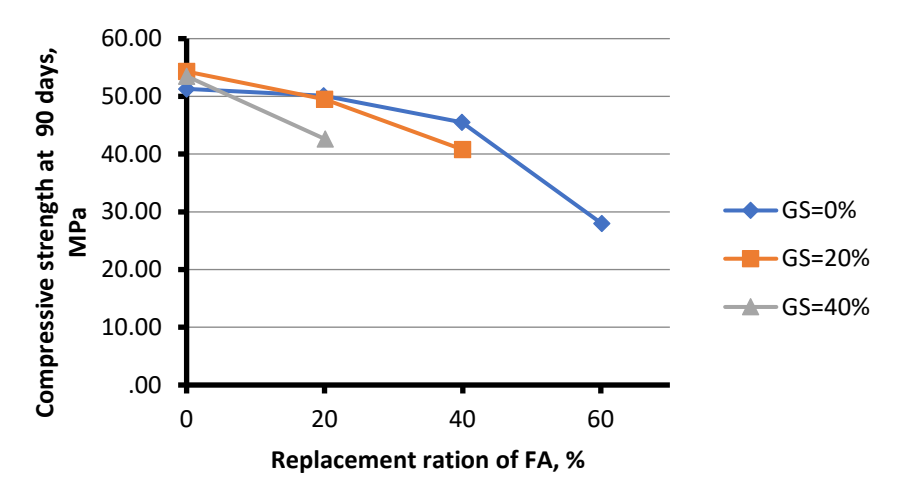


Figure 4. Effect of FA on the compressive strength of concrete at 90 days.

The above data shows that when replacing a part of the cement with mineral additives, the absolute value of the strength may decrease, but the strength development at longer ages is greater than that of the control mixture without mineral admixture. When replacing cement with GGBFS at the ratio of 20 wt.% to 60 wt.% of cementitious materials, the compressive strength at 90 days can increase from 25 % to 33 %, while replacing with FA increases from 30 % to 40 %. Replacement of cement with the mixture of GGBFS+FA can increase strength by 25 %. The above results are similar to studies [10, 16, 17] and show that concrete using mineral admixtures will be effective in structures where the strength is specified at longer ages.

Table 4 presents the ratio of the compressive strength of concrete at each age to the compressive strength of reference concrete (without mineral admixtures) at 28 days.

Table 4. The compressive strength rate	tion at 28 days.
--	------------------

No	ID	Ratio of strength of concrete to the strength of reference concrete at 28 age, % at age, days					
		3	7	28	60	90	
1	S0.F0	64	85	100	108	113	
2	S2.F0	54	77	94	112	119	
3	S4.F0	44	62	88	109	117	
4	S6.F0	33	56	82	97	103	
5	S0.F2	49	65	84	100	110	
6	S0.F4	36	49	72	88	100	
7	S0.F6	17	29	44	57	61	
8	S2.F2	33	55	87	106	109	
9	S2.F4	23	45	74	81	89	
10	S4.F2	23	44	76	84	93	

The data in Table 4 shows that concrete using mineral admixtures can achieve strength not less than 28 days strength of reference concrete when the GGBFS replacement ratio is up to 40 wt.% at 60 days and up to 60 wt.% at 90 days. These ratios of FA were 20 wt.% at 60 days and 40 wt.% at 90 days. When using the combination of GGBFS+FA, the concrete strength only reaches the reference concrete strength at the age of 28 days when the replacement ratio of each type is 20 wt.% (total replacement ratio 40 wt.%). The results obtained in the study are different from some studies in the world. The reason may be due to differences in local raw material characteristics, different chemical compositions, and fineness.

To evaluate the contribution effect on concrete's strength of the mineral admixture, we estimate the k-value in Equation (1) at different ages. To calculate the k factor, we determine the regression between compressive strength and the cement-to-water ratio in concrete without using mineral admixture at different ages. Based on the actual strength of concrete with mineral admixture and established regression, we calculate the equivalent amount of binder, thereby determining the k-value. Table 5 presents the estimated k-value.

Table 5. Efficiency factor k-value.

No	in	Efficiency factor k-value at age, days					
	ID	3	7	28	60	90	
1	S2.F0	0.60	0.70	0.78	1.16	1.28	
2	S4.F0	0.57	0.54	0.75	1.00	1.09	
3	S6.F0	0.56	0.61	0.75	0.84	0.86	
4	S0.F2	0.37	0.20	0.34	0.64	0.89	
5	S0.F4	0.40	0.29	0.40	0.59	0.74	
6	S0.F6	0.32	0.24	0.20	0.28	0.29	
7	S2.F2	0.31	0.39	0.70	0.92	0.89	
8	S2.F4	0.40	0.46	0.62	0.62	0.67	
9	S4.F2	0.40	0.45	0.65	0.66	0.73	

Obviously, in Table 5, the k-value for both admixtures tends to increase over time from 3 days to 90 days. The increase of the k-value depends on the type of admixture and the replacement ratio. Previous studies have also noted this upward trend [18, 27, 29, 30]. Compared with the recommended value in EN 206, the determined k-value has a certain difference as mentioned in the studies [1, 26, 29]. It shows that in practice, to improve the efficiency of mineral admixture, it is advisable to determine and apply the k-value for each different local source of raw materials.

The k-value of mineral admixtures depends on the replacement ratio. Regarding the GGBFS and GGBFS+FA, the k-value at a replacement ratio of 20 wt.% is higher than that of 40 wt.% and 60 wt.% at all ages from 3 days to 90 days. FA has a different behavior. The FA k-value at a replacement ratio of 40 wt.% is highest only at the ages of 3 days to 28 days. At 60 days and 90 days, the FA k-value at a replacement ratio of 20 wt.% is higher than that of 40 wt.% and 60 wt%.

The efficiency of GGBFS is higher than that of FA. When the replacement ratio increased from 20 wt.% to 60 wt.%, the efficiency factors of both admixtures tended to decrease. At a replacement ratio of 60 wt.%, the efficiency factor of FA is dramatically reduced, indicating that, for materials used in the study, a replacement ratio of FA of more than 40 wt.% may not be beneficial in the strength aspect.

Regarding the use of a combination of two admixtures, the efficiency factor of the combined admixture has an intermediate value between these values of each admixture at the corresponding replacement ratio. When replacing cement with GGBFS at the ratio of 20 wt.% and 40 wt.%, the k-value at 60 days and 90 days is greater than 1.00, showing that the efficiency of GGBFS in strength is more than that of cement. These results can be used for selecting concrete proportions using GGBFS and FA admixtures.

4. Conclusions

Partial cement replacement with GGBFS and FA at a ratio of up to 60 wt.% improves concrete slump as shown by reducing the required water-reducing admixture to maintain the same slump when the water content remains unchanged. The effect on slump improvement of FA is greater than that of GGBFS.

GGBFS and FA replacement increases the initial and final setting time of concrete mixtures. In particular, the increase in setting time when using FA is more than when using GGBFS.

Replacing up to 40 wt.% of cement with GGBFS improves concrete strength at 60 days and 90 days, even in combination with 20 wt.% FA. Replacing cement with FA at the replacement ratio in the study decreases concrete strength at all ages. Based on the experimental results, the mineral admixture efficiency factor k-value was calculated at specific replacement ratios and different ages. These values can be used for selecting concrete proportions using mineral admixtures.

References

- 1. Papadakis, V.G. Effect of fly ash on Portland cement systems: Part I. Low-calcium fly ash. Cement and Concrete Research. 1999. 29(11). Pp. 1727–1736. DOI: 10.1016/S0008-8846(99)00153-2
- 2. Oner, A., Akyuz, S., Yildiz, R. An experimental study on strength development of concrete containing fly ash and optimum usage of fly ash in concrete. Cement and Concrete Research. 2005. 35(6). Pp. 1165–1171. DOI: 10.1016/J.CEMCONRES.2004.09.031
- 3. Cho, Y.K., Jung, S.H., Choi, Y.C. Effects of chemical composition of fly ash on compressive strength of fly ash cement mortar. Construction and Building Materials. 2019. 204. Pp. 255–264. DOI: 10.1016/J.CONBUILDMAT.2019.01.208
- 4. Luan, C., Wu, Z., Han, Z., Gao, X., Zhou, Z., Du, P., Wu, F., Du, S., Huang Y. The effects of calcium content of fly ash on hydration and microstructure of ultra-high performance concrete (UHPC). Journal of Cleaner Production. 2016. 415. Article no. 137735. DOI: 10.1016/j.jclepro.2023.137735
- 5. Hwang, K., Noguchi, T., Tomosawa, F. Prediction model of compressive strength development of fly-ash concrete. Cement and Concrete Research. 2004. 34(12). Pp. 2269–2276. DOI: 10.1016/J.CEMCONRES.2004.04.009
- 6. Yildirim, H., Sümer, M., Akyüncü, V., Gürbüz, E. Comparison on efficiency factors of F and C types of fly ashes. Construction and Building Materials. 2010. 25(6). Pp. 2939–2947. DOI: 10.1016/J.CONBUILDMAT.2010.12.009
- Sumer, M. Compressive strength and sulfate resistance properties of concretes containing Class F and Class C fly ashes. Construction and Building Materials. 2012. 34. Pp. 531–536. DOI: 10.1016/J.CONBUILDMAT.2012.02.023
- 8. Cho, Y.K., Jung, S.H., Choi, Y.C. Effects of chemical composition of fly ash on compressive strength of fly ash cement mortar. Construction and Building Materials. 2019. 204. Pp. 255–264. DOI: 10.1016/J.CONBUILDMAT.2019.01.208
- 9. Oner, A., Akyuz, S. An experimental study on optimum usage of GGBS for the compressive strength of concrete. Cement and Concrete Composites. 2007. 29(6). Pp. 505–514. DOI: 10.1016/J.CEMCONCOMP.2007.01.001
- 10. Pal, S.C., Mukherjee, A., Pathak, S.R. Investigation of hydraulic activity of ground granulated blast furnace slag in concrete. Cement and Concrete Research. 2003. 33(9). Pp. 1481–1486. DOI: 10.1016/S0008-8846(03)00062-0
- 11. Ganesh Babu, K., Sree Rama Kumar, V. Efficiency of GGBS in concrete. Cement and Concrete Research. 2000. 30(7). Pp. 1031–1036. DOI: 10.1016/S0008-8846(00)00271-4
- 12. Shariq, M., Prasad, J., Masood, A. Effect of GGBFS on time dependent compressive strength of concrete. Construction and Building Materials. 2010. 24(8). Pp. 1469–1478. DOI: 10.1016/J.CONBUILDMAT.2010.01.007
- 13. Barnett, S.J., Soutsos, M.N., Millard, S.G., Bungey, J.H. Strength development of mortars containing ground granulated blast-furnace slag: Effect of curing temperature and determination of apparent activation energies. Cement and Concrete Research. 2005. 36(3). Pp. 434–440. DOI: 10.1016/J.CEMCONRES.2005.11.002
- 14. Sanjuán, M.A., Piñeiro, A., Rodríguez, O. Ground Granulated Blast Furnace Slag Efficiency Coefficient (k Value) in Concrete. Applications and Limits. Materiales De Construcción. 2011. 61(302). Pp. 303–313. DOI: 10.3989/mc.2011.60410
- 15. Szcze'sniak, A.S., Zychowicz, J., Stolarski, A. Influence of Fly Ash Additive on the Properties of Concrete with Slag Cement. Materials. 2020. 13(15). Article no. 3265. DOI: 10.3390/ma13153265
- 16. Juang, C.U., Kuo, W.T. Properties and Mechanical Strength Analysis of Concrete Using Fly Ash, Ground Granulated Blast Furnace Slag and Various Superplasticizers. Buildings. 2023. 13(7). Article no. 1644. DOI: 10.3390/buildings13071644
- 17. Rivera, R.A., Sanjuán, M.Á., Martín, D.A. Granulated Blast-Furnace Slag and Coal Fly Ash Ternary Portland Cements Optimization. Sustainability. 2020. 12(14). Pp. 5783. DOI: 10.3390/SU12145783
- 18. Chore, H.S., Joshi, M.P. Strength evaluation of concrete with fly ash and GGBFS as cement replacing materials. Advances in concrete construction. 2015. 3(3). Pp. 223–236. DOI: 10.12989/ACC.2015.3.3.223
- 19. Elaine Jin, Y., Yazdani, N. Substitution of Fly Ash, Slag, and Chemical Admixtures in Concrete Mix Designs. Journal of Materials in Civil Engineering. 2003. 15(6). Pp. 602–608. DOI: 10.1061/(ASCE)0899-1561(2003)15:6(602)

- 20. Bouzoubaâ, N., Foo, S. Use of Fly Ash and Slag in Concrete: A Best Practice Guide. Government of Canada Action Plan 2000 on Climate Change, 2005. 40 p.
- 21. Phul, A., Jaffar, M., Shah, S.N.R., Sandhu, A., GGBS And Fly Ash Effects on Compressive Strength by Partial Replacement of Cement Concrete. Civil Engineering Journal. 2019. 5(4). Pp. 913–921. DOI: 10.28991/cej-2019-03091299
- 22. Qu, Z., Liu, Z., Si, R., Zhang, Y. Effect of Various Fly Ash and Ground Granulated Blast Furnace Slag Content on Concrete Properties: Experiments and Modelling. Materials. 2020. 15(9). Article no. 3016. DOI: 10.3390/ma15093016
- Nataraja, M.C., Shivakumara, M.J., Dalawai, V.N. Effect of design parameters on the proportioning of mass concrete using fly ash and ground granulated blast furnace slag. Materials Today: Proceeding. 2022. 62(8). Pp. 5329–5335. DOI: 10.1016/J.MATPR.2022.03.410
- 24. Wang, L., Uji, K., Ueno, A. Evaluation on reaction efficiency coefficient of fly ash based on threshold value of effective replacement ratio. Proceedings of the Cement & Concrete Society. 2017., 71(1). Pp. 645-652. DOI: 10.14250/cement.71.645
- Babu, K.G., Nageswara Rao, G.S. Efficiency of fly ash in concrete. Cement and Concrete Composites. 1993. 15(4).
 Pp. 223–229. DOI: 10.1016/0958-9465(93)90025-5
- Magalhães, M.S., Cezar, B.F., Lustosa, P.R. Influence of Brazilian fly ash fineness on the cementing efficiency factor, compressive strength and Young's modulus of concrete. Developments in the Built Environment. 2023. 14. Article no. 100147. DOI: 10.1016/j.dibe.2023.100147
- Härdtl, R. The k-value concept applied for GGBFS-Principles and experiences. Proceedings of the International RILEM Conference on Material Science (MatSci).
 Additions Improving Properties of Concrete (AdIPoC). RILEM Publications SARL, 2010. Pp. 189–198.
- 28. Boukhatem, B., Ghrici, M., Kenai, S., Tagnit-Hamou, A. Prediction of Efficiency Factor of Ground-Granulated Blast-Furnace Slag of Concrete Using Artificial Neural Network. ACI Materials Journal. 2011. 108(1). Pp. 55–63.
- 29. Papadakis, V.G., Antiohos, S., Tsimas, S. Supplementary cementing materials in concrete: Part II: A fundamental estimation of the efficiency factor. Cement and Concrete Research. 2002. 32(10). Pp. 1533–1538. DOI: 10.1016/S0008-8846(02)00829-3
- Bijen, J., Van Selst, R. Cement equivalence factors for fly ash. Cement and Concrete Research. 1993. 23(5). Pp. 1029–1039.
 DOI: 10.1016/0008-8846(93)90162-3

Information about the authors:

Minh Duc Hoang, PhD

ORCID: https://orcid.org/0000-0001-8413-8741

E-mail: hmduc@yahoo.com

Quoc Toan Tran,

E-mail: trqtoans@gmail.com

Sang Hyun Lee,

E-mail: paulus@lotte.net

Received 27.08.2023. Approved after reviewing 17.10.2024. Accepted 17.10.2024.



Magazine of Civil Engineering

ISSN 2712-8172

journal homepage: http://engstroy.spbstu.ru/

Research article UDC 621.82

DOI: 10.34910/MCE.131.4



Antifriction fluoroplastic materials for sliding layers in bridge supports

L.A. Bokhoeva ¹ 🖾 🗓 , V.E. Rogov ² D, A.S. Chermoshentseva ³ D

- ¹ East-Siberian State University of Technology and Management, Ulan-Ude, Russian Federation
- ² Baikal Institute of Nature Management Siberian branch of the Russian Academy of Sciences, Ulan-Ude, Russian Federation
- ³ Bauman Moscow State Technical University, Moscow, Russian Federation

⊠ bohoeva@yandex.ru

Keywords: deterioration, bridge sliding bearings, sliding elements, polytetrafluoroethylene, metalfluoroplastic, fluoroplastic composite

Abstract. The requirements for reliability and durability are increasing every year for the critical elements of bridge structures, as there is a steady increase in the number of vehicles and volumes of cargo movement. Such structural elements include bearing parts of spans of bridges, which perceive loads from the mass of spans, transport cargo and compensate for deformations from thermal expansion and contraction. Antifriction polymeric materials are used in all newly developed designs of bearing parts. The reliability and durability of bridges as a whole depend on the physical, mechanical and operational properties of such materials. The change in the length of spans due to temperature fluctuations is carried out due to sliding along the polymer layers. The article presents a critical analysis of the polymer and metalpolymer materials used as sliding supports. A review and analysis of standardized anti-friction materials for possible use as sliding layers in the bearing parts of bridges have been carried out. The most promising fluoroplastic composite materials capable of operating without lubricant are presented. An analysis of metalfluoroplastic sheet materials was made, new metal composites were proposed, in which various mesh materials with a high polymer content in the working layer are used as an anti-friction layer. Such materials can be used as guides for the moving bearing parts of the bridge without the use of lubricants. It is shown that the use of the described modern wear-resistant anti-friction materials will significantly increase the bearing capacity and service life of sliding bearings.

Funding: The work has been carried out within the framework of the state task of the SB RAS Baikal Institute of Nature Management No. 0273-2021-0007, Grant RB under agreement No. 505.

Citation: Bokhoeva, L.A., Rogov, V.E., Chermoshentseva, A.S. Antifriction fluoroplastic materials for sliding layers in bridge supports. Magazine of Civil Engineering. 2024. 17(7). Article no. 13104. DOI: 10.34910/MCE.131.4

1. Introduction

The article presents a study on the bearing capacity of sliding elements in bridge sliding bearings. The object of the study is sliding elements in the construction of a linearly movable support part of the bridge. Currently, there is a significant increase in the load on transport facilities and their supporting elements [1–3], which is associated with a steady increase in the number of vehicles and the volume of goods, material and other tangibles movement around the world. In Russia, there is also an active development of land transport infrastructure aimed at efficient transport communication within the country

and with neighboring states [4]. The requirements for strength, reliability, durability and non-repair periods of operation of transport structure elements in general and bridge structures in particular have increased significantly [5-7]. This has led to the increasing number of scientific and engineering developments in bridge building aimed at improving bridge structures [8–12], introducing new materials with improved performance properties [13, 14], changing the configuration of bearing parts, optimizing the thickness and position of sliding layers [15], etc. One of the critical elements of bridge structures are the supporting parts [16–18]. During operation, the bearing parts perceive various static and dynamic loads from superstructures, rolling-stock and deformations of steel spans of bridges associated with daily temperature changes. The movement of bridge spans from thermal expansion takes place in various ways. For example, compensation for the thermal expansion of old massive arch bridges of small length usually occurs due to joint deformation with the soil massifs of the banks. The progressive movements of the movable bearing parts are divided into three groups during implementation: deformation, rolling and sliding. Bearing parts that move due to rolling bearings are bulky and require constant care and lubrication control. Sliding bearings use polymeric materials [19-21] with high antifriction properties in the fluid friction mode. Not a single transport structure can do without polymeric materials used as thin sliding layers to move bridge spans. At present, more length of spans and higher cargo flows has increased the load acting directly on the steel-polymer sliding pair, leading to a change in the performance of bridges as a whole. Moreover, recommendations for the design and installation of polymer bearing parts of bridges 1 have not been reviewed for a long time.

The analysis of literary sources of the current state of bridge support elements and the introduction of new materials that can significantly increase the durability and reliability of the sliding support without structural changes to the assembly as a whole can be considered a useful and relevant task.

The purpose of the work is to summarize the literature data and patent sources on the bearing capacity and service life of sliding elements in the construction of a linearly movable bridge support part. Research objectives: 1) review of literature and patent sources on the bearing capacity of sliding elements in sliding bridge supports; 2) analysis of polymer materials to optimize the operation of critical sliding elements of transport and logistics systems; 3) choosing the optimal material for use in sliding bearings to change the supporting parts and increase the service life of sliding pairs due to increased wear resistance.

2. Methods

The collection of information began with studying the sources of printed materials, including the authors' articles. A selection of literature sources on antifriction fluoroplastic materials has been made and optimal composite, metal fluoroplastic materials have been proposed to be used in bridge structure supports. With the objective information on the study, a critical analysis of the materials used for sliding layers in bridge supports has been carried out. The data can be used to determine the required dimensions of sliding elements for newly created bridge structures for a load given. According to the research, fluoroplastic composites can significantly increase the bearing capacity and the service life of bridge structure sliding bearings.

2.1. Sliding Knots and Materials Used

The structures of the supporting parts with movable sliding bearings are shown in Figs. 1 and 2. The slip plate rests on the middle support element, which is a cup cover (Fig. 1) and an upper balance bar (Fig. 2). A sliding element made of polished steel sheet is attached to the plate. Sheet polymeric material is fixed on the upper surface of the middle supporting element. Linear movements of the support units are provided by a sliding pair of polished stainless steel – fluoroplast. In spherical bearing parts, an additional polymeric anti-friction material is installed between the balancers. For smooth movement of the plates along the guide elements, metal-fluoroplastic material (MFL) is used, in the form of strips (Fig. 1, pos. 5 and Fig. 2, pos. 6).

¹ Rekomendacii po proektirovaniyu i montazhu polimernyh nesushchih chastej mostov [Recommendations for the design and installation of polymer load-bearing parts of bridges]. Rosavtodor. 20.02.2008. No. 73-r. Moscow, 2008. 115 p. [Online]. URL: https://docs.cntd.ru/document/1200062263 (reference date: 23.07.2024).

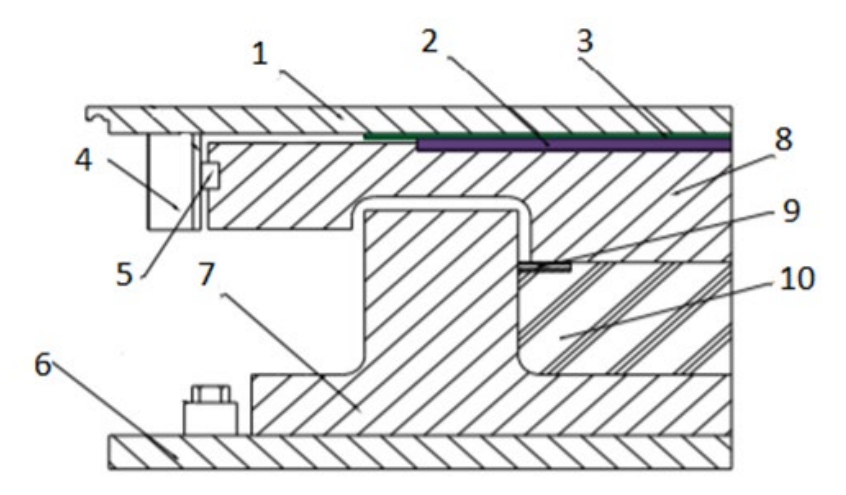


Figure 1. Design of a linearly movable bearing part of the bridge:
1 – top plate, 2 – polished steel sheet, 3 – anti-friction gasket made of polymeric material,
4 – guide, 5 – metal-fluoroplastic strip, 6 – bottom plate, 7 – glass, 8 – cover, 9 – sealing rings,
10 – rubber insert.

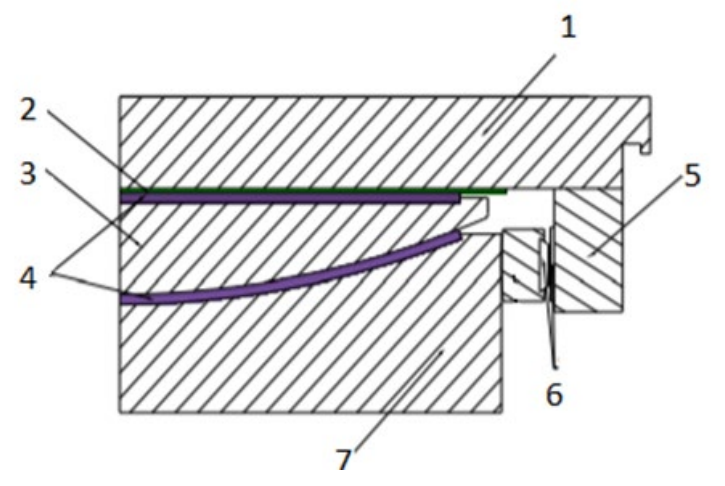


Figure 2. Design of the ball segment bearing part of the bridge:
1 – sliding plate, 2 – polished steel sheet, 3 – upper balancer,
4 – anti-friction gasket made of polymeric material, 5 – guide, 6 – friction pair, 7 – lower balancer.

In sliding tribocouplers, it is recommended to use polymer plates made of fluoroplast-4 (polytetrafluoroethylene) grades P, PN, which are located in grooves (balancers, covers, plates)1. In sliding pairs with fluoroplast, sheet corrosion-resistant chromium-nickel steel Russian State Standard GOST 5582-75 with a polished contact surface is used. According to the analysis of the work, the recommended sliding pair can work with lubricant during the planned time in case when the amplitude of displacement of the bridge spans is insignificant. With a displacement amplitude of several tens of centimeters per day and an increased load, the service life of the sliding support may decrease due to the increased wear rate of polytetrafluoroethylene (PTFE) [20] and the cold flow of the material. Such movements are typical for bridges located in areas with a severe continental climate. In slip pairs, PTFE was chosen ¹ because of its a low coefficient of friction. PTFE was also experienced in bridge piers located in European countries with a temperate climate. The undoubted prospect of using PTFE in sliding bearings is due to the presence of a number of unique properties: an anomalously low coefficient of friction among structural materials (0.04-0.05 for steel without lubrication), high thermal stability (decomposition onset temperature 4150C), high chemical resistance, excellent insulating properties. Along with these qualities, PTFE has insufficient wear resistance in tribocouplings (PTFE wear during friction is 4-5 times greater than that of caprolon, polyamide, polyethylene, and filled materials based on them) and increased creep (fluidity) under prolonged loads. It is known [22] that irreversible plastic deformation develops in PTFE products at low loads and at low temperatures (below the glass transition temperature). At room temperature and a load of 10 MPa, which is 2-3 times lower than the rupture strength of PTFE, its irreversible deformation develops within 100 hours (more than 200%) [23]. Unfortunately, the scientific literature review does not prove that there are practically any experimental studies of the stress-strain state of PTFE samples under compressive loads in a free or constrained state. Therefore, for a long time, researchers considered it impossible to use fluoroplastic in heavily loaded sliding bearings due to its cold flow (creep) [20]. A decrease

in the creep of PTFE products in sliding bearings of bridges is observed due to design solutions in the form of placement of fluoroplastic plates in recesses – undercuts. To improve the wear resistance of PTFE in world practice, two main approaches have been developed, which can be defined as physical and chemical modification methods. The first one is based on the creation of composite materials by introducing finely dispersed (recently, ultrafine and nanosized) fillers (graphite, coke, chopped glass fiber and carbon fiber, metal oxides, nanodiamonds, etc.) into the fluoroplast [24, 25]. The second method is based on the copolymerization of tetrafluoroethylene with other partially or fully fluorinated monomers. Both methods made it possible to obtain a series of new materials with one or another improved characteristic, which are used mainly as structural materials.

Composite materials based on PTFE are distinguished by higher wear resistance and elastic properties, which leads to a significant increase in the durability and reliability of friction units. It is known that one of the most effective ways to ensure the reliability and durability of movable interfaces of mechanisms and minimize energy losses during operation is the use of lubricants. However, the use of lubricating fluids requires special devices, constant monitoring and maintenance, which leads to additional costs, while negatively affecting the environment. Based on the fact that recent years witness more attention to the environmental friendliness of friction units, in the long term, sliding bearings of bridge structures will work in tandem with polymeric materials with a low coefficient of friction and without the use of a lubricant.

Given the above, it is necessary to consider industrial fluoroplastic composite materials according to the following criteria:

- maintenance without the use of lubricants;
- higher wear resistance compared to that of the main polymer by at least 1000 times;
- the material works in pairs with steel;
- the coefficient of friction being equal to or slightly higher than the original polymer.

3. Results and Discussion

From more than three dozen standardized PTFE-based composites, we have selected the following materials, presented in Table 1.

Table 1. Comparative tribotechnical characteristics of industrial fluoroplastic composite materials.

	Trademarks of fluoroplastic composites							
Indicators	F-4	F4K15M5	F4K15UV5	Flubon-20	Fluvis-20	Fluvis-20 PHO		
	GOST 10007- 72	TC 6-05-1412	TC 6-05-041- 781	TC301-05- 16	RB 0353	5279.071		
Fillers, %	-	Coke – 15, $MoS_2 - 5$	Coke – 15, carbon fiber – 5	Carbon fibers UTM-8 - 20		arbon fibers plasma – 20		
Coefficient of friction on steel	0.04	0.1–0.39	0.08–0.35	0.05	0.05	0.05		
Reverse friction pair	Steel	Steel	Steel	Steel	Steel	Steel		
Relative wear resistance	1	1000	1000	2000	2000	3500		
Working conditions		Moisture, condensation, no lubrication	In various environments without lubrication	Liquid, gaseous media, without lubrication	Aggressive media, without lubrication			

Table 1 shows that among the studied fillers, carbon and carbon fibers are promising ones, since they significantly increase the wear resistance of fluoroplastic composites. In addition to the presented materials based on fluoroplast-4, a new material has been developed, its structure changed due to joint temperature and radiation modifications. L.Ya. Karpov Research Institute of Physics and Chemistry manufactures F-4RK grade material [26, 27] produced according to TC 2213-103-00208982-2007, obtained by radiation modification of finished fluoroplastic products. This modification of PTFE made it possible to significantly increase the operational and wear-resistant characteristics of the polymer, which are shown in

Table 2. Modification of finished products is carried out by irradiation with gamma rays above the melting point of the crystalline phase of the polymer. After such processing, the operational properties of fluoroplastic blanks increase sharply. The F-4RK material obtained in this way has higher elastic modulus and yield strength compared to the initial material. Creep decreases up to 100 times, wear resistance increases 103–104 times, with a low friction coefficient [28].

Indicators	F-4	F-4PM
Density, kg/m3	2180	2200
Tensile strength, MPa	25	14.2
Relative elongation at break, %	350	125
Tensile modulus, MPa	350	630
Compressive stress at deformation 10%, MPa	15	25
Deformation in compression under a load of 14 MPa in 24 hours, %	16	6.8
Residual deformation 24 hours after unloading, 14 MPa	9.8	0.6
Coefficient of friction on steel	0.08	0.08
Wear intensity during friction on steel 30KhGSA under a load of 2.4 MPa and a speed of 0.3 m/s, mm/km	3.0	0.003
Brinell hardness, MPa	35	45
Maximum operating temperature, 0C	260	260

The search conducted showed that there are proposals from other companies offering antifriction fluoroplastic materials, without presenting their technical characteristics and disclosing methods of obtaining. Flontekh LLC ² and RPE Arflon LLC ³ advertise wear-resistant polymer materials of the ARFLON brand (AR100 and AR200) obtained by high-temperature physicochemical modification of the original PTFE. Such materials can be used in the construction of railway bridges, road junctions and overpasses as a sliding layer for reciprocating and angular movements of span support units. Innovative fluoroplastic technologies LLC ⁴ produces a radiation-modified fluoroplastic – 4 called RAFLON, which is widely used in railway rolling stock. In our opinion, all the presented companies produce the same F-4RM material, but under different names, since any change in the irradiation dose entails changes in the properties of the material. Thus, when advertising a material called ARFLON, the company does not even report its radiation exposure, while the enterprise [27] RAFLON has a trademark that can be placed on all manufactured products. According to the authors of [29], the F-4RM material is widely used in various products and is manufactured at more than 50 enterprises. The Internet advertised the products of the company LLC "Konstanta-2":

- "Constaftor 300" PTFE filled with the particles of chemically modified carbon fibers, which reduces creep under load, sharply increases wear resistance and strength at elevated temperatures;
- "Constaftor 400" a highly filled composition based on F-4, characterized by an increased yield strength, heat resistance and very low creep, especially at elevated temperatures;
- "Constaftor 500" a bronze-filled PTFE-based composition with low creep and high compressive strength, as well as good wear resistance.

Unfortunately, the company does not provide comparative technical characteristics of its materials in relation to industrial materials. In our opinion, the fillers used by this company, approved by many researchers, cannot lead to a significant increase in the performance characteristics of fluoroplastic composites compared to known materials.

The second bottleneck in sliding bearings are elements – guides, which must provide low friction and anti-seize properties during the movement of plates during the entire guaranteed service life. Such properties are typical for sheet MFLs. Traditional MFLs have been developed for plain bearings in various

² Technical characteristic of antifriction fluoroplastic materials of FLONTEKH LLC [Onljne]. URL: https://flonteh.ru/material/ (application date: 23 07 2024)

³ Technical characteristic of antifriction fluoroplastic materials of NPP Arflon. [Onljne]. URL: http://www.arflon.ru/Products/properties.html (reference date: 23.07.2024).

⁴ Technical characteristic of antifriction fluoroplastic materials of Innovacionnye ftoroplastovye tekhnologii LLC [Onljne]. URL: https://studylib.ru/doc/5000618 (reference date: 23.07.2023).

industries where the use of a lubricant is not desirable or acceptable. MFLs are produced in the form of metal strips, on which a porous layer of spherical particles of tin bronze is applied through a thin layer of copper. The protruding peaks of the outer bronze particles are covered with a polymer coating made from a mixture of fluoroplastic with various fillers, which acts as a lubricant. MFL production is automated and high-tech: plain bearings of various diameters, made from these tapes, in the form of rolled bushings, have a minimum running-in layer. In Russia, such bearings are produced at the machine-building enterprises of the country: Ftoroplast LLC, Bugulma, Promsnabkomplekt LLC, Promgleks-M CJSC, Kineshma. Foreign-made MFLs of the brands DU and DP (The USA) and MU (Italy) are also known. A comparative analysis of bushings made of MFL from various manufacturers, including Russian ones, showed that plain bearings made from grades DU and DP have the highest wear resistance [30]. The Russian MFL [31] loses to foreign products in terms of wear-resistant properties in dry friction due to the fact that the limiting wear of the fluoroplastic coating is concentrated in the surface layer with a thickness of 0.025–0.05 mm, which directly affects the durability of products as a whole. The wear limit is caused by the insufficient thickness of the fluoroplastic layer located in the pores of the bronze particles.

It can be stated that materials scientists failed to sufficiently firmly bond PTFE with a porous metal layer [32] (because of complete "unwillingness" of the polymer to stick to anything, the presence of a "shape memory effect" of the material during heat treatment, and a high coefficient of thermal expansion). In this regard, in most cases, these bearings provide the necessary resource of friction units when using lubricants. Bushings made of strip bimetallic materials are used in a wide variety of friction units (in pumps for pumping oil, various rotary mechanisms, hydraulic boosters, etc.). Based on these data, it can be stated that guides in the form of MFL platinum cannot ensure the guaranteed operation of this sliding unit without the presence of a lubricant. After the loss of the fluoroplastic coating, friction processes without lubricant are carried out along the tops of antifriction bronze particles with a possible loss of antifriction properties.

Thus, for the successful operation of the guides in the absence of lubrication, new anti-friction sheet materials are needed. There are known methods [33, 34] for producing MFLs in the form of plates where instead of the traditional porous bronze layer of spherical particles, various mesh woven materials are used, which are specially fixed on a metal surface. The polymer layer is fixed in the mesh pores after PTFE particles are pressed into the mesh space and sheet products are sintered in tightly compressed cassettes [32]. The resulting materials represent a metal composite with a heterogeneous structure. The working surface is a regularly alternating sections of a solid base (bronze mesh) and a polymer. The use of antifriction layers in the form of grids on the metal surface made it possible to increase the proportion of the polymer in the working layer. In the pores of bronze-brass meshes, the thickness of the fluoroplastic layer can be more than 1 mm. Such a thickness of the polymer layer makes it possible to significantly increase the durability and reliability of friction units without the use of a lubricant [35, 36]. Unfortunately, these metalfluoroplastic mesh materials have not found proper application in plain bearings in the form of bushings. The main disadvantage is that at the initial moment of rotation, the contact between the sleeve and the shaft is carried out along the grid vertices, that is, along the minimum contour area, which leads to wear and, in most cases, when stable operation of the friction unit is achieved, the bearing clearances go beyond the limit value of the linear wear value.

In our opinion, this material is promising for sliding units for guide plates, since changing the dimensions of the interface by a few hundredths of a mm will not affect the operation of the unit as a whole. In addition to traditional MFLs and bearings, fundamentally new imported metal-polymer bearings of the Fritex type made by Technymon appeared ⁵. These bearings are rolled bushings from a three-layer system consisting of a bronze substrate with a thickness of 0.50 to 2.70 mm and a fluoroplastic fabric adhesively connected to it. The fabric, woven with special fibers, has a thickness of 0.40 mm. This thickness of the fluoroplastic coating in the form of a woven material may indicate the long-term operational reliability of the bearing. In terms of technical characteristics, when operating without lubrication at maximum allowable load and operating temperatures, Fritex bearings are not significantly inferior to MFL (Russia). The operating temperature range of such bearings is in the range from -100 to + 260 °C. A similar material, consisting of a metal substrate, an adhesive sublayer, and a fluoroplastic layer reinforced with fiberglass, is also advertised by Konstanta-2 LLC [30]. Technical characteristics of the material, unfortunately, are not provided by the producer. In our opinion, it is possible to adhesively connect a fluoroplastic fabric with a metal surface only if fabrics are created in the form of three-dimensional woven structures. Such fabrics consist of bulk layers intertwined with various threads in a special way into a single structure [37], where fluoroplastic fibers are on the surface, and the carrier threads, made of another synthetic material, have strength properties and increased adhesion to adhesives.

⁵ Technical characteristics of FRITEX-B [Onljne]. URL: https://technymon.com/product/self-lubricated-bearings/fritex-b/ (reference date: 23.07.2024).

4. Conclusion

- The paper presents wear-resistant polymeric materials with hundreds and thousands of times increased operational characteristics when working in friction units in the absence of lubrication compared to the original polymer. This fact suggests that the replacement of sliding elements made of PTFE-4 with the materials described above in the sliding bearings will optimize the operation of the critical sliding elements of transport and logistics systems, significantly increasing their bearing capacity and service life.
- The most promising material to replace PTFE is radiation-modified PTFE grade F-4RK (TU 2213-103-00208982-2007), then industrial fluoroplastic composite materials grades Fluvis-20PHO, Flubon-20, Fluvis-20, F4K15M5 and F4K15UV5.
- 3. Among PTFE materials, the longest non-lubricated mating work can be done with DU or DP materials. Promising materials can be metal-fluoroplastic sheets where various mesh materials with an increased proportion of polymer in the working layer are used as an anti-friction layer.
- 4. Further clarifications, calculations and more detailed research and experimental studies are needed to search for and select antifriction materials that are optimal in terms of wear resistance and reliability when operating without lubrication, providing the required service life of sliding elements in bridge sliding bearings.

References

- 1. Proske, D. Bridge Collapse Frequencies versus Failure Probabilities. Springer. Cham, 2018. 126 p.
- 2. Ruzov, A.M. Ekspluataciya mostovogo parka [Operation of the bridge park]. Moscow: Akademiya, 2007. 176 p.
- 3. Singh, S., Martinetti, A., Majumdar, A., van Dongen, L.A.M. Transportation systems: Managing performance through advanced maintenance engineering. Springer Singapore. Singapore, 2019. 221 p. DOI: 10.1007/978-981-32-9323-6
- 4. Blinkin, M., Koncheva, E. A Forecast for Transport System Development in Russia. Springer. Cham, 2016. Pp. 273–293. DOI: 10.1007/978-3-319-47800-5 10
- Ovchinnikov I.I., Majstrenko I.YU., Ovchinnikov I.G., Uspanov A.M. Failures and collapses of bridge constructions, analysis of their causes. Part 4. Russian journal of transport engineering. 2018. 1(5). DOI: 10.15862/05SATS118
- Ye, S., Lai, X., Bartoli, I., Aktan, A.E. Technology for condition and performance evaluation of highway bridges. Journal of Civil Structural Health Monitoring. 2020. 10. Pp. 573

 –594. DOI: 10.1007/s13349-020-00403-6
- Su, M., Wang, J., Peng, H., Cai, C.S., Dai, G.L. State-of-the-art review of the development and application of bridge rotation construction methods in China. Science China Technological Sciences. 2021. 64. Pp. 1137–1152. DOI: 10.1007/s11431-020-1704-1
- 8. Patent US no. 3349418 A,1965.
- 9. Beyer, Ye., Wintergerst, L. New bridge storage, new pillar shape. Der Bauingenleur. 1960. 35(6). Pp. 227-230.
- 10. Huang, W., Pei, M., Liu, X., Wei, Y. Design and construction of super-long span bridges in China: Review and future perspectives. Frontiers of Structural and Civil Engineering. 2020. 14. Pp. 803-838. DOI: 10.1007/s11709-020-0644-1
- 11. SHul'man S.A., Sluckaya M.N., Dvorkin N.Ya., Sovershaev I.V., Ivanov S.A., Antonov A.N. Opornaya chast' mosta [Bridge support]. Patent Russia no. 202383, 2021.
- Sitnikov S.L., Sitnikov A.S. Opornaya chast' mosta i sposob ee izgotovleniya (Nesushchaya chast' mosta i sposob ee izgotovleniya) [Bridge support part and method of its manufacture (Bearing part of the bridge and method of its manufacture)]. Patent Russia no. 2731300, 2018.
- Vasilev, A.P., Struchkova, T.S., Okhlopkova, A.A. Effects of Complex Fillers on the Mechanical and Tribological Properties of Polytetrafluoroethylene Composites. Materials Science Forum. 2020. 992. Pp. 739–744. DOI: 10.4028/www.scientific.net/MSF.992.739
- 14. Balyakin, V.B., Khatipov, S.A. Pilla, C.K. Experimental studies of tribotechnical characteristics of radiation-modified PTFE to use in rotor supports. Journal of Friction and Wear. 2015. 36. Pp. 346–349. DOI: 10.3103/S1068366615040030
- 15. Adamov, A.A., Kamenskikh, A.A., Nosov, Yu.O. Deformational behavior of the flat sliding layer of the spherical bearing. International Journal of Civil Engineering and Technology. 2019. 10(5). Pp. 99–107.
- 16. Eggert, H., Kauschke, W. Structural bearings. Ernst & Sohn. Berlin, 2002. 405 p.
- Xue, J., Briseghella, B., Chen, B.-C., Zhang, P.Q. Optimal Design of Pile Foundation in Fully Integral Abutment Bridge. Springer Tracts on Transportation and Traffic. 9. Developments in International Bridge Engineering. Springer. Cham, 2016. Pp. 3–16. DOI: 10.1007/978-3-319-19785-2
- Beben, D. Soil-Steel Bridges: Design, Maintenance and Durability. Springer. Cham, 2020. 214 p. DOI: 10.1007/978-3-030-34788-8
- 19. Yi, X., Du, S., Zhang, L. Composite Materials Engineering. 1. Fundamentals of Composite Materials. Springer Singapore. Singapore, 2018. 765 p. DOI: /10.1007/978-981-10-5696-3
- 20. Wang, Q.J., Chung, Y.W. Encyclopedia of Tribology. Springer New York. NY, 2013. 4139 p. DOI: 10.1007/978-0-387-92897-5
- 21. Spiridonov, A.M., Okhlopkova, A.A., Sokolova, M.D. Polymer Composite Materials Based on Ultra-High-Molecular-Weight Polyethylene Filled with Organomodified Zeolite. Polymer Science. Series D. 2020. 13(3). Pp. 311–314. DOI: 10.1134/S1995421220030181
- 22. Hatipov S.A., Cvelev V.M., Alekseev S.V. Aktual'nye voprosy proektirovaniya kosmicheskih sistem i kompleksov [Current issues in the design of space systems and complexes]. 6. Moscow: Block-Inform-Express, 2005. P. 53.
- 23. Khatipov, S.A., Artamonov, N.A. Creation of a new antifriction and sealing material based on radiation-modified polytetrafluoroethylene. Rossijskij Khimicheskij Zhurnal. 2008. 52(3). Pp. 89–96.

- Kalistratova, L.F., Mashkov, Y.K., Egorova, V.A. Calculation of X-ray Density of Amorphous—Crystalline Polymer Taking into Account Degree of Ordering of Amorphous Phase. Inorganic Materials: Applied Research. 2018. 9(4). Pp. 687–692. DOI: 10.1134/S2075113318040147
- 25. Kornopoltsev, N.V., Rogov, V.E., Lenskaya, E.V., Kornopoltsev, V.N. Development of materials and coatings based on polytetrafluoroethylene. Chemistry for Sustainable Development. 2004. 12(6). Pp. 681–686.
- 26. Hatipov S.A., Sichkar' V.P., Voronina E.N., Ivanchenko V.K., Sobolev G.P., Bruk M.A. Sposob termoradiacionnoj obrabotki izdelij iz politetraftoretilena [Method of thermoradiation treatment of products made of polytetrafluoroethylene]. Patent Russia no. 2211228, 2003.
- 27. Artamonov, N.A. Sposob radiacionno-himicheskogo modificirovaniya politetraftoretilena i materiala na ego osnove [Method for radiation-chemical modification of polytetrafluoroethylene and materials based on it]. Artamonov N.A., Hatipov S.A. Patent Russia no. 2304592, 2007.
- 28. Hatipov, S.A., Konova E.M., Artamonov N. A. Politetraftoretilen, modificirovannyj radiaciej: struktura i svojstva [Radiation-modified polytetrafluorethylene: structure and properties]. Rossijskij Khimicheskij Zhurnal. 2008. 52(5). Pp. 64–72.
- 29. Sytyj, YU.V., Chursova L.V., Hatipov S.A., Sagomonova, V.A. Properties and application of F-4RM radiation-modified fluoroplastic (polytetrafluoroethylene). Aviation Materials and Technologies. 2012. 4(25). Pp. 48–55.
- 30. Bychkov S.A., Lavrenko I.G., Nechiporenko O.YU., Mladinov S.D. Issledovanie harakteristik metalloftoroplastov razlichnyh proizvoditelej dlya elementov aviacionnyh konstrukcij Open Information and Computer Integrated Technologies. 2013. 59. Pp. 343–354.
- 31. Mashkov YU.K., Ovchar Z.N., Bajbarackaya M.YU., Mamaev O.A. Polymeric compound materials in tribotechnique. Moscow: Nedra, 2004. 262 p.
- 32. Rogov, V.Ye Gur'ev A. M., Nikiforov S.O. Metalloftoroplastovye materialy dlya mashinostroeniya: osobennosti razrabotki, proizvodstva i primeneniya [Metal fluoroplastic materials for mechanical engineering: features of development, production and application]. Polzunovskij al'manah. 2010. 1. Pp. 51–57.
- 33. Buznik V.M., Kornopol'cev V.N., Kornopol'cev N.V., Mognonov D.M., Rogov, V.Ye Sposob polucheniya bimetallicheskogo materiala [Method for producing bimetallic material]. Patent Russia no. 2277998, 2006.
- 34. Kornopol'cev V.N., Kornopol'cev N.V., Rogov, V.Ye Mognonov D.M., Greshilov A.D. Sposob polucheniya bimetallicheskogo metalloftoroplastovogo materiala [Method for producing bimetallic fluoroplastic material]. Patent Russia no. 2212307, 2003.
- Kornopol'cev V.N., Mognonov D.M., Ayurova O.Z., Buyantuev S.L. Novye tribologicheskie kompozity na osnove politetraftoretilena. Neorganicheskie materialy: prikladnye issledovaniya. 2017. 8(1). S. 108-111. DOI:10.1134/S2075113317010208
- 36. Kornopol'cev V.N. Sheet antifriction material with specified structure. Journal of Friction and Wear. 2010. 31(5). 359–363. DOI: 10.3103/S1068366610050077
- 37. Rogov, V.Ye., Bohoeva, L.A., Chermoshenceva, A.S. Reinforced composites with 3D fabric structures. Russian Engineering Research. 2021. 3. 71–74. DOI: 10.36652/0042-4633-2021-3-71-74

Information about the authors:

Lubov Bokhoeva, Doctor of Technical Sciences ORCID: https://orcid.org/0000-0001-6986-4307

E-mail: bohoeva@yandex.ru

Vitaliy Rogov, Doctor of Technical Sciences ORCID: https://orcid.org/0000-0002-2249-0827

E-mail: rogov54v@mail.ru

Anna Chermoshentseva, PhD in Technical Sciences

ORCID: https://orcid.org/0000-0003-0764-598X

E-mail: asch-13@ya.ru

Received 17.05.2022. Approved after reviewing 17.09.2024. Accepted 18.10.2024.



Magazine of Civil Engineering

ISSN 2712-8172

journal homepage: http://engstroy.spbstu.ru/

Research article UDC 624

DOI: 10.34910/MCE.131.5



Geotechnical characteristics of saline soft soils improved by chemical agents

A.M. Al-Kinani^{1 \(\infty\)}, M.Y. Fattah²

- ¹ Civil Engineering Department, University of Thi-Qar, Nassyriah, Iraq
- ² Civil Engineering Department, University off Technology Iraq, Baghdad, Iraq

□ aali-majid@utq.edu.iq

Keywords: Saline soft soils, consistency limits, chemical agents, geotechnical properties.

Abstract. Chemical stabilization is a typical method for enhancing salinity in soils. In this regard, an effort has been made to evaluate the effect of chemical substances and stabilizers of Portland cement on the geotechnical characteristics of salt soils. Due to their geologic makeup, textural characteristics, and climatic factors, the majority of the soils in the southern part of Iraq are notable for having a wide variety of formations. Because the soil particles in the saline regions of Thi-Qar governorate are encircled by molecules of chlorides, sulfates, or other salt species that function as link agents to fill in the gaps in the dry state, these soils may generally be categorized as saline soils. The sort of salt in such soil determines how it should be disposed of. The objective of this study is to investigate the effect of adding different types of salt compounds including NaCl, MgCl₂, Na₂SiO₃, and CaCl₂ with various percentages 2, 4, 8, and 10 % and Portland cement for improving the consistency limits and shear strength of saline soft soils. It was found that adding cement materials and a group of chlorides NaCl, MgCl₂, Na₂SiO₃, and CaCl₂ increased the unconfined compressive strength of the soil from 290 to 814, 506, 404, 574, and 422 kPa, respectively, and decrease the consistency limits.

Citation: Al-Kinani, A.M., Fattah, M.Y. Geotechnical characteristics of saline soft soils improved by chemical agents. Magazine of Civil Engineering. 2024. 17(7). Article no. 13105. DOI: 10.34910/MCE.131.5

1. Introduction

The sides of the Euphrates River bank are formed by fine sediments of silt or silty clay, and mud accumulating on the bank and at the top portion of the natural flood zone level, which work to obstruct the flow of the river and seem like a steep barrier. River water is diverted from the neighboring plains and utilized to build car parks and many engineering structural compounds like dams, bridges, liquefaction-pumping stations, etc. When the sides of rivers are safe and stable, the procedure of exploiting them becomes easier. If they are unstable and on the verge of collapsing, the process of exploitation is delayed. The soils along the Euphrates River bank in the southern region of Iraq were classified as saline soft soils. When the subgrade is fine soil, a tricky issue arises in civil engineering applications [1].

Many studies were conducted on the topic of soil stabilization utilizing different additives. The usual process for clayey soil stabilization is stabilization by adding lime and cement. Nevertheless, there is justification for studying inexpensive additives, which can be utilized to modify the features of soils. Any mechanical, hydrological, physicochemical, biological, or any combination of these approaches used to modify specific features of natural soil deposits is referred to as ground improvement or ground modification. The goal of ground improvement is to enhance the strength and minimize the settlement of existing soils, or to modify their permeability [2]. Saline soils are created from hydrated gypsum natural resources CaSO₄.2H₂O, SiO₂, calcite CaCO₃, or NaCl salt, which covers ground surface. When the moisture content is raised up because of capillary action and evaporation of the water from the ground, and the salinity of

water increase for these soils to the limits of sedimenting of salts because of water evaporation. So, the water table acts an essential way to the presence of salty soil [3, 4]. With a chloride salt level greater than 3%, salty soil is a highly conductive system [5]. Saline ions penetrate electric porous media with water migration and subsequently react with soil atoms [6]. The hydration range of chloride ions is likewise greater, and they can absorb water [7]. Without treatment, such filling would not fulfill the required strength and anti-deformation standards for use in construction due to physical and chemical issues, such as salt expansion, dissolution, and moisture absorption [8]. The microstructures of treated soil are affected by chloride ions, as are the strength properties [9]. In the short and long term, chloride ions have a significant impact on the strength of improved soil [10, 11].

Because the presence of significant amounts of saline indicates that the geotechnical properties of clayey soils may change in the presence of infiltrating water, engineering properties of clayey soils mixed with sodium chloride revealed that the plasticity index and unconfined compressive strength (UCS) decrease as salt content is increased [12]. The addition of chloride salt improved the structure of the lime-soil combination significantly. It increased the amount of coarse soil particles while decreasing the soil's overall surface area. The degree of homogeneity was lowered by increasing the salt level, whereas the salt amount had a linear connection with the microstructure's characteristics, such as the bone area, appearance ratio, and roundness [13]. Addition of up to 8 % calcium chloride improved lateritic soil. Calcium chloride is not convenient as an independent stabilizer but can be passable as a modifier or as an admixture in the cement stability of lateritic soil [14]. In Shatt Al-Arab Southern Iraq, the influence of salinity on the geotechnical properties of fine grain soil was investigated. Atterberg limits, standard compaction, consolidation, and soil shear strength are examples of laboratory testing. The presence of detectable amounts of dissolved salts in water can cause changes in the engineering characteristics of the soil [15].

The effect of magnesium chloride (MgCl₂) emulsion on the geotechnical properties of clay soils was evaluated by different researches. Turkoz et al. [16] explained that the increasing the MgCl₂ content decreased the soil consistency (Atterberg limits). The fact that addition of NaCl, CaCl₂, and MgCl₂ filled up the voids between particles of soil as particle size of NaCl, CaCl₂, and MgCl₂ is smaller than soil particles and can be easily replaced the voids. The compression index and swelling index were decreased with increasing the chloride compound percentage [17]. Moayedi et al. [18] studied affected of sodium silicate system binders of the physicochemical characteristics of the soft soil. It was conducted a number of batch tests. According to the results, adding 3 mol/L of Na₂SiO₃ may raise the UCS of soil in group testing by up to 220 % of its baseline strength, while adding activators CaCl₂ and/or Al₂(SO₄)₃ can boost UCS values by up to 270 %. Additionally, adding CaCl2 at greater concentrations (such as 1 mol/l) had no appreciable impact on the UCS findings. The objective of this study is to investigate the effect of adding different types of salt compounds including NaCl, MgCl₂, Na₂ SiO₃, and CaCl₂ with various percentages 2, 4, 8, and 10 % and Portland cement for improving the consistency limits and compressive strength of saline soft soils. The methodology of this study includes: First, collecting soil from the study area and conducting a series of conventional tests to know its geotechnical properties. Second, mixing the natural soil with a variety of salts each added with different percentages as demonstrated in experimental work section to obtain saline soil samples. Third, testing the samples. Finally, analyzing the obtained results.

2. Methods

2.1. Salinity's Impact on the Physical Properties of Soils

The invading water also has a tendency to flow into the voids between the platelets due to the relatively higher concentration of ions close to the platelet, which causes the platelets to become further separated. When there is too much space between the platelets, dispersion takes place, which results in the platelets being carried away by the flowing water and perhaps getting stuck in big soil pores, further reducing the rate of absorption. The top layer of soil may expand and become saturated if water cannot get through it. Sodium has the opposite effect of salinity on soils. The primary physical processes associated with high sodium concentrations are soil dispersion and clay platelet and aggregate swelling. The forces that bind clay particles together are disrupted when too many large sodium ions come between them. When this separation occurs, the clay particles expand, causing swelling and soil dispersion. So, the hydraulic conductivity of the soil is impacted by soil dispersion in addition to reducing the quantity of water that enters the soil. Hydraulic conductivity describes how quickly water enters the subsoil. For instance, soils with welldefined will have a lot of microspores, fractures, and fissures that allow water to move through the soil very quickly. The hydraulic conductivity is also decreased when sodium-induced soil dispersion causes the degradation of soil structure. Hanson et al. [20] explained that the soil dispersion causes clay particles to plug soil pores, resulting in reduced soil permeability. Their ion layers tend to overlap as two platelets get close to one another, and electrical repulsive forces emerge as a result of positively charged clay particles having charged ions "attached" to them make an effort to repel one another.

The clay platelets are often kept apart with forces, resulting in the swelling of the soil. When soil is repeatedly wetted and dried, and clay dispersion occurs, it then reforms and solidifies into almost cement-like soil with little or no structure. The three main problems caused by sodium-induced dispersion are reduced infiltration, reduced hydraulic conductivity, and surface crusting. Salts that contribute to salinity, such as calcium and magnesium, do not have this effect because they are smaller and tend to cluster closer to clay particles as shown in Fig. 1. Calcium and magnesium will generally keep soil flocculated because they compete for the same spaces as sodium to bind to clay particles. Increased amounts of calcium and magnesium can reduce the amount of sodium-induced dispersion. Because sodium ions are less attracted to the platelets than are calcium ions, the layer of sodium ions extends further from the platelet, thus increasing the separation distance between adjacent platelets and inducing more swelling. Calcium ions are more strongly attracted to the platelets, and as a result, the ion layer does not extend as far from the platelets compared with sodium ions. This means a smaller separation distance between platelets and less swelling of the soil. Thus, replacing exchangeable sodium with calcium can reduce swelling and improve infiltration.

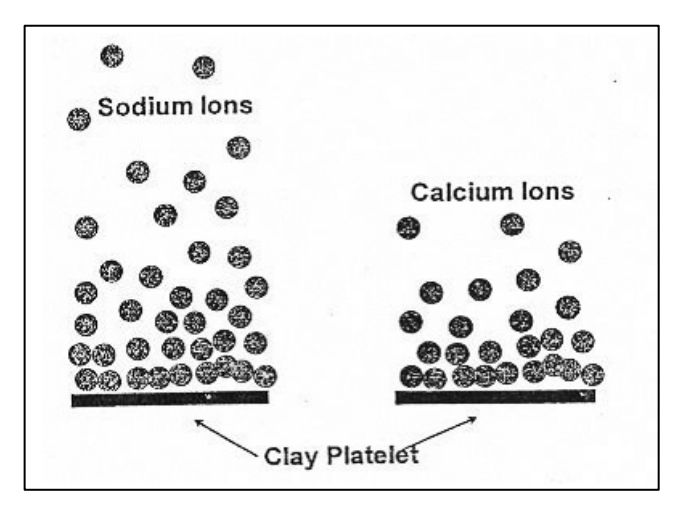


Figure 1. Behavior of sodium and calcium attached to clay particles [21].

2.2. Geotechnical Properties of the Study Area

Grayish silty clay soils were brought from south of Iraq representing a generally typical soil in the saline area at Southern Iraq. Disturbed soil samples were collected from a depth of 0.5–1 m from Al-Nasiriyah city located in the southern part of Iraq (Coordinate: Latitude = 628069, Longitude = 3427088). The study area was chosen to be between the bank of Euphrates River and the public estuary project that is considered one of the major development projects in Iraq due to its importance in transporting saline water for messages from the reclamation of agricultural lands in Central Iraq as shown by the blue mark in Fig. 2. This site has a high potential for increasing the salinization because of the drought exposed in the area. According to the standard specification ASTM D 2487-11 [21], the soil can be classified as ML (Fine grained soil). Geotechnical and chemical tests were conducted after transferring the samples to the laboratories of Civil Engineering Departments in the College of Engineering at the University of Thi-Qar. Table 1 summarizes the basic geotechnical properties of the natural soil and chemical properties.



Figure 2. Satellite image of the location of the test points for samples extraction.

Table 1. The geotechnical properties of the tested soil.

Soil property	Value	Specifications
D ₁₀ (mm)	< 0.0007	
D ₃₀ (mm)	0.0022	
D ₅₀ (mm)	0.0037	ASTM D422 [22]
D ₆₀ (mm)	0.0047	
Liquid limit, LL (%)	49	ASTM D4318 [22]
Plastic limit, PL (%)	38	ASTM D4318 [22]
Plasticity index, PI (%)	11	
Specific gravity, GS	2.65	ASTM D854 [22]
Maximum dry unit weight, γd max (g/cm³)	1.61	ASTM 698 [22]
Optimum water content (%)	20	
Undrained shear strength of the natural soil, c_u (kPa)	28	A CTM D0466 (00)
Undrained shear strength after compaction (kPa)	145	ASTM D2166 [22]
CI (%)	1.5	
Organic matter, OM (%)	6.78	
Total dissolved salts, TDS (%)	9.2	DC 4277 [22]
SO₃	4.1	BS. 1377 [23]
Gypsum content (%)	9.3	
рН	8.41	

3. Results and Discussion

The laboratory tests of the soil samples began immediately after receiving the samples in the laboratory. The tests were conducted in the College of Engineering, Thi-Qar University laboratory. Subsequent laboratory tests were executed to determine the physical and engineering properties of disturbed soil samples. All tests on the site have a high potential for increasing salinization because of the drought that exposed the area.

3.1. Compaction Test

The Proctor compaction test was carried out to determine the moisture content–dry density relationship according to ASTM (D 698) [22]. The soil was compacted into 937 cm³ mold in 3 layers. Fig. 3 shows the dry density–moisture content relation for the soil and preparation of proctor compaction.

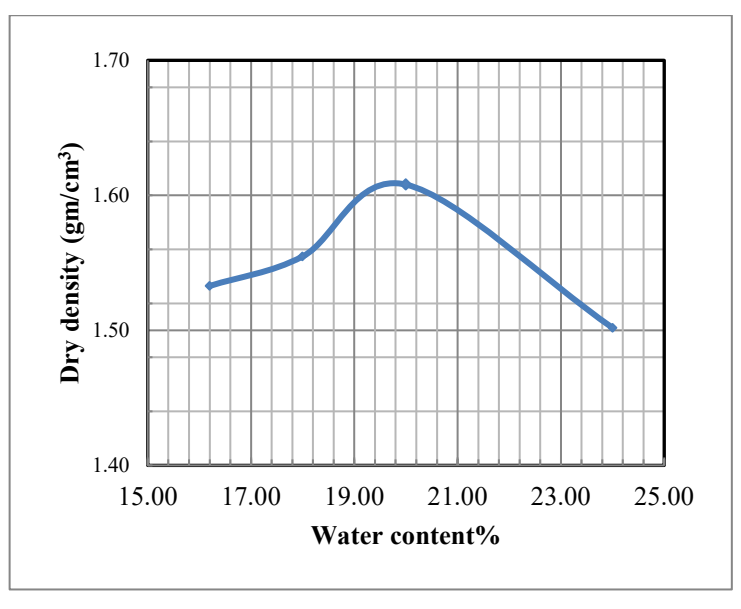


Figure 3. Results of compaction test.

3.2. Atterberg Limits

The liquid limit test has been accomplished using the Cassagrande apparatus according to ASTM D423-66 [21]. The plastic limit test was conducted according to the ASTM D 424-59 [21]. The chloride

compounds (NaCl, MgCl $_2$.6H $_2$ O, CaCl $_2$.2H $_2$ O, and Na $_2$ SiO $_3$) were dissolved in water and mixed with soil. These tests were carried out to investigate the effect of addition of salt on the consistency limits. Fig. 4 shows the effect of additive content on the Atterberg limits. The figure shows that the increase in additive content decreases the liquid limits for all additives. While in the case of the plastic limits, there was a fluctuation in the soil behavior and a decrease in the values of the plastic limits by adding additives, although there was a significant increase with the addition of Portland cement.

On the other hand, the all-values of plasticity index decrease with adding the additive. The dissolution of salts in water and soil leads to a change in their physicochemical properties. Changes in its physical and chemical properties as a result of the different interactions between the exchange complex and the soil solution, which lead to a change in the composition and concentration of the soil solution. The behavior of the soil with saline water depends on its physical properties at the beginning and on the adsorption capacity of ions, which in turn affect its hydrophysical properties. The initial chemical composition of the soil affects the ion exchange processes during contact of water with the soil. In addition to the accumulation of some elements, especially sodium, which leads to the deterioration of soil construction and a decrease in the movement of water and air. Finally, the amount of salt causes flocculation and agglomeration of soil particles, which results in a reduction in liquid limit. The results show that when the salinity of the pore media increases, the soil's liquid and plastic limits decrease. These results are consistent with the findings of Shariatmadari et al. [22] and Yukselen-Aksoy et al. [23].

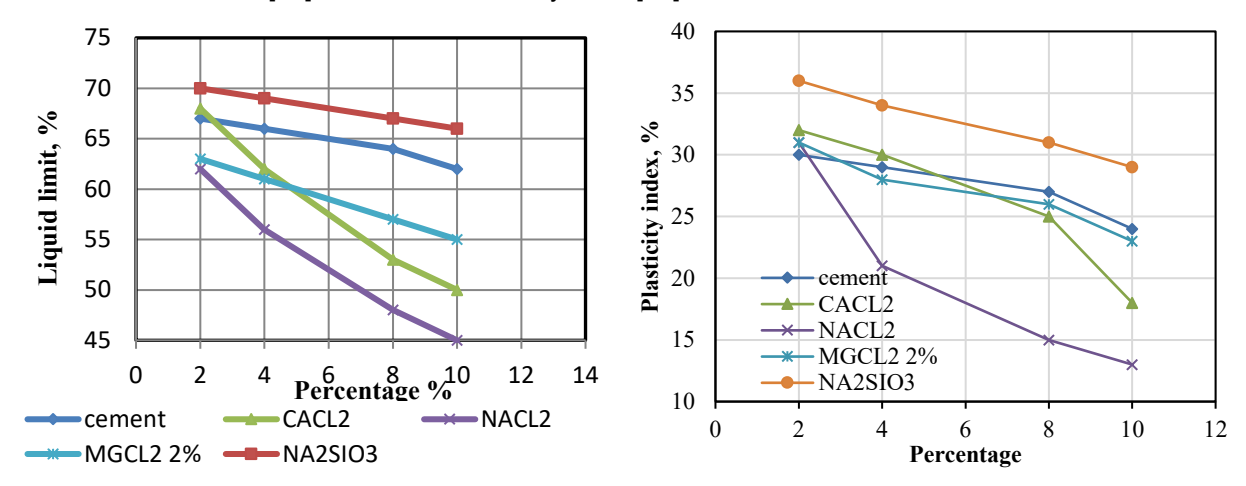


Figure 4. Consistency limits of salinity soil under different percentage of additives.

3.3. Shear Strength Results

The shear strength of soils treated with additives was investigated using UCS testing. To obtain the highest dry unit weight and optimum water content, the sample was compacted into three layers using the Harvard miniature compaction device. The compacted specimen's diameter was 33 mm and 70 mm in length. The results of the undrained shear strength were treated by adding (Portland cement, NaCl, MgCl₂.6H₂O, CaCl₂.2H₂O, and sodium silicate) under different percentages of additives (0, 2, 4, 8, and 10)% are shown in Table 2.

	Unconfined compressive strength, UCS (kPa)						
Additive, %	Natural compacted soil	NaCl	MgCl ₂ .6H ₂ O	CaCl ₂ .2H ₂ O	Portland cement	Na ₂ SiO ₃	
0				290			
2		282	404	422	682	574	
4	290	506	316	352	814	518	
8		484	206	304	582	422	
10		200	208	250	506	326	

Table 2. The undrained shear strength results for different chemical agents.

Portland cement was added at 0, 2, 4, 8, and 10 %, respectively, to the natural clay soil and obtained UCS as shown in Fig. 5. According to the UCS test, the UCS increased as the percent of common cement increased. However, it was discovered that when ordinary cement was mixed with 8 and 10 % of cement mixing, the results were unsatisfactory due to the absence of bonding between the cement and the soil.

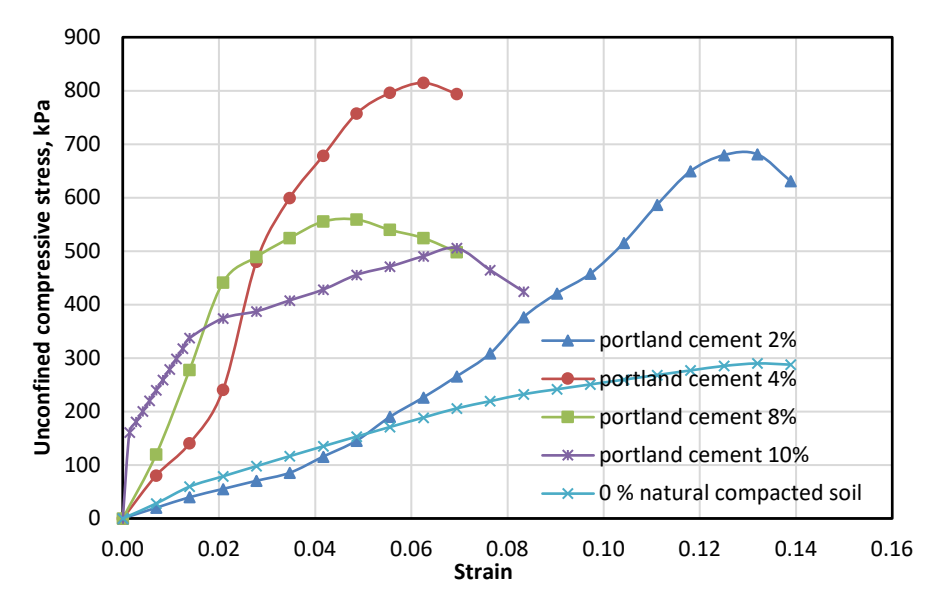


Figure 5. Unconfined shear strength of soil treated with several percentage of Portland cement.

Soil can also be stabilized by chemical stabilization. Sodium chloride is the ionic compound of sodium and chloride. The results show that sodium chloride can be effectively dissolved in water quickly and provide enough sodium ions for exchange ionic reactions with clayey soil. The function of this chemical (sodium chloride) is to form a cluster of fine particles and bind them together. The sodium chloride dosage is added in 2, 4, 8, and 10 % by weight of soil. The UCS increases from 290 to 506 kN/m² upon the addition of 4 % sodium chloride. However, it was discovered that when sodium chloride was mixed with 8 and 10 % of salt mix, the results showed a decrease in the undrained shear strength as shown in Fig. 6.

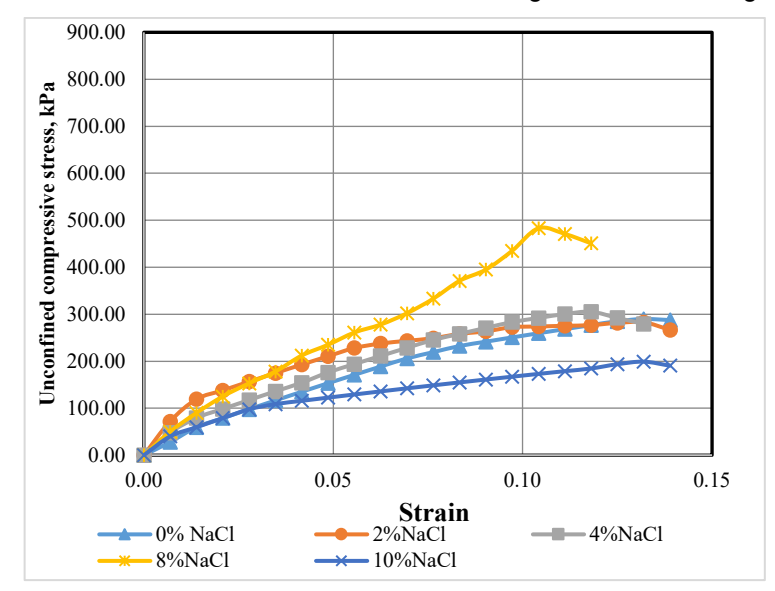


Figure 6. Strength test results for soil under different percentage of sodium chloride.

An inorganic salt called calcium chloride is created as a by-product of making sodium carbonates. The property of calcium chloride is hygroscopicity. This is how calcium chloride attracts and absorbs water. Both temperature and relative humidity influence this. When exposed to its own moisture, it could liquefy very fast. Conversely, calcium chloride has a lower freezing point than water and a higher surface tension. Saylak et al. [25], demonstrated that the significant water-absorbing capacity of solid calcium chloride. Solid CaCl₂ can absorb 16.6 times its water weight at a relative humidity of 95 %. Even at a 30 % humidity condition, it can absorb approximately all of its own weight of water. Because it may change the strength, compressibility, and permeability of materials, calcium chloride has been utilized as a stabilizer. Essentially, the purpose of this chemical is to bind and aggregate small particles. So that the soil's UCS increases to 422 kN/m² when 2 % calcium chloride is added. Nevertheless, it was noted that the results showed a reduction in UCS when calcium chloride was mixed with 4, 8, and 10 % of the salt mix as shown in Fig. 7.

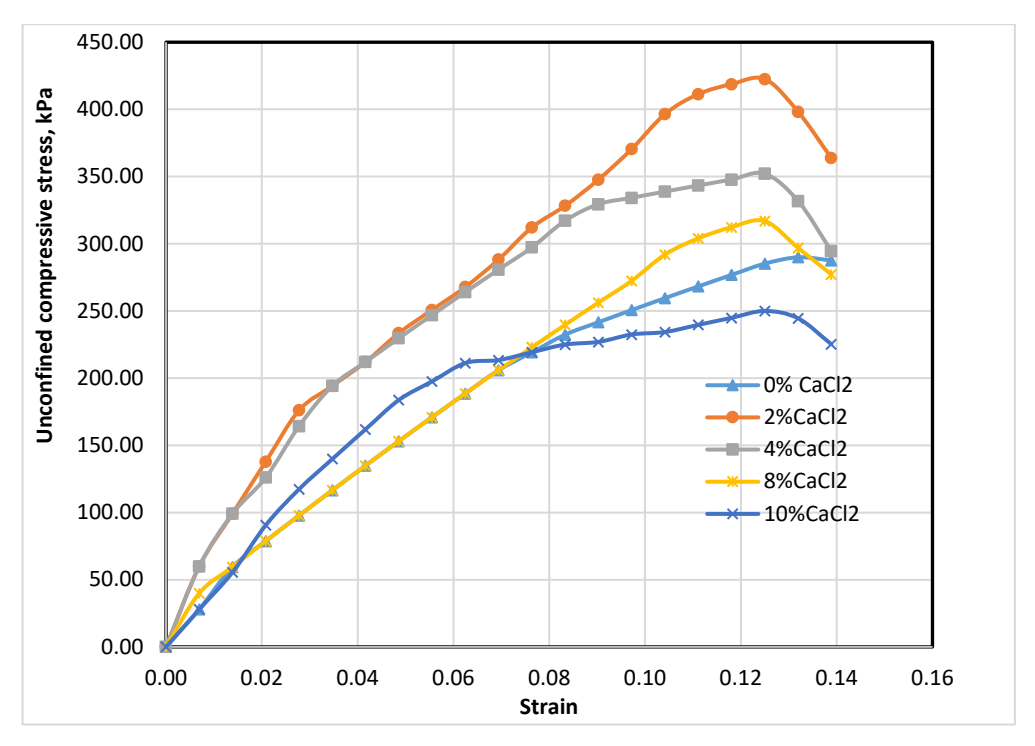


Figure 7. Strength test results for soil under different percentage of calcium chloride.

Bischofite, also known as "magnesium chloride hexahydrate" (MgCl₂.6H₂O), is a non-traditional stabilizer that has lately attracted the attention of researchers. Magnesium chloride is a sea salt that is used as a green stabilizer since it does not hurt plants or animals and does not corrode asphalt, concrete, pavements, or cars. On the other hand, magnesium holds an atomic number of 12, and its electronic configuration is 2, 8, 2. Thus, it has two more electrons than the closest stable electronic configuration of a noble gas, neon. As a result, magnesium tends to lose two electrons from its outermost shell and obtains a stable electronic configuration, resulting in magnesium cation (Mg $^{+2}$) as shown in Fig. 8. When a magnesium atom joins two chlorine atoms, two electrons are transferred from the magnesium to the chlorine, resulting in a magnesium chloride molecule. Thus, both atoms have a stable octet electronic configuration.

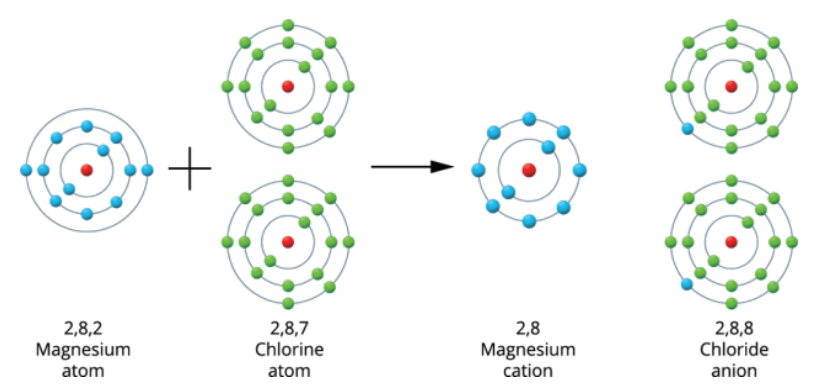


Figure 8. Ionic bond formation in magnesium chloride.

When 2 % magnesium chloride is added to soil, the UCS increases to 404 kN/m². However, it was discovered that when magnesium chloride was mixed with 4, 8, and 10 % of salt mix, the results showed a decrease in UCS as shown in Fig. 9.

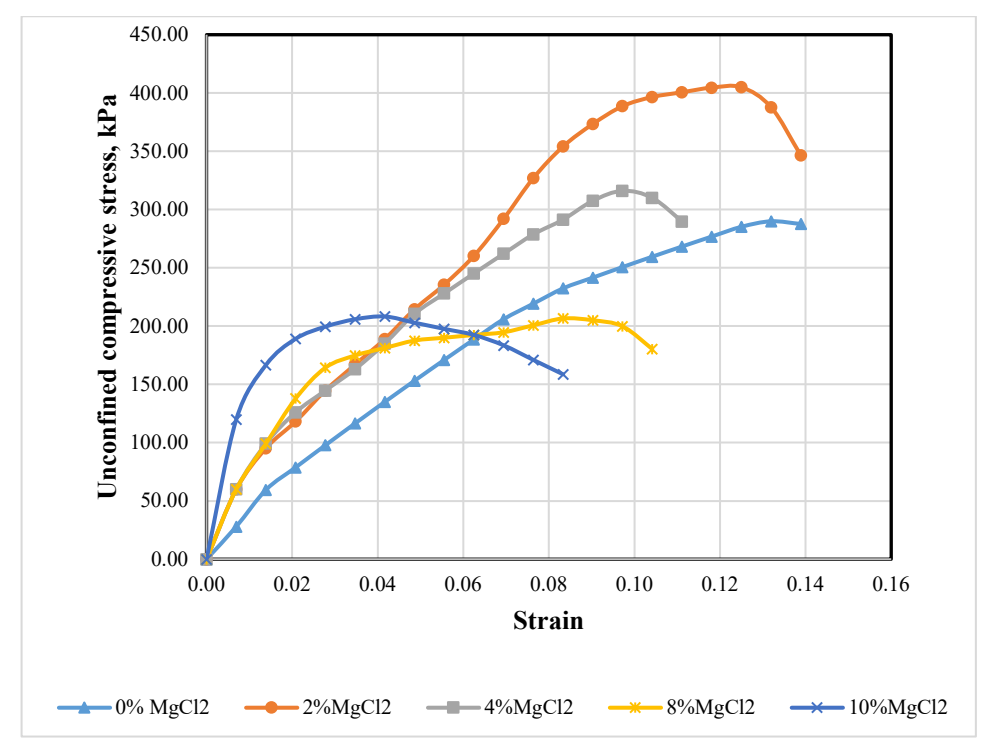


Figure 9. Strength test results for soil under different percentage of magnesium chloride.

Sodium silicates are inorganic, polymeric, alkaline silica-based materials. All silicates are made of three basic components: silica (SiO₂) for which sand is the raw material, alkali (Na₂O or K₂O) for which soda ash or potash is the raw material and water. The researcher discovered that when 2 % of sodium silicates was added to soil, the UCS increases to 574 kN/m². However, it was discovered that when magnesium chloride was mixed with 4, 8, and 10 % of salt mix, the results showed a decrease in UCS as shown in Fig. 10.

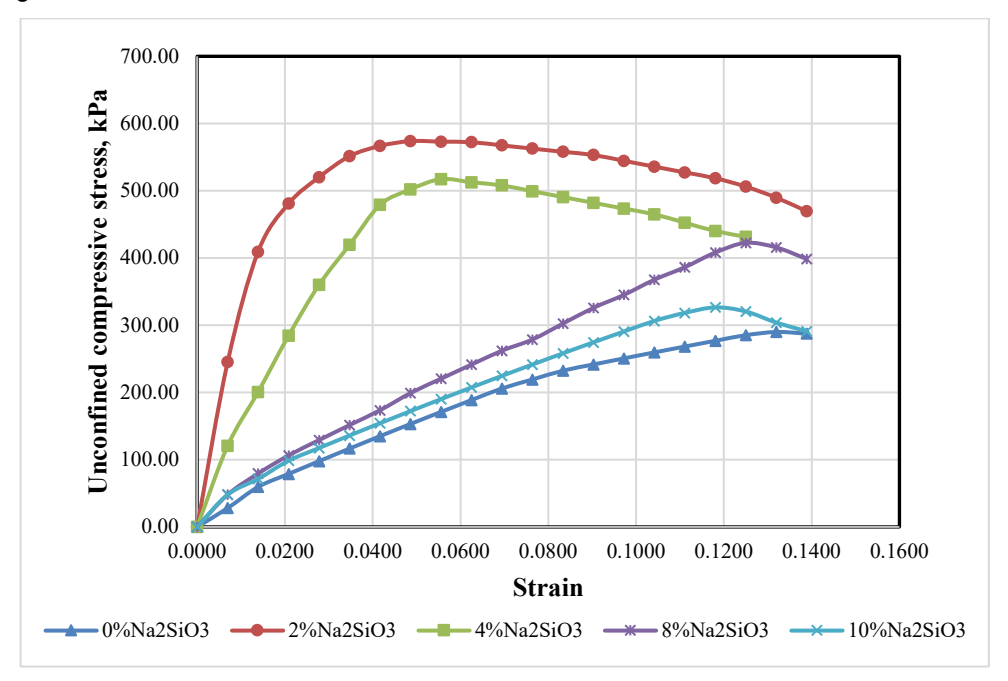


Figure 10. Strength test results for soil under different percentage of sodium silicates.

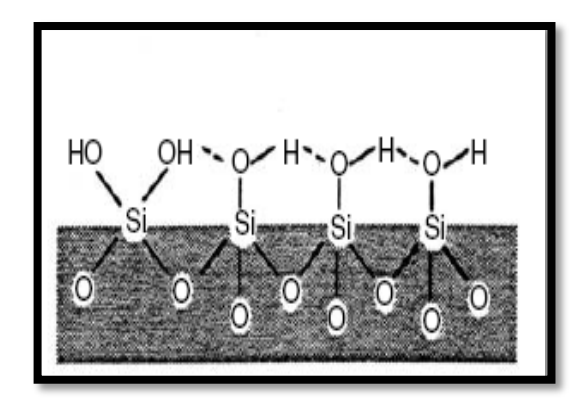
Fattah et al. [26] stated that soils located above the groundwater table are generally unsaturated and possess negative pore-water pressures. Soil suction is one of the most important parameters describing the moisture condition of unsaturated soils. They concluded that the suction increases with the decrease of the degree of saturation. The sodium silicate contains the groups called "silanol", which may be found not only on the surface of colloidal but also within the structure of colloidal particles. The silicate attraction with water increases the hydroxide ions on the surface and within the silanol as shown in Fig. 11. The remaining (OH) experiences very weak hydrogen bonding, while if the proportion of water is low then the

result will be more proportion of sodium hydroxide on silanol surface and an increase in the negative charge on the silica so high strength develops due to adhesion with soil particles.

The sodium silicate concentration effect on bonding because there are three conditions and the typical forms of the strength curve of silica concentration as illustrated in Fig. 12. The first case, if the concentration of silica is too high and drying the silica gel is by hydration of water, then the bridges crack and become weak as in Fig. 12a. The second case, when the colloidal silicate is too small in concentration, the refractory particles come together and approximate close packing, but there is no enough colloidal silicate to fully reinforce all the contact positions as in Fig. 12b. The third case is when the colloidal silicate is in optimized concentration, the refractory particles attain close packing and colloidal reaches its gel concentration simultaneously as in Fig. 12c. Therefore, if water quantity is small or dehydrated from silica or evaporated, two things will happen:

- The colloidal silica concentration will increase.
- The volume of the system will decrease.

So, when we use sodium silicate ratio more than 10 %, the soil sample becomes softer and cannot be molded, so we thank that this ratio of silicate is adequate for this purpose.



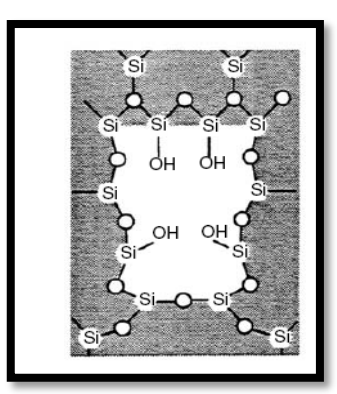
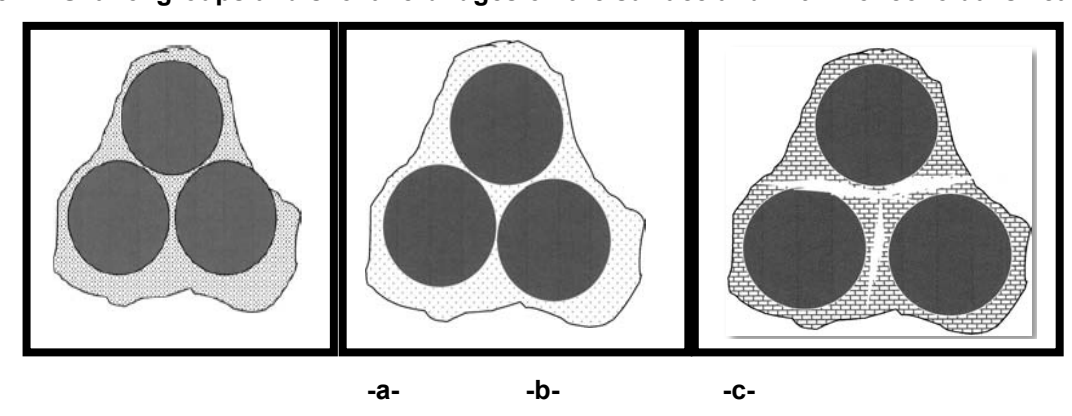


Figure 11. Silanol groups and siloxane bridges on the surface and within of colloidal silicate [28].



- a. Colloidal silica concentration too high
- b. Colloidal silica concentration too small
- c. Colloidal silica at optimum concentration

Figure 12. Bond strength of colloidal silica in solution [28].

For comparison of UCS of salinity soils after treated and natural soil were expressed in percent ratio of (qu(improved)/qu(natural)), the results are illustrated in histograms as shown in Fig. 13 for various percentages 2, 4, 8, and 10 %.

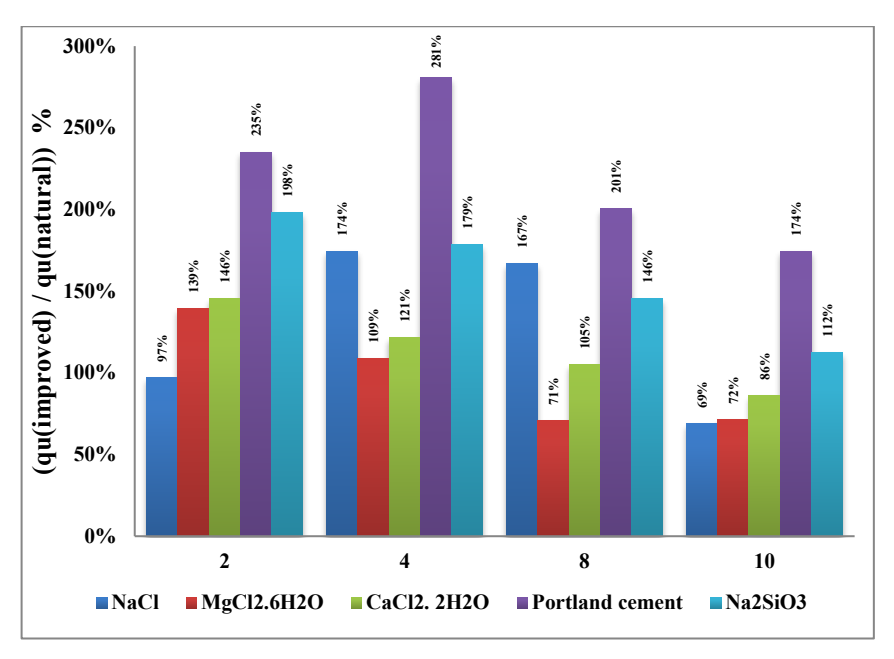


Figure 13. Strength improvement percent in saline clayey soil.

When comprising the results obtained unconfined compressive strength of salinity soils after treated and natural soil were expressed in percent ratio of (qu(improved)/qu(natural)) as illustrated above, it is possible to state that:

- NaCl varied considerably to 174 % for adding 4 % and the decreasing to 69 % at 10 %.
- MgCl₂.6H₂O varied considerably to 139 % for adding 2 % and the decreasing to 69 % at 8 %.
- CaCl₂.2H₂O varied considerably to 146 % for adding 2 % and the decreasing to 86 % at 10 %.
- Na₂SiO₃ varied considerably to 198 % for adding 2 % and the decreasing to 112 % at 10 %. Portland cement varied considerably to 281 % for adding 4 % and the decreasing to 174 % at 10 %.

4. Conclusions

To investigate the effect of different types of salts on geotechnical characteristics, different concentrations of salts (0, 2, 4, 8, and 10 %) were added to the soil. The most important conclusions were as follows:

- As salinity has risen, shear strength parameters increased. The growth of salt crystals in soil
 pores, as well as the location of the cement, have all been ascribed to an increase in
 attractive forces between soil particles, the establishment of adhering between them, and
 the development of attractive forces between soil particles. In the case of the low proportion
 of clay in the soil, a tiny portion of these changes is due to a reduction in the thickness of the
 double layer.
- Increasing the salt content of the soil by more than 10% has a negative impact on the shear strength of the soil.
- Generally, sodium silicate and Portland cement mostly act as active stabilizers because of their ability to alter material properties, such as strength. Essentially, the act of this chemical is to lump fine particles together and join them together.
- Adding any of the chemicals (NaCl, MgCl₂.6H₂O, CaCl₂.2H₂O, Na₂SiO₃, and Portland cement) decreased the liquid limit, plastic limit, and plasticity index of the salinity soil.

References

- 1. Fattah, M.Y., Baqir, H.H., Al-Rawi, O.F. Field and Laboratory Evaluation of A Soft Clay Southern Iraq. 4th Jordanian Civil Engineering Conference. Amman, 2006. Pp. 28–30.
- 2. Fang, Hsai-Yang, Daniels, John L. Introductory Geotechnical Engineering. CRC Press. London, 2017. 576 p. DOI: 10.1201/9781315274959
- 3. Abu-Taleb, M.G., Egeli, I. Some Geotechnical Problems in the Eastern Province of Saudi Arabia. Proceedings, Symposium on Geotechnical Problems in Saudi Arabia. Riyadh, 1981. 2. Pp. 799–811.

- Johnson, H.S., Kamil, M.R., Pierson, G.O., Ramsay, J.B. Sabkhas of Eastern Saudi Arabia. Quarterly Period in Saudi Arabia. Springer. Berlin, 1978. Pp. 84–93.
- 5. Jiang-Beng, G.A.O., Yong-Gang, Y.U. Research progress in engineering and mechanical properties of the saline soil. Mechanics in Engineering. 2011. 33(4). Pp. 1–7.
- Koniorczyk, M. Salt transport and crystallization in non-isothermal, partially saturated porous materials considering ions interaction model. International Journal of Heat and Mass Transfer. 2012. 55(4). Pp. 665–679. DOI: 10.1016/j.ijheatmasstransfer.2011.10.043
- 7. Flatt, R.J. Salt damage in porous materials: how high supersaturations are generated. Journal of Crystal Growth. 2002. 242(3–4). Pp. 435–454. DOI: 10.1016/S0022-0248(02)01429-X
- 8. GB 50021-2001. Code for investigation of geotechnical engineering. 2009.
- 9. Modmoltin, C., Voottipruuex, P. Influence of salts on strength of cement-treated clays. Proceedings of the Institution of Civil Engineers-Ground Improvement. 2009. 162(1). Pp. 15–26. DOI: 10.1680/grim.2009.162.1.15
- 10. Calvello, M., Lasco, M., Vassallo, R., Di Maio, C. Compressibility and residual shear strength of smectitic clays: influence of pore aqueous solutions and organic solvents. Italian Geotechnical Journal. 2005. 1. Pp. 34–46.
- De Carteret, R., Buzzi, O., Fityus, S., Liu, X. Effect of Naturally Occurring Salts on Tensile and Shear Strength of Sealed Granular Road Pavements. Journal of Materials in Civil Engineering. 2013. 26(6). Pp. 1–13. DOI: 10.1061/(ASCE)MT.1943-5533.0000938
- 12. Rahil, F.H., Al-Soudany, K.Y., Abbas, N.S., Hussein, L.Y. Geotechnical Properties of Clayey Soils Induced by the Presence of Sodium Chloride. IOP Conference Series: Materials Science and Engineering. 2019. 518(2). Article no. 022064. DOI: 10.1088/1757-899X/518/2/022064
- 13. Li, M., Chai, S., Du, H., Wang, C. Effect of chlorine salt on the physical and mechanical properties of inshore saline soil treated with lime. Soils and Foundations. 2016. 56(3). Pp. 327–335. DOI: 10.1016/j.sandf.2016.04.001
- 14. Sani, J.E., Etim, R.K., Joseph, A. Compaction Behaviour of Lateritic Soil-Calcium Chloride Mixtures. Geotechnical and Geological Engineering. 2019. 37. Pp. 2343–2362. DOI: 10.1007/s10706-018-00760-6
- Al-Obaidi, A., Ihssan, A., Allawi, H. Studying of the combined salts effect on the engineering properties of clayey soil. MATEC Web of Conferences. 2018. 162(2). Article no. 01011. DOI: 10.1051/matecconf/201816201011
- 16. Türköz, M., Savaş, H., Acaz, A., Tosun, H. The effect of magnesium chloride solution on the engineering properties of clay soil with expansive and dispersive characteristics. Applied Clay Science. 2014. 101. Pp. 1–9. DOI: 10.1016/j.clay.2014.08.007
- 17. Afrin, H. Stabilization of Clayey Soils Using Chloride Components. American Journal of Civil Engineering. 2017. 5(6). Pp. 365–370. DOI: 10.11648/j.ajce.20170506.18
- 18. Moayedi, H., Huat, B.B.K., Moayedi, F., Asadi, A., Parsaie, A. Effect of Sodium Silicate on Unconfined Compressive Strength of Soft Clay. Electronic Journal of Geotechnical Engineering. 2011. 16. Pp. 289–295.
- 19. Hanson, B., Grattan, S., Allan, F. Agricultural Salinity and Drainage. University of California. University of California Irrigation Program, Davis, 1999. 160 p.
- 20. Annual Book of ASTM Standards 2021. American Society for Testing and Materials. USA, 2021. 1685 p.
- 21. BS 1377-2: Methods of test for soils for civil engineering purposes Classification tests and determination of geotechnical properties. British Standarts Institution, 1990.
- 22. Aljanabi, K.R., Abdullah, B.M. Effects of inorganic salt solution on some properties of compacted clay liners. Journal of Engineering Science and Technology. 2017. 12(12). Pp. 3188–3202.
- 23. Yukselen-Aksoy, Y.A.K., Ören, A.H. Seawater effect on consistency limits and compressibility characteristics of clays. Engineering Geology. 2008. 102(1–2). Pp. 54–61. DOI: 10.1016/j.enggeo.2008.07.005
- 24. Saylak, D., Mishra, S.K., Shon, C.S. Fly ash-calcium chloride stabilization in road construction. Transportation Research Record. 2008. 2053(1). Pp. 23–29. DOI: 10.3141/2053-04
- 25. Bergna, H.E. Colloid Chemistry of Silica: An Overview. Surfactant Science Series. 2006. 131. Pp. 9-35.
- 26. Fattah, M.Y., Yahya, A.Y., Al-Hadidi, M.Th., Ahmed, B.A. Effect of salt content on total and matric suction of unsaturated soils. European Scientific Journal. 2013. 9(9). Pp. 228–245.
- Roberts, W.O. Manufacturing and Applications of Water-borne Colloidal Silica. Surfactant Science Series. 2006. 131. Pp. 131– 175.

Information about the authors:

Ali Majid Al-Kinani,

E-mail: aali-majid@utq.edu.iq

Mohammed Y. Fattah, PhD E-mail: myf 1968@yahoo.com

Received 29.11.2022. Approved after reviewing 12.07.2023. Accepted 02.08.2024.



Magazine of Civil Engineering

ISSN 2712-8172

journal homepage: http://engstroy.spbstu.ru/

Research article UDC 628.1/3

DOI: 10.34910/MCE.131.6



Improving the efficiency of cleaning metal pipes of the sewerage system of the city of Yerevan

G. Chibukhchyan 🖾, H. Chibukhchyan 👵

National Polytechnic University of Armenia, Yerevan, Armenia

☑ hovhannesch@gmail.com

Keywords: pipeline, sewerage, restoration, cleaning, ultrasonic vibrations, magnetostrictive transducer, small-sized, power

Abstract. About 2,200 km³ of wastewater is discharged into the environment annually: municipal (including households), industrial and agricultural (including drainage water) - at the same time, as indicated in the UN World Report on the State of Water Resources for 2023. Over the past 40 years, global water use has been increasing by about 1 % per year and is expected to grow at this rate until 2050 as a result of the combined impact of factors, such as population growth, socio-economic development and climate change consumption patterns. With increasing consumption of water resources, the volume of their pollution increases, which creates serious environmental, economic and social problems. In this regard, the preservation of water and food security through sustainable management of water resources, universal quality provision of water supply and sanitation services are global problems all over the world and require an integrated approach involving government agencies, private business, academia and public organizations. The water supply and sewerage industry has an extremely important social character, as it directly affects the health of the population and the environment. This requires the use of new effective environmentally friendly technologies for cleaning blockages and improving the mechanical characteristics of sewer pipelines, which will significantly increase their service life and reduce repair costs. The conducted studies have proved the effectiveness of using small-sized ultrasonic devices with an ultrasonic generator with a power of 0.1–10 kW, a frequency of 20–40 kHz, and a magnetostrictive transducer.

Funding: This work was supported by the Higher Education and Science Committee of RA (Research project no. 22YR-2D040)

Citation: Chibukhchyan, G., Chibukhchyan, H. Improving the efficiency of cleaning metal pipes of the sewerage system of the city of Yerevan. Magazine of Civil Engineering. 2024. 17(7). Article no. 13106. DOI: 10.34910/MCE.131.6

1. Introduction

Modern urban sewerage is a complex engineering system, the function of which is the purification and subsequent discharge of wastewater generated in populated areas. Currently, there are no precise criteria to assess the condition of sewer networks and the potential hazards associated with the destruction of their structures, depending on the nature and extent of damage. The creation of a centralized sewerage and water supply system for large cities and megacities in many countries of the world has become a good and effective tool for solving problems arising from the vital activity of the urban population and eliminating their environmental consequences. It is obvious that sewage systems do not last forever, and the service life of sewer pipelines is often much shorter than the design one due to errors made during the construction and operation of networks [1]. The destruction of sewage pipelines annually causes billions of dollars in damage to the economies of developed and developing countries [2]. These are not only large financial costs to eliminate their consequences but also social and moral costs.

In modern cities, the sewage system of both the residential and industrial sectors is constantly experiencing very high loads and often large natural overloads. This leads to the accumulation of large amounts of silt and plaque of various compositions on the inner surfaces of the pipes, which gradually reduces their throughput. All this can cause the waste to stop flowing from various structures and subsequently lead to a complete shutdown of the entire system, which means serious environmental consequences. In order to avoid more complex blockages and emergencies in residential areas and industrial sectors of the city and to ensure the normal functioning of the sewer system, it is necessary to carry out its regular preventive cleaning [3].

It is widely known that as a result of human activity and various technological processes, large amounts of waste and products are generated that are not suitable for further use. For their disposal, relatively expensive technologies and means are generally not used, but are simply disposed of by draining them through networks of city sewer pipelines. This leads, in relatively short periods of time, to the rapid formation of oil and salt deposits on their walls, the thickness of which constantly increases over time, as a result of which, as can be seen in Fig. 1, the pipeline section is partially or completely clogged [4–8].





Figure 1. Partially or completely clogged sewer pipes [4-8].

In Armenia, the water supply and sewerage system are serviced by CJSC "Veolia Jour" (a subsidiary of the French firm Veolia Generale des Eaux) and is a single operator of water supply and drainage in Yerevan and several other regions of Armenia for the period 2016–2031, the company serves 45 cities and more than 350 settlements. The drainage and sewerage system consists of 2,945 km of sewer network, 6 treatment plants, 350 km of surface and rainwater drainage system. More than 55 % of the total length of the pipelines of existing water pipelines was built more than 30 years ago. As a result, losses during their operation amount to almost 70 % of the total volume of supplied water. Currently, many engineering communications and structures of water supply and sewerage systems are in a pre-emergency condition. Sewer collectors and more than 60 % of the total length of network sewer pipelines are also in a preemergency state. Since 2000, the Armenian government has begun to pay serious attention to the restoration and development of municipal water supply with the involvement of private entrepreneurs and international investments. The total length of the sewerage system in Yerevan is more than 1,700 km. More than 60 % of the sewerage network in Yerevan requires urgent repair and replacement. In 2022, 5,954 m of the sewer network were reconstructed and repaired. In December 2023 alone, the company carried out 4,035 cleaning operations throughout the republic to eliminate blockages in sewer pipes, of which 863 times in Yerevan, repair and construction work was carried out on 754 m, in Yerevan 222 m1.

As a result of blockages of sewer pipes, every year only in Yerevan, a large number of works are carried out to flush and eliminate blockages, which cost consumers large financial and moral losses. Only in 2023, the number of blockages in the sewerage system of Yerevan exceeded 10 thousand times, and the construction and reconstruction of sewer lines amounted to more than 2 thousand meters, which is very far from satisfactory.

There are three types of blockages in Yerevan sewer pipes:

- Accumulative. Fats, hair and organic products gradually settle on the walls of the pipes, which leads to a narrowing of the diameter of the latter and a decrease in the intensity of the water flow. Cumulative blockage is considered the most common.
- Technical. Occurs due to errors in the design of the sewer system. Blockages in this case are formed due to improper laying of pipelines or the use of small diameter pipes.
- Instant. Such a blockage occurs due to the ingress of large objects into the pipe.
 Accumulative types of blockages are most often observed in the sewerage system of Yerevan. A clean sewer system is the basis for pipe safety, which guarantees the absence of leaks and unpleasant odors, comfort and a normal environment, and a reduction in

¹ Financial statement 2024 year of "Veolia Group" - "Veolia Jur" CJSC- "State Water Committee of the Republic of Armenia" [Online]. URL: https://www.veolia.am/en/publications (date of access: 17.09.2024)

significant annual costs for removing blockages. Because blockages can lead to a serious accident or a pipe break.

For internal sewage systems, which can have a diameter of up to 150 mm, the most common causes of blockage are:

- accumulation of silty deposits;
- getting rags, clothes and any other pieces of fabric into the sewer pipes;
- formation of fat deposits;
- various deposits on the walls of sewer pipes, calcium, rust and some others.

The efficiency and service life of water supply and sewerage infrastructures and highways depend on timely identified damages, types of pipeline defects and their effective elimination. The main reason for the current state of underground pipelines in Yerevan is the unjustifiably large use of metal pipes: more than 70 % steel and no more than 10 % cast iron [9].

In practice, various methods of cleaning and restoring sewer pipelines are used [4–8, 10–18]:

- mechanical with cylindrical piston pigs made of polyurethane with an additional coating of a fleecy metal cartridge – the cleaning method is used for pipeline diameters of 80–150 mm;
- water-air method, which is used for pipelines with a diameter of 200–250 mm in the presence of loose rust deposits and the length of the treated area in one pass is up to 2000 m;
- hydraulic based on jet heads or hydrocavitation nozzles the method can be used for any
 pipe diameter, while achieving a mirror shine, and at the same time an anti-corrosion internal
 protective coating can be applied;
- hydrodynamic using high-pressure jets (pressure up to 350 MPa), which allows you to
 process pipelines with a diameter of up to 400 mm and a length of up to 1200 m in one pass,
 as well as for cleaning sewer pipelines with a diameter of up to 750 mm, into which the roots
 of trees and shrubs penetrate;
- hydrochemical, which consists in the use of chemical reagents to remove iron oxides and carbonate deposits from the internal walls of pipelines using specially prepared solutions;
- biological, implemented using foam herbicides, which are pumped into an emptied sewer
 pipeline and disrupt the normal development of the roots of trees and shrubs, penetrating
 into open cracks in the pipelines and carried by the flow of water into the nearest inspection
 wells:
- pulse, which produces a hydraulic shock that destroys deposits on the walls of pipelines the method is effective for cleaning pipelines with a diameter of up to 300 mm and a length of up to 300 m:
- ultrasonic, which is realized due to ultrasound propagating in a liquid medium or in the material of the equipment being cleaned;
- ice, the basis of which is the use of specially prepared ice to absorb contaminants located on the inner surface of pipes and remove them from the pipeline.

The above methods for cleaning pipelines have certain advantages and disadvantages. The ultrasonic method of cleaning pipelines has currently received limited use, despite such undeniable advantages as low energy intensity, the use of less concentrated cleaning solutions to ensure high quality cleaning without causing damage to the internal surfaces of pipelines [15–18].

Ultrasound is elastic vibrations and waves with a frequency higher than 15–20 kHz, which, when applied to liquid, causes specific physical, chemical and biological effects, such as cavitation, capillary effect, dispersion, emulsification, degassing, disinfection, local heating and many others. The lower the frequency, the easier it is to obtain cavitation, and the more aggressive the effect the latter has on the object being processed, which is why many devices use ultrasound with a frequency of 20–22 kHz [19, 20].

As is known [18, 21, 22], ultrasonic vibrations (USV) in a liquid medium are created by means of piezoceramic or magnetostrictive ultrasonic vibration transducers. At the same time, piezoceramic ultrasonic transducers provide higher efficiency compared to magnetostrictive ones – 0.8...0.9 and have a simpler design and low manufacturing cost, and also do not require additional water cooling² [18, 21–23]. The disadvantages of piezoceramic ultrasonic transducers include their relatively low specific acoustic

² Ultrasonic cleaning of products: simple about the complex. Journal "ISUP"(Informatization and control systems in industry). 2023. No. 4(106). Pp. 117–119. [Online]. URL: https://isup.ru/upload/pdf-zhurnala/2023/4/116 119 Sp-sonic.pdf (date of access: 17.09.2024)

power, ranging from 1...2.5 W/cm² [15, 19–22, 26–30], as well as the need to ensure its high-quality sealing from the liquid medium, since their penetration at best, it will lead to their breakdown; at worst, there will be a short circuit in the output of the ultrasonic testing generator and there will be a possibility of damaging operating personnel with high-frequency electric current. Therefore, to provide the required power needed for cleaning sewer pipelines, bulky composite piezoceramic ultrasonic transducers of the overhead type are used.

Note that magnetostrictive ultrasonic transducers have a much higher specific acoustic power, ranging from 80...120 W/cm² [17, 18, 21, 24–26], but low efficiency – 0.4...0.5. Therefore, during the operation of magnetostrictive ultrasonic transducers, large losses of electrical energy occur, which leads to heating of both its winding and the magnetic circuit, as a result of which such converters are equipped with an additional water cooling system, which is considered to be its main disadvantage.

In this regard, in the case of using magnetostrictive ultrasonic transducers for cleaning sewer lines, this disadvantage becomes its advantage, since for cleaning pipelines, rinsing water can be used to cool the ultrasonic transducer, and the heated rinsing water can be used to increase the efficiency of the cleaning process. To solve this problem, it is necessary to have powerful, small-sized and through-the-pipe magnetostrictive ultrasonic transducers.

The purpose of the work is to increase the efficiency of cleaning through-flow sewer pipelines using powerful small-sized magnetostrictive ultrasonic transducers.

Methods for manufacturing magnetostrictive ultrasonic transducers. To manufacture single-rod magnetostrictive ultrasonic transducers, rectangular plates are stamped from a tape made of magnetoelastic material, a magnetic circuit package is assembled from them, the end of which is soldered to the waveguide. Gaskets made of heat-resistant electrical insulating material are installed on the magnetic core, onto which the ultrasonic excitation winding is wound [28, 29].

This method of manufacturing a single-rod magnetostrictive ultrasonic transducer is distinguished by its simplicity of technology, since the excitation winding can be manufactured in the form of a separate ready-made coil, which is immediately installed on the magnetic core. It should be noted that this method of manufacturing magnetostrictive ultrasonic transducers allows the use of waste-free technology for stamping rectangular plates from magnetostrictive material and winding the electromagnetic field excitation coil in a separate automated technological operation. The main disadvantage of such a magnetostrictive ultrasonic transducer is its low efficiency [28, 29]. This is due to the fact that the electrical energy of the windings is converted into the energy of the magnetic field, it creates through the magnetic circuit and air space, where there are large magnetic losses, and the efficiency of such converters is within 10...15 % [28, 29].

The noted disadvantages are absent in the methods of manufacturing two, three or more rod magnetostrictive ultrasonic transducers, in which rectangular holes are cut out in a magnetoelastic rectangular material along its length and in its middle, and after assembling the magnetic circuit package, a window is formed, through which the ultrasonic excitation winding is wound onto them [28, 29].

The main advantage of manufacturing such two, three or more rod magnetostrictive ultrasonic transducers is that the electrical energy of the ultrasonic excitation winding is converted into the energy of a magnetic field, in which the magnetic flux lines pass in a closed magnetic circuit, as a result of which magnetic losses are significantly reduced, and so on. p.d. of such converters increases to 45...50 % [28, 29].

2. Methods

Currently, magnetostrictive ultrasonic transducers are being manufactured using this method to produce high-power ultrasound for various ultrasonic processing plants manufactured in the USA, Germany, Japan, England, Russia, China, etc., which allow ultrasonic testing with a power of up to 10 kW or more. Such magnetostrictive ultrasonic transducers are assembled from stamped plates – magnetically elastic tapes with a thickness of 0.08...0.2 mm and the required width. A package of magnetic circuits of the required size is assembled from these plates, the end of which is soldered to the waveguide, gaskets made of heat-resistant insulating material are installed on the rods of the magnetic circuit and an ultrasonic excitation winding is wound through the formed windows on the magnetic circuit. The presence of windows in the magnetic circuit and the need for manual winding of the excitation winding leads to a complication of equipment for manufacturing plates with rectangular holes, a decrease in the utilization rate of expensive magnetically elastic material and a decrease in its effective power. At the same time, the loss of magnetically elastic material is up to 35 %, which leads to an increase in the cost of manufacturing an ultrasonic vibration transducer. The National Polytechnic University of Armenia (NPUA) has developed a new method for manufacturing double-rod magnetostrictive ultrasonic transducers, in which rectangular

plates are stamped from a tape made of magnetically elastic material, from which a package of magnetic wires is assembled, the end of which is soldered to a waveguide [29]. The magnetic core body is divided into two rods of the same thickness, on which gaskets made of heat-resistant insulating material are installed, on which ultrasonic excitation windings are wound. A gasket made of heat-resistant electrical insulating material is installed between these windings, the windings are compressed and in contact with each other through the gasket, and the free ends of the rods of the magnetic circuit are rigidly connected to each other [29]. This method of manufacturing double-rod magnetostrictive ultrasonic transducers provides a waste-free technology for cutting rectangular plates of a magnetic core, due to the absence of rectangular holes in them. However, with the same power, the overall dimensions of the speaker system remain relatively large, and with its limited overall dimensions, the ultrasonic radiation power remains relatively low.



Figure 2. Experimental setup with an ultrasonic generator.

The experiments were conducted in the Research and Innovation Laboratory of the NPUA using the newest ultrasonic generator. Comparative tests were performed with both piezoceramic and magnetostrictive transducers, allowing for a detailed evaluation of their performance and efficiency under identical experimental conditions.

3. Results and Discussion

To obtain powerful small-sized three-rod magnetostrictive ultrasonic transducers, a magnetic core package assembled from rectangular plates of magnetically elastic material was divided into three rods, resulting in the formation of a middle rod and two adjacent outer cores of the magnetic core (Fig. 3) [28, 29].



Figure 3. Experimental sample of a magnetostrictive transducer.

In this case, the thickness of the middle rod is taken to be twice the thickness of the outer rods, which makes it possible to obtain a three-rod magnetostrictive ultrasonic transducer with a uniformly distributed magnetic flux throughout the magnetic core and ensures a uniform magnetic flux along the entire cross-section of the magnetic core body (Fig. 3). This method also provides the possibility of manual winding of the excitation winding of the ultrasonic transducer in the form of a separate coil, wound automatically as a separate technological process, and immediately installed without additional technological processes.



Figure 4. Piezoceramic transducer.

The tests conducted on the experimental setup demonstrated that ultrasonic testing using our magnetostrictive transducer for 5 minutes reduces the thickness of blockages and deposits by 50 %. This significant reduction highlights the practical efficiency of the magnetostrictive transducer without requiring additional complex technologies or significant human intervention. Furthermore, compared to piezoceramic transducers, our magnetostrictive transducer offers higher specific acoustic power (80–120 W/cm² versus 1–2.5 W/cm² for piezoceramic). While piezoceramic transducers provide higher efficiency (0.8–0.9) under standard conditions, they require meticulous sealing to prevent damage from liquid environments and often demand bulky configurations to achieve comparable power. Conversely, our magnetostrictive transducer combines compactness, robustness and a high-power output, making it more suitable for intensive applications like cleaning sewer pipelines. Moreover, its integrated cooling feature – using rinsing water – enhances operational efficiency and ensures sustainability during prolonged use.

4. Conclusions

- Traditional methods of cleaning sewer pipes are limited by factors, such as the composition of deposits, the diameter and length of the cleaning section, and environmental conditions. Among the most promising environmentally friendly technologies is the use of ultrasonic vibrations generated by mobile and compact devices.
- 2. A relatively powerful, small-sized three-rod magnetostrictive transducer with an ultrasonic concentrator has been successfully developed for cleaning sewer pipelines.
- 3. It has been established that the newly developed method for manufacturing three-rod magnetostrictive ultrasonic transducers allows for a 25.5 % increase in output power compared to two-rod ultrasonic transducers, while also reducing the overall dimensions by 15 %.
- 4. Theoretical calculations and experimental results demonstrate that the use of a three-rod magnetostrictive transducer with an ultrasonic concentrator increases the efficiency of cleaning sewer pipelines by up to 10 %, while significantly reducing the cleaning time.

References

- Vasilev, V.M., Pankova, G.A., Stolbikhin, Yu.V. Deterioration of sewage tunnels and in-line structures as a result of microbiologic corrosion. Vodosnabzhenie i sanitarnaya tekhnika [Water Supply and Sanitary Technique]. 2013. No. 9. Pp. 67–76. (rus).
- 2. Wells, T., Melchers, R.E., Bond, P. Factors involved in the long term corrosion of concrete sewers. Corrosion & Prevention. Australia: Australasian Corrosion Association Inc, 2009. Pp. 1–12.
- Chibukhchyan, O.S. Improving the Efficiency of Treatment of Sewage Systems. Occupational Safety in Industry. 2024. No. 2. Pp. 69–74. (rus). DOI: 10.24000/0409-2961-2024-2-69-74
- 4. Karsten, M. Zustandserfassung von Kanalisationen. WWT: Wasserwirt. Wassertechn. 2007. No. 3. Pp. 10–15.
- 5. Kuliczkowski, A., Kuliczkowska, E., Zwierzchowska, A. Technologie bezwykopowe w inynierii rodowiska. Wydawnictwo Seidel-Przywecki Sp. z o.o. 2010. 735 p.
- 6. Ishmuratov, R., Orlov, V., Andrianov, A. The spiral wound pipeline rehabilitation technique for pipe networks: An application and experience in Moscow City. 31 International Conference and Exhibition NO-DIG'2013, Sydney (Australia).

- Zwierzchowska, A. Technologie bezwykopowej budowy sieci gazowych, wodociagowych i kanalizacyjnych. Kielce: Wydawnictwo Politechniki Świętokrzyskiej, 2006. 180 p.
- 8. Rabmer-Koller U. No-dig technologies innovative solution for efficient and fast pipe rehabilitation. 29 International Conference and Exhibition NO-DIG'2011, Berlin (Germany).
- 9. Chibukhchyan, H.S., Chibukhchyan, G.S. Improving the mechanical characteristics of water supply and sewerage pipes in urban areas. Chernye metally. 2024. No. 11. Pp. 69–73. DOI: 10.17580/chm.2024.11.12
- 10. Levchenko, E.P., Petrenko, A.V., Chernyshov, E.A., Ivanova, E.O. Practical application of methods and means for mechanical defouling of water supply and sewerage nets. Collection of scientific papers of DonGTI. 2021. 22 (65). Pp. 114–121. (rus)
- 11. Hovhannes, C., Aram, B., Boris, B. Increasing the rigidity of thin-walled machine parts made of aluminium alloys by reducing its grain size by two-way ultrasonic smoothing. Materials Science Forum. 2021. 1022. Pp. 142–151. DOI: 10.4028/www.scientific.net/MSF.1022.142
- 12. Stephenson M. Ice Pigging a NO-DIG Technique for Cleaning Pressurized Pipes. NO-DIG 2013, Sydney (Australia).
- 13. Orlov, V.A., Meshkova, N.I. Ultrazvukovaya sistema Piglet. Vnutrenniy osmotr i prochistka truboprovodov [Ultrasonic system Piglet. Internal inspection and cleaning of pipelines]. Tekhnologii mira. 2012. No. 5. Pp. 43–44. (rus)
- Wu, Q., Zhu, C.P., Yao, C., Wang, B., Yin, Y.Z., Chen, B.Y., Ren, Q.G., Han, Q.B., Tang, Y.B., He, Z.B., Chen, G.C., Li, Z.X., Chen, J. Ultrasonic Cleaning Device with Adjustable Power for Submerged Structure. AMM. 2014. 578-579. 1087. DOI: 10.4028/www.scientific.net/AMM.578-579.1087
- Xu, Y., Langbauer, C., Hofstaetter, H. The Application of Ultrasonic Technology for Cleaning Oil Contaminated Sand. SPE Asia Pacific Health, Safety, Security, Environment and Social Responsibility Conference. Kuala Lumpur, 2017. DOI: 10.2118/185261-MS
- 16. Khmelev, V.N., Shalunov, A.V., Shalunova, A.V. Ultrasonic atomization of liquids: monograph. Altai State Technical University named after I.I. Polzunov, BTI. Biysk: Publishing house of Altai State Technical University, 2010. 250 p. (rus)
- 17. Khmelev, V.N., Leonov, G.V., Barsukov, R.V. Ultrazvukovyye mnogofunktsionalnyye i spetsializirovannyye apparaty dlya intensifikatsii tekhnologicheskikh protsessov v promyshlennosti, selskom i domashnem khozyaystve [Ultrasonic multifunctional and specialized devices for intensification of technological processes in industry, agriculture and households]. Barnaul: Alt. gos. tekhn. un-t, 2007. 399 p. (rus)
- 18. Khmelev, V.N., Shalunov, A.V., Khmelev, S.S., Tsyganok, S.N. Ultrazvuk. Apparaty i tekhnologii: monografiya [Ultrasound. Devices and technologies: monograph]. Biysk: Izd-vo Altayskogo gos. tekhnich. un-ta, 2015. 688 p. (rus)
- 19. Venkittaraman, A., Roberts, P.M., Sharma, M.M. Ultrasonic removal of near-wellbore damage caused by fines and mud solids. SPE Drilling & Completion. 1995. 10. Pp. 193–197. DOI: 10.2118/27388-PA
- Frizzell, L.A. Biological Effects of Acoustic Cavitation, in Ultrasound: Its Chemical, Physical and Biological Effects, Suslick, K. S. (Ed.), VCH Publishers, New York, 1988.
- 21. Khmelev, V.N., Shalunov, A.V., Shalunova, K.V. Ultrazvukovaya koagulyatsiya aerozoley: monografiya [Ultrasonic coagulation of aerosols: monograph]. Biysk: Izd-vo Altayskogo gos. tekhnich. un-ta, 2010. 227 p. (rus)
- 22. Khmelev, V.N., Shalunov, A.V., Golykh, R.N., Nesterov, V.A. Ultrazvuk. Vozdeystviye na sistemy s nesushchey zhidkoy fazoy [Ultrasound. Effect on systems with a carrier liquid phase: monograph. Biysk: Izd-vo Altayskogo gos. tekhnich. un-ta, 2018. 275 p. (rus)
- 23. Novitskiy, B.G. Primeneniye akusticheskikh kolebaniy v khimikotekhnologicheskikh protsessakh [Application of acoustic vibrations in chemical engineering processes]. Moscow: Khimiya, 1983. 192 p. (rus)
- Golovnev, I., Marzul, V., Using ultrasound treatment to intensify and improve the efficiency of biological cleaning of waste water and improve the properties of raw suction. Bulletin of Polotsk State University. 2019. Series B. Pp. 129–136 (rus)
- 25. Stepanenko, D.A. Theoretical substantiation of the possibility of amplifying ultrasonic vibrations using composite ring elastic elements. Technical acoustics. 2017. 2. Pp. 13. (rus)
- 26. Balasanyan, B.S., Khristaforyan, S.Sh. Sposob izgotovleniya magnitostriktsionnykh preobrazovateley ultrazvukovykh kolebaniy [Method for manufacturing magnetostrictive transducers of ultrasonic vibrations]. Patent RA 2443 A2. Ofitsialnyy byulleten. No. 8. 2010. 24 p.
- 27. Novikov, V., Rubanik, V., Synthesis and analysis of ultrasonic oscillatory systems of drawing machines. Bulletin of Vitebsk State Technological University. Pp. 68–73 (rus)
- Arshakyan, A.L., Balasanyan, A.B., Chibukhchyan, O.S., Balasanyan, B.A., Grigoryan, V.Sh. Kompaktnyy magnitostriktsionnyy
 preobrazovatel ultrazvukovykh kolebaniy [Compact magnetostrictive ultrasonic transducer]. Collection of scientific articles
 Proceedings of National Polytechnic University of Armenia. 2019. 2. Pp. 285–291.
- Balasanyan, B.S., Arshakyan, A.L., Balasanyan, A.B., Chibukhchyan, O.S., Balasanyan, B.A., Grigoryan, V.Sh., Oganisyan, O.A. Sposob izgotovleniya magnitostriktsionnykh preobrazovateley ultrazvukovykh kolebaniy [Method for manufacturing magnetostrictive transducers of ultrasonic vibrations]. Patent RA 3265 A2. 2019
- 30. Ukhanova, Y., Perova, N., Ukhanov, A. Ultrasound: efficiency of application and technical. News of the Samara State Agricultural Academy. 2019. 2. Pp. 57–63 (rus)

Information about the authors:

G. Chibukhchyan, PhD in Technical Sciences

E-mail: hovhannesch@gmail.com

H. Chibukhchyan, PhD in Technical Sciences ORCID: https://orcid.org/0000-0003-0746-2091 E-mail: grigor.chibukhchyan@gmail.com



Magazine of Civil Engineering

ISSN 2712-8172

journal homepage: http://engstroy.spbstu.ru/

Research article UDC 674.816.2

DOI: 10.34910/MCE.131.7



Strength and thermal conductivity properties of thermowood-cement composition and factors influencing these indicators





V.Yu. Chernov¹ D, I.G. Gaisin¹ D, E.M. Maltseva², A.N. Nosova¹



- ¹ Volga State University of Technology, Yoshkar-Ola, Mari El, Russian Federation
- ² Construction Materials Plant "Amarant". LLC. Yoshkar-Ola, Mari El, Russian Federation

Keywords: strength class, compressive strength, thermal conductivity, thermally modified wood, TMW, thermal wood concrete, TMC, TMW-cement composition

Abstract. The paper studies the ways that technological characteristics of thermal wood concrete (TWC) production have on its strength and thermal conductivity properties. TWC is a new, effective wood-cement composition of authors' development. To produce it the authors used crushed thermally modified wood (TMW) with a certain shape and size as a filler. The research is rationalized by the fact that currently we are facing a lack of both fundamental and applied experimentally confirmed data on TWC. The paper discusses the studies of the compressive strength and thermal conductivity of four groups of TWC samples that were obtained with three types of filler, differing in size and shape, molding method and strength class of cement-sand mortar. The authors determined general impact patterns of the above-mentioned factors on strength and thermal conductivity properties, as well as specific indicators. Moreover, the paper describes the strength classes and grades of TWC that ranged from B1.5 to B3.5 and from M25 to M50, respectively. Thermal conductivity for standard samples ranged from 0.21 to 0.4 W/(mK). It has been concluded that TWC with a finer TMW filler has the most balanced combination of strength, thermal conductivity and deformation properties. Following the results, the authors proposed practical recommendations for TWC production, and further courses for its improvement and research.

Funding: The research work was supported by the Russian Science Foundation (RSF, no. 22-79-00098)

Citation: Chernov, V.Yu., Gaisin, I.G., Maltseva, E.M., Nosova, A.N. Strength and thermal conductivity properties of thermowood-cement composition and factors influencing these indicators. Magazine of Civil Engineering. 2024. 17(7). Article no. 13107. DOI: 10.34910/MCE.131.7

1. Introduction

While developing new materials, an important task is seen in acquiring fundamental knowledge on their operational, technological and other properties. Thermowood-cement composition or thermal wood concrete (TWC) is a new, previously unstudied building material of original development. The paper studies its strength, thermal conductivity properties, as well as technological factors that influence them. Standard TWC samples made in the laboratory are the objects under study.

Being environmentally friendly and with high thermophysical properties, nevertheless, the modern wood-cement compositions have a number of disadvantages associated with the properties of natural wood [1-5], namely:

1) hyper sorption of water and moisture, as well as associated shrinkage loss and swelling;

© Chernov, V.Yu., Gaisin, I.G., Maltseva, E.M., Nosova, A.N., 2024. Published by Peter the Great St. Petersburg Polytechnic University.

- 2) discomfort and danger of operation due to the formation of mold and fungal lesions accompanied by destruction;
 - 3) content of extractives and acids that negatively affect the formation of cement stone in composites.

Nowadays, the work is underway and a number of technological solutions have been offered to boost the properties of wood-cement compositions that can be done by minimizing the negative factors from arise when using natural wood [6–8]. Those solutions cover a wide range of methods for wood aggregate pretreating [9], adding chemicals and other substances to mixtures [10–13] and employing chemical modification of wood [14–16]. Despite the successful results, the above-mentioned solutions did not bring any breakthrough improvements in the strength and protective properties of wood-cement compositions.

An effective solution to these problems can be the use of thermally modified wood (TMW) filler [17–22].

In this regard, we are witnessing a rising interest in developments done to create wood-cement compositions based on the use of TMW, namely wood-polymer composition (WPC), plywood and wood concrete [23]. The authors discuss current researches in modeling the processes of thermal modification of crushed wood, determining the hygroscopicity and swelling pressure of TMW, as well as the degree of thermal modification. As it concerns the operational and technological properties, so far, we may give only experimental data on compressive strength, the search for a rational water-cement ratio, the bulk density of particles (fillers) estimations from TMW and others.

Other relevant works [24] that study mortars based on hydraulic binders, where crushed TMW obtained from waste. It was proved that compared to mortar with untreated wood particles, mortars with wood chips showed better flexural strength and compressive strength due to improved adhesion between the wood aggregate and the cement stone. Compared the standard solution the crushed wood aggregate has lower strength, nevertheless, it shows higher levels of flexural toughness and impact strength.

However, some major features that differ TWC from wood concrete and mortars based on TMW, can be found in fine aggregate (sand), a various shape and size of the TMW aggregate, the general recipe, the processes of preparing raw materials and molding. Hence, resting on the results of exploratory studies, we can refer to higher density, physical-mechanical and other properties of TWC compared to analogues [25].

By analyzing research works, the authors concluded that the developed material has no close analogues and is essentially new.

Therefore, based on individual scientific, technical and technological approaches in the field of thermal modification and production of building materials supervised by Dr. V.Yu. Chernov (Yoshkar-Ola), the authors started the development and piloted research aimed at creating innovative, effective TMW-cement composite materials [26]. The use of TMW as the main coarse aggregate in concrete minimizes the negative properties of natural wood described above.

Today in the field of industrial production of new composite material at the Scientific and Production Association "MariTermoWoodIndustries" (Yoshkar-Ola) developed and implemented technology and equipment for thermal modification of wood (Patent Russia no. 2724421), which allowed to reduce significantly the cost of production of TMW and thereby, according to preliminary calculations, ensure the profitability of TWC production (Patent Russia no. 2790390) and products made from it.

The objective of this paper is to study the strength and thermophysical properties of the proposed TWC, as well as to estimate the influence the production (technological) factors might bring. The tasks include the production of standard TWC samples of several groups with different mix formulations and molding methods, studies on compressive strength and thermal conductivity, additionally, determining technological factors that influence the properties under study.

2. Methods

2.1. Obtaining Development Samples

The research in this work is piloted, since there are no objective data on the material being developed, its recipe production parameters and technological requirements. The authors of the work were facing with the issue of creating the first samples with properties close to the maximum expected – these are low thermal conductivity (at the level of aerated concrete), average compressive strength (at the level of expanded clay concrete), low moisture and water absorption (at the level of heavy weight concrete with mineral fillers). The authors decided on the size and shape of the coarse TWC aggregate, the class of the cement-sand mortar and the molding method to be used as variable factors when obtaining TMW samples. These factors are significant as based on the existing general provisions of wood science and concrete

science and have the most impact on the physical, mechanical and thermophysical properties of wood-cement compositions.

Thus, to study the general influence of variable factors, 4 varieties (groups) of samples were described (Table 1, Fig. 1).

Table 1. Description of the characteristics of the development samples groups.

- T U K	Die 1. Description of the chai	acteristics of the deve	iopinent samples groups.
Group #	Name of sample	Relative content of components, % of volume: (cement / sand / TMW chips / water)	Description of the key features of sample manufacturing
1	Vibrocast TWC samples with large TMW filler and class of cement-sand mortar M150 (class B12.5). Main group	7 / 27 / 55 / 11	The filler used was crushed TMW in the form of an oblique parallelepiped with all dimensions (length, width, thickness) in the range from 15 to 20 mm (Fig. 1, a).
2	Vibrocast TWC samples with large TMW filler and class of cement-sand mortar M400 (class B30). Comparing group	13 / 22 / 53 / 13	Compared to other groups, the strength of the cement-sand mortar was higher by increasing the content of the cement binder. The rest is similar to the 1st group.
3	Vibrocast TWC samples with medium TMW filler and class of cement-sand mortar M150 (class B12.5). Comparing group	7 / 27 / 55 / 11	The filler used was crushed TMW in the form of an oblique parallelepiped with dimensions: length from 15 to 20 mm, width from 10 to 20 mm and thickness from 5 to 10 mm (Fig. 1, b). The rest is similar to the 1st group.
4	Vibration-pressed samples of TWC with fine TMW filler and class of cement-sand mortar M150 (class B12.5). Comparing group	7 / 29 / 60 / 4	Samples obtained by pressing a semi-dry mixture with preliminary soaking of TMW filler, having dimensions: length from 10 to 20 mm, width from 5 to 20 mm and thickness from 2 to 5 mm (Fig. 1, c). The sizes and shapes varied.

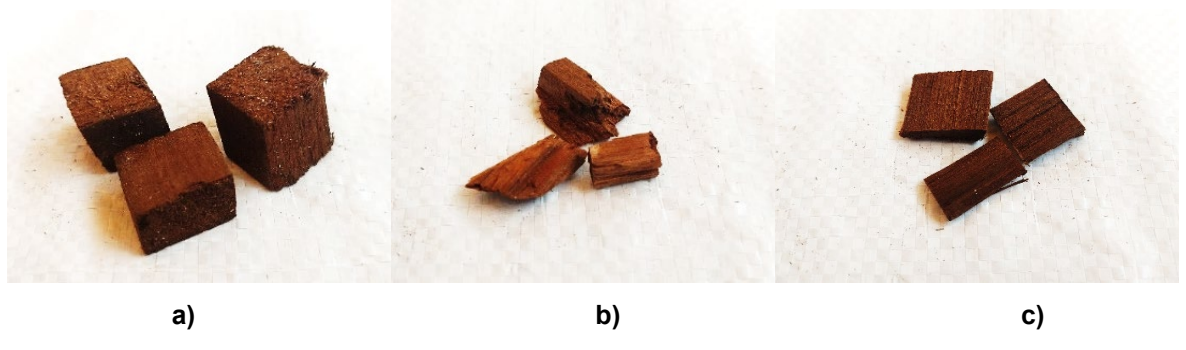


Figure 1. Relative comparison of size and shape of TMW filler.

The filler for all groups of samples was used from TMW of predominantly deciduous species (*Tilia europaea*, *Populus tremula*) with the COLOR+ treatment modes using AST technology (185 °C) (Patent Russia no. 2724421). However, the existing equipment for grinding wood was not suitable due to the difference in the elastic properties of natural and TMW, which affects the cutting process, namely, such material, during high-speed cutting in standard grinding equipment, broke and crushed into a dusty form. This is not suitable for obtaining TMW-cement composition. Therefore, grinding to the specified sizes and forms of thermal modification chips was performed on specially designed equipment (Patent Russia no. 2804105).

While producing the development samples, in addition to the TMW filler, the mixture included Portland cement M 500 (marked 42.5N (CEMII/A-K)) (GOST 25328-82), clean pit sand of class I of fine and medium fraction (GOST 8736-2014) and process water (GOST 23732-2011) in appropriate proportions to obtain a solution of class B12.5 (M150) and B30 (M400) without chemical additives and other components.

2.2. Setting the Research

In accordance with standard research methods, for each of the described groups and separately for each type of a test, the authors made 10 pieces of cubic samples with dimensions of 100×100×100 mm (Fig. 2).



Figure 2. Appearance of the finished sample of group 4 for research (the side surface is cut off at the front to visualize the interior distribution of crushed TMW filler).

The mixture was prepared in a gravity-type concrete mixer, thus, subsequently the samples were produced using a vibrating table in specially made steel matrices with a removable bottom. The same matrices were used for vibrocasting as for vibrocompression, however, tiles were added to squeeze from above and form a sample from a semi-dry TMW-cement mixture. Uniform distribution, compaction and better adhesion between the cement paste and the TMW particles (Fig. 2) occur as a result of the simultaneous action of compression and vibration, namely, with the help of pressure arising from the punch and the operation of the platform vibrator. The size and shape of the sample corresponds to the matrix in which the TMW-cement composition is placed.

Subsequent exposure for both molding methods employed a simplified non-standard method and included exposure for 28 days until the design (grade) strength was reached at a temperature of 20 °C and a relative humidity of 60±5 %. Such conditions were chosen to obtain the material under less favorable hardening conditions, which is typical for simple and low-tech (non-factory) production conditions.

2.3. Methodology for Studying Strength and Thermal Conductivity Properties

Methods for studying the strength and thermal conductivity properties of TWC were in accordance with the basic requirements for testing concrete comparably with current standards (GOST 10180-2012 and 30256-94), as well as taking into account practical recommendations for the use of test measuring equipment.

The authors used a universal testing machine (UTM) SHIMADZU 50 kN (Shimadzu Corp, Japan) to study the strength of the TWC. Data processing and calculation of compressive strength (R, MPa) was performed on the maximum destructive load and the working cross-sectional area of the sample according to the formula:

$$R = \alpha \frac{F}{A}$$
,

where F – maximum breaking load, H; A – sample working section area, mm²; α – scale factors (equal to 0.95 for the indicated shapes and sample sizes).

Thermal conductivity of the TWC was carried out with an automatic thermal conductivity meter by the probe method MIT-1 (LLC Scientific Development and Production Enterprise Interpribor, Chelyabinsk). For this purpose, a blind hole with a diameter of 6.2 mm and a depth of 80 mm was made in the central part of the samples. Litol-24 lubricant was used for tighter contact in the hole of the measuring probe rod with the material.

Studies of thermal conductivity of a wall block manufactured using a standard industrial method based on the vibrocompression method are also of scientific and practical interest. Therefore, the blocks with "euro holes" with dimensions 390×190×190, which are most popular in practice, were also manufactured (Fig. 3). Thermal conductivity studies on them were carried out by obtaining a hole and measuring in the central part of the block, namely in the center of the middle partition, from the side wall (Fig. 3).

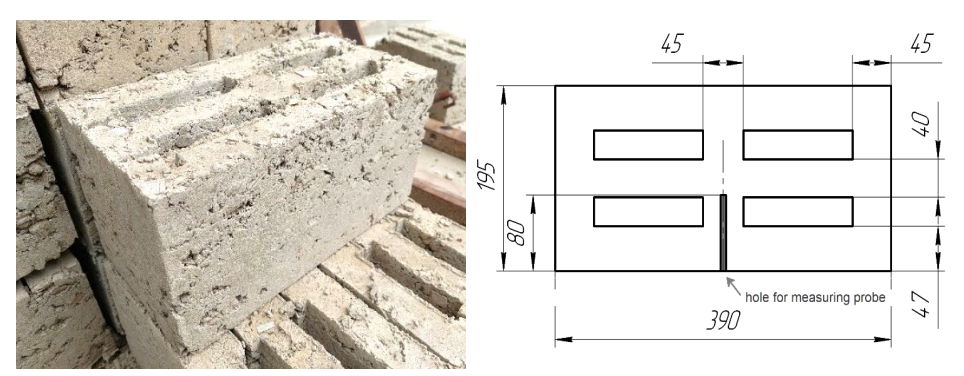
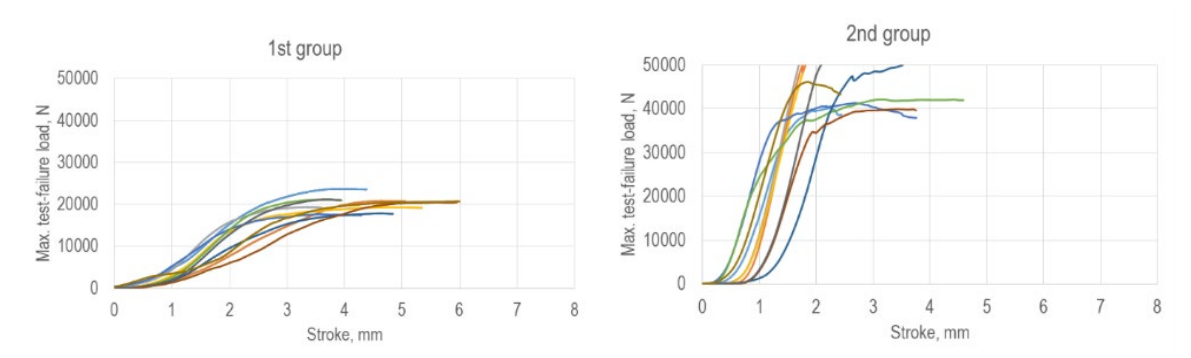


Figure 3. Appearance of blocks ready for research (left) and their dimensions with the location of the hole for the thermal conductivity meter (right).

3. Results and Discussion

3.1. Studies on the Strength of Thermal Wood Concrete

TWC strength studies were performed individually for each 10 pieces-group of samples. The main results are given in Table 2 and Fig. 4, as well as group-averaged diagrams of loading (Fig. 5).



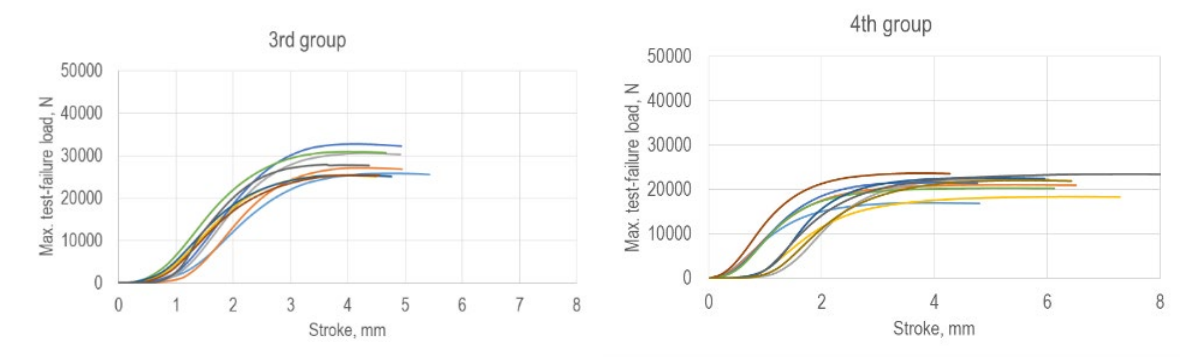


Figure 4. Sample diagrams of loading for each group (see Table 1).

Due to technical limitations of the specified UTM, it was impossible to construct complete diagrams of loading in dynamics for the 2nd group of samples. However, the results for the maximum breaking load were gained on another hydraulic testing machine without constructing diagrams and were taken into account in subsequent data processing and calculation of the average compressive strength for the group.

Table 2. Main statistical indicators of TWC strength.

able 2. Main statistical indicators of TWC strength.						
Statistical indicators of TWC	Groups of samples					
strength, MPa	1	2	3	4		
Average (R)	1.98	4.53	2.67	2.11		
Maximum	2.34	5.00	3.05	2.47		
Minimum	1.82	3.99	2.29	1.74		
Standard deviation	0.162	0.367	0.242	0.229		

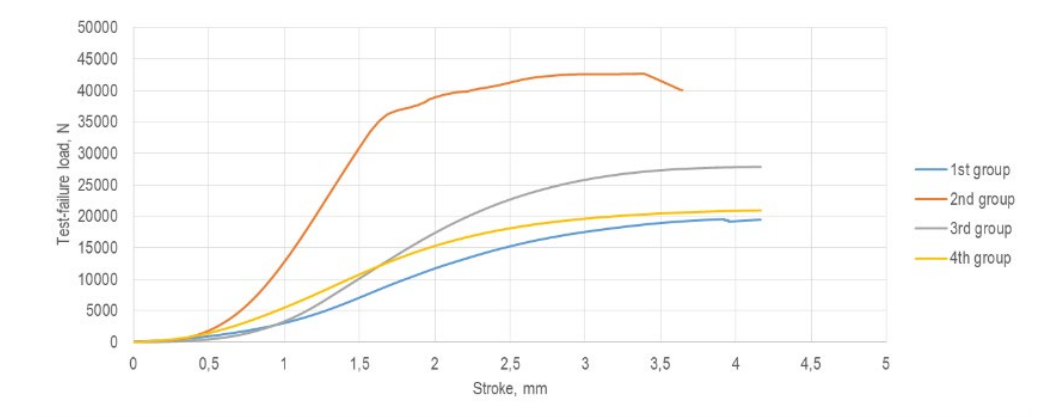


Figure 5. Average loading curves of samples for each group.

3.2. Studies of Thermal Conductivity of Thermal Wood Concrete

Studies of the thermal conductivity of TWC were also performed for samples in a volume of 10 pieces in each group. The main results are given in Table 3 and Fig. 6.

Table 3. Main statistical indicators of TWC thermal conductivity.

Statistical indicators of TWC	marcators	Thickened block with "euro holes"			
thermal conductivity, W/(mK)	1	2	3	4	
Average (λ)	0.32	0.28	0.40	0.21	0.31
Maximum	0.37	0.35	0.49	0.29	0.38
Minimum	0.26	0.21	0.31	0.16	0.25
Standard deviation	0.041	0.051	0.062	0.038	0.052

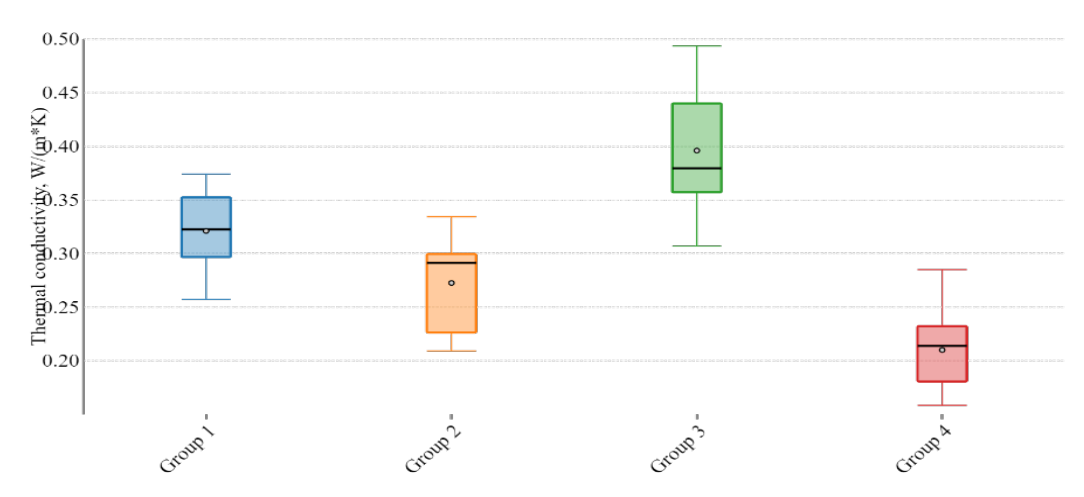


Figure 6. Diagrams of the range of TWC thermal conductivity by groups.

3.3. Comparative Analysis and Discussion

The increased content of cement binder and the grade (class) of cement-sand mixture (mortar) used to produce it both have a significant influence on the strength of TWC. When comparing the average data, the excess strength of samples from grade M400 mortar (the 2nd group) relative to grade M150 (the 1st group) was 2.3 times or 129 %.

Initially, the authors expected an increase in thermal conductivity due to an increase in the strength of the material, but the results turned out to be the opposite, namely, for samples with a higher grade of mixture, an insignificant decrease in thermal conductivity was observed by approximately 1.14 times or 12.5 %. Probably, this may be explained by the difference in thermal conductivity of the hydraulic cement binder and fine mineral filler and the difference in their relative content in the resulting mixture. That is, while manufacturing the M400 mixture, a smaller amount of fine filler in the form of sand and a larger amount of Portland cement were used, which could have a similar effect. However, this disclosure should be tested by performing special studies in this course. In this case, we can draw a general conclusion that the increased content of cement binder has a positive effect on the strength and thermophysical properties of the material under study.

The size of crushed thermally modified filler (the 1st, 3rd and 4th groups) does not have a significant effect on the strength properties of TWC. However, in the 3rd group with medium-sized TMW fillers (see Table 1), we observe a higher strength of the samples, exceeding the 1st group (main) by 35 %, and in the 4th group samples with the smallest filler sizes (see Table 1) strength also turned out to be 7 % higher than the first group. Along with strength and thermal conductivity, the 3rd group of samples had the highest value, which differed from the main group by 25 %, and the 4th group, on the contrary, had the lowest thermal conductivity, which was lower than the relative main group by 34 %.

The authors compared the results given with wood concrete based on natural wood [3, 4] and TMW [6, 23], which proved the advantages of choosing a smaller aggregate size for thermal wood concrete in terms of thermal conductivity properties and the nature of destruction. Nevertheless, the samples with an average aggregate size (the 3rd group) showed the best results in terms of strength.

Based on the nature of the destruction of the samples, we can conclude that the cement content and the size of the TMW filler affect the pattern and nature of the deformation of the wood-cement composition. In compression tests, samples with large TMW filler (the 1st and 2nd groups) were destroyed along the boundary of the filler and the hardened cement-sand mortar, and the nature of destruction according to GOST 10180-2012 had a satisfactory appearance, close in shape to a sand-glass. On the contrary, in the 3rd group during testing there was less destruction of the structural integrity of the samples, and in the 4th group we observed only slight surface damage in the particles of thermally modified filler.

At the end of testing samples of the 3rd group and especially the 4th group, elastic recovery after compression was noticeable, which indicates the high elastic-deformable properties of TWC, which probably have an inverse relationship with the size of the wood filler. For a proper understanding of the deformations and destruction of TWC, it is reasonable to perform special studies in this course.

The data obtained as a result of the tests made it possible to determine the strength class and grade strength of TWC (Table 4).

Table 4. Classification of TWC by strength.

	Groups of samples				
Strength indicators	1	2	3	4	
The coefficient of variation, %	8	8	9	11	
Brand strength	M25	M50	M25	M25	
Strength class	B1.5	B3.5	B2	B1.5	

Overall, the results for studying the compressive strength of TWC are close to those for testing wood concrete based on TMW [23, 24] and are approximately equal to 5 MPa. Still, direct comparing will be wrong, since the materials are not homogeneous, besides, the variable factors adopted in the studies do not correspond to each other.

The 4th group of samples proved to have the best thermal conductivity indicator, which is associated with the smallest size of the crushed thermally modified aggregate among the presented groups and, consequently, with a smoother distribution throughout the material and a higher percentage in the cement-sand mixture.

The 3rd group of samples is also of high interest, as it is highly thermally conductive and has increased strength compared with other materials similar in recipe. Initially, the authors expected that the 3rd group would show average values between the 1st and 2nd group of samples. Additional studies would be preferable.

TWC blocks showed higher thermal conductivity than the 4^{th} group of samples similar in recipe and production method. This could be explained by the fact that the probe of the thermal conductivity meter was inserted into the hole obtained in the middle partition wall of the block, with a 50 mm thickness, instead of the permissible minimum standard 100 mm. Based on the known ratios of thermal conductivity of solid and hollow blocks (on average 1.5–1.75 times), the expected thermal conductivity of hollow blocks made of TWC (Fig. 3) ranged from 0.12 to 0.14 W/(mK).

Thus, the most heat-efficient material is the 4th group TWC – obtained from fine TMW filler (see Table 1) corresponding to standard technological wood chips in shape and size, and also used for the production of wood concrete. The size and shape of the TMW filler do not have a significant role on the strength of the composition, therefore, one should use cement-sand mortar of increased grade strength to obtain TWC with increased strength properties. Samples of the 2nd and 4th groups have the most balanced thermophysical and strength properties, additionally the authors recommend their production methods for

practical implementation. However, studies should be performed on moisture and water absorption, water resistance and frost resistance of TWC in order to obtain the thorough and objective information on the material (composition) under study.

4. Conclusions

- 1. The greatest influence on the strength properties of TWC is exerted by the cement binder content in the cement-sand paste (the 2nd group), while with an increase in the amount of cement, the compressive strength also increases by more than 2 times. The size of the TMW filler has a noticeable effect. It was found that the TMW-cement composition has a strength 1.3–1.4 times higher than that of similar samples (the 1st group) with other filler sizes. There is also a difference in the strength of TWC concrete of different molding methods, namely, the strength of the TMW-cement composition obtained by vibration casting is 1.3–1.4 times higher than that of the vibration-pressed one.
- 2. The best ratio of strength and thermal conductivity properties were found within TWC made with the use of TMW filler characterized by the following dimensions: length from 10 to 20 mm, width from 5 to 20 mm and thickness from 2 to 5 mm the 4th group. These dimensions are the closest to technological wood chips. While performing strength tests, these TWC samples were most efficient in preserving their structural integrity and showed the highest elastic recovery after unloading.
- 3. The grade and increased content of cement hydraulic binder in the cement-sand mixture used to make TWC both have a positive impact on the strength properties of TWC. Meanwhile, cement hydraulic binder slightly reduces the thermal conductivity of TWC.
- 4. The strength of the recommended TWC samples is 2.11 MPa (the 4th group) and 4.53 MPa (the 2nd group), which corresponds to grades M25 and M50 or strength classes B1.5 and B3.5, respectively. Their thermal conductivity is 0.21 W/(mK) and 0.28 W/(mK), accordingly. It is necessary to note that in case the TMW filler of the 2nd group samples was coarse, then based on the identified patterns when using fine TMW filler as in the 4th group, samples of the 2nd group would have shown better strength and thermal conductivity properties.
- 5. The thermal conductivity can be in the range of 0.12–0.14 W/(mK) when manufacturing a hollow building material from TWC, for example, in the form of a standard block with "euro holes".
- 6. We should note that for this work specifically, the authors obtained the strength and thermophysical properties of TWC under simplified curing conditions, without heat and moisture treatment and any chemical additives that increase plasticity, strength, frost resistance and other properties. Thence, one can improve the properties of TWC, like other concrete with the indicated methods.
- 7. The results and patterns acquired in this work are fundamental and can serve as the basis for more in-depth research of the material, as well as finding optimal ratios of recipe factors and making high-quality TMW-cement compositions. Furthermore, the authors are expecting to continue researches on moisture and water absorption, water resistance, frost resistance, etc., as well as to develop an optimization model and method for getting the material, relying on the functional purpose (the ratio of physical-mechanical and thermophysical properties) and the economic efficiency of the production of TWC.

References

- 1. Gornostaeva, E.Yu., Gornostaeva, E.Yu., Lasman, I.A., Fedorenko, E.A., Kamoza, E.V. Wood-cement compositions with structures modified at macro-, micro-, and nano-levels. Stroitel'nye Materialy [Construction Materials]. 2015. 11. Pp. 13–16.
- 2. Nanazashvili, I.Kh. The "quick-to-erect" low-rise monolith buildings from the arbolite. Part 1. Construction Materials, Equipment, Technologies of the XXI Century. 2009. 11. Pp. 14–15.
- 3. Nanazashvili, I.Kh. Proizvodstvo arbolita iz drevesnyh othodov [Production of wood concrete from wood waste]. Moscow: CBNTI Minpromstroya SSSR, 1974. 47 p.
- 4. Krutov, P.I. Sklizkov, N.I., Nanazashvili, I.Kh., Sirotkina, R.B., et al. Ispol'zovanie othodov drevesiny dlya polucheniya effektivnyh stroitel'nyh materialov: Obzor [The use of wood waste to produce efficient building materials: Review]. Moscow: ONTI TsNIIEPselstroy, 1978. 24 p.
- Sanaev, V.G., Zaprudnov, V.I., Gorbacheva, G., Oblivin, A.N. Factors affecting the quality of wood-cement composites. Bulletin
 of the Transilvania University of Braşov. Series II: Forestry. Wood Industry. Agricultural Food Engineering. 2016. 9(58). Pp. 63
 70.
- 6. Safin, R.G., Stepanov, V.V., Khairullina, E.R., Gainullina, A.A., Stepanova, T.O. Modern building composite materials based on wood waste. Bulletin of the Kazan Technological University. 2014. 17(20). Pp. 123–128.
- Fu, Q.N., Yan, L., Thielker, N., Kasal, B. Effects of Concrete Type, Concrete Surface Conditions and Wood Species on Interfacial Properties of Adhesively-bonded Timber – Concrete Composite Joints. International Journal of Adhesion and Adhesives. 2021. 107. Article no. 102859. DOI: 10.1016/j.ijadhadh.2021.102859

- 8. Nemati, G.A., Fu, Q.N., Yan, L., Kasal, B. The effect of adhesive amount and type on failure mode and shear strength of glued timber-concrete joints. Construction and Building Materials. 2022. 345. Article no. 128375. DOI: 10.1016/j.conbuildmat.2022.128375
- Khajrullina, E.R., Safin, R.G., Tuntsev, D.V., Khajrullina, M.R. The effectiveness of the use of pretreatment of wood filler in the production of wood-cement composition. Systems. Methods. Technologies. 2021. 3(51). Pp. 85–91. DOI: 10.18324/2077-5415-2021.3-85-91
- Long, Xi., Liu, Z., Li, Xi., Zhou, H., Han, Ch. Surface modification of wood and its effect on the interfacial bonding properties of cement-based wood composites. European Journal of Wood and Wood Products. 2023. 81. Pp. 897–909. DOI: 10.1007/s00107-023-01926-7
- 11. Ramdane, R., Leila, Kh., Assia, A., Belachia, M. Influence of Biomass Ash on the Performance and Durability of Mortar. Civil and Environmental Engineering Reports. 2022. 32(2). Pp. 53–71. DOI: 10.2478/ceer-2022-0019
- 12. Verma, Sh., Singh, A., Gupta, R., Sundriyal, S. The Effect of Wood Ash on the Workability, Water Absorption, Compressive Strength in Cement Mortar. International Journal for Modern Trends in Science and Technology. 2023. 9(4). Pp. 368–373. DOI: 10.46501/IJMTST0904054
- Kostic, S., Merk, V., Berg, J., Hass, P., Burgert, I., Cabane, E. Timber-mortar composites: The effect of sol-gel surface modification on the wood-adhesive interface. Composite Structures. 2018. 201. Pp. 828-833. DOI: 10.1016/j.compstruct.2018.06.108
- 14. Liu, Z., Han, Ch., Li, Q., Li, Xi., Zhou, H., Song, Xi., Zu, F. Study on wood chips modification and its application in wood-cement composites. Case Studies in Construction Materials. 2022. 17. Article no. e01350. DOI: 10.1016/j.cscm.2022.e01350
- 15. Liu, Z., Han, Ch., Li, Xi., Zhou, H., Song, Xi., Zu, F. Study on Wood Chips Modification and its Effect on the Mechanical Properties of Wood-Cement Composite Material. SSRN Electronic Journal. 2022. DOI: 10.2139/ssrn.4020085
- 16. Hill, C., Stevens, C.V. Wood Modification: Chemical, Thermal and Other Processes. John Wiley and Sons, Ltd, 2006. 239 p.
- 17. Altgen, M., Adamopoulos, S., Militz, H. Wood defects during industrial-scale production of thermally modified Norway spruce and Scots pine. Wood Material Science & Engineering. 2017. 12. Pp. 14–23. DOI: 10.1080/17480272.2014.988750
- 18. Boonstra, M.J., Van Acker, J., Kegel, E.M. Optimisation of a two-stage heat treatment process: durability aspects. Wood Science and Technology. 2007. 41. Pp. 31–57. DOI: 10.1007/s00226-006-0087-4
- 19. Cai, Ch., Heräjärvi, H., Haapala, A. Effects of environmental conditions on physical and mechanical properties of thermally modified wood. Canadian Journal of Forest Research. 2019. 49(11). Pp. 1434–1440. DOI: 10.1139/cjfr-2019-0180
- 20. Hill, C., Altgen, M., Rautkariauri, L. Thermal modification of wood a review: chemical changes and hygroscopicity. Journal of Materials Science. 2021. 56(11). Pp. 6581–6614. DOI: 10.1007/s10853-020-05722
- Militz, H. Thermal treatment of wood: European processes and their background. The 33rd annual meeting of The International Research Group on Wood Preservation, 12–17 May. Cardiff, 2002. 4. Pp. 1–17.
- 22. Hakkou, M., Petrissans, M., Gerardin, P., Zoulalian, A. Investigations of the reasons for fungal durability of heat-treated beech wood. Polymer Degradation and Stability. 2006. 91(2). Pp. 393–397. DOI: 10.1016/j.polymdegradstab.2005.04.042
- 23. Hasanshin, R.R. Thermal modification of wood filler in the production of composite materials. Doctoral dissertation. Kazan National Research Technological University, 2019.
- 24. Guo, A., Bu, A., Osama, A.O., Satyavolu, J., Sun, Zh. Impact of thermally modified wood on mechanical properties of mortar. Construction and Building Materials. 2019. 208. Pp. 413–420. DOI: 10.1016/j.conbuildmat.2019.03.016
- 25. Chernov, V.Yu., Gaisin, I.G., Palkin, A.A., Maltseva, E.M. The Concrete Based on TMW Filler: Features of the Material and Prospects of Use. Actual Problems and Prospects for the Development of the Timber Industry: Materials of the IV International Scientific-Practical Conference. Kostroma: Kostroma State University, 2021. Pp. 103–106.
- Chernov, V.Yu., Sharapov, E.S., Mal'tseva, E.M., Pegushina, E.N. Investigation of the effect of thermal modification of wood on the adhesive and strength properties of a wood-cement composition. Bulletin of MGSU. 2023. 18(9). Pp. 1394–1407. DOI: 10.22227/1997-0935.2023.9.1394-1407

Information about the authors:

Vasilii Chernov, PhD in Techhnical Sciences ORCID: https://orcid.org/0000-0001-9496-7340

E-mail: chernovvy@volgatech.net

Ilschat Gaisin, PhD in Techhnical Sciences ORCID: https://orcid.org/0000-0002-3707-1342

E-mail: GaisinIG@volgatech.net

Elena Maltseva,

E-mail: <u>kcm.amarant@mail.ru</u>

Anzelika Nosova,

ORCID: https://orcid.org/0009-0009-9788-9929

E-mail: NosovaAN79@mail.ru

Received 24.10.2023. Approved after reviewing 19.10.2024. Accepted 23.10.2024.



Magazine of Civil Engineering

ISSN 2712-8172

journal homepage: http://engstroy.spbstu.ru/

Research article UDC 532.517

DOI: 10.34910/MCE.131.8



Method of integrated consideration of factors for calculation of anchor system of pontoons

G.L. Kozinetc, V.L. Badenko 🗓 , D. Sharapov 🖾 🗓 , E.V. Shonina 🗓







Peter the Great St. Petersburg Polytechnic University, St. Petersburg, Russian Federation

Keywords: Neva Bay, hydraulic structures, wave load, ice load, wind load, pontoons, mooring system, information model

Abstract. The work is devoted to the study and analysis of hydrodynamic and climatic loads on hydraulic structures of the Neva Bay - the eastern part of the Gulf of Finland, which is exposed to significant anthropogenic and natural impacts. The geographical position of the Neva Bay, as well as the complex of flood protection structures of St. Petersburg, affect the predicted load levels. In these conditions, special attention is paid to the design and operation of pontoons and other hydraulic structures resistant to waves, ice cover and wind loads. The study calculated the wave-protective characteristics and stability of pontoons used in the Neva Bay as moorings for small vessels. The main parameters of wave loads were estimated using wave models, which made it possible to take into account irregular water oscillations and their effect on the dynamic behavior of structures. A test was carried out for the stability of pontoons with various configurations of anchor systems that ensure their fixation at a given point in the water area. The simulation showed that under conditions of irregular waves and changing water levels, floating structures experience significant loads that are distributed to the anchor system and require accurate calculations to ensure reliability. Additionally, ice and wind load on hydraulic structures, loads associated with thermal expansion of ice, changes in water levels, and wind effects were studied, taking into account the characteristics of ships of different lengths and above-water heights. The simulation results make it possible to identify key operating conditions for protective and berthing structures in the Neva Bay and provide information for inclusion in the information model of the water area, which will allow predicting the behavior of structures under changing natural and climatic conditions.

Funding: The study was supported by a grant from the Russian Science Foundation No. 23-19-20062 and the St. Petersburg Science Foundation, agreement No. 23-19-20062.

Citation: Kozinetc, G.L., Badenko, V.L., Sharapov, D., Shonina, E.V. Method of integrated consideration of factors for calculation of anchor system of pontoons. Magazine of Civil Engineering. 2024. 17(7). Article no. 13108. DOI: 10.34910/MCE.131.8

1. Introduction

The object of this work is the development and analysis of an anchoring system for pontoons designed to serve as mooring facilities for small vessels in the Neva Bay, located in the eastern part of the Gulf of Finland. This work addresses the engineering challenges associated with ensuring the stability and durability of pontoon structures under variable environmental loads, including wave, wind, and ice pressures, as well as the effects of erosion and sedimentation.

The study focuses on creating an information model that considers the hydrodynamic and climatic conditions specific to Neva Bay, with an emphasis on developing mathematical models for predicting the behavior of waves and currents under changing external conditions. The research highlights the

© Kozinetc, G.L., Badenko, V.L., Sharapov, D., Shonina, E.V., 2024. Published by Peter the Great St. Petersburg Polytechnic University.

advantages of pontoons over fixed structures, including their adaptability to water level changes and ease of relocation, and investigates the mechanics and durability of anchoring systems under diverse loading conditions. This involves calculations of anchor fastenings, analysis of mooring systems, and assessment of potential structural defects in the anchoring devices.

The aim of this work is to provide a scientifically grounded approach to optimizing the stability and operational characteristics of pontoons, specifically for applications in a harbor near Kotlin Island. The findings contribute to enhancing the reliability and safety of floating hydraulic structures in coastal areas subject to intensive shipping and high anthropogenic impact.

Hydraulic structures play a key role in the development of coastal infrastructure, providing protection of coastal areas and objects from the impact of natural factors, such as waves, currents, ice and wind. This issue is especially relevant for water areas with intensive shipping and a high degree of anthropogenic impact, which includes the Neva Bay. This is a water area in the eastern part of the Gulf of Finland of the Baltic Sea, located between the Neva River delta and Kotlin Island. Its unique location and specific hydrological regime necessitate the use of complex engineering solutions, such as the St. Petersburg Flood Protection Complex, which provides reliable protection of the city from rising water levels [1, 2]. However, the creation and operation of such structures require a comprehensive analysis and consideration of many natural and man-made factors, which makes the development of an information model of the Neva Bay an urgent scientific and practical task. A special feature of the Neva Bay is its relatively limited water space, which changes as a result of anthropogenic factors and natural processes, such as erosion and sedimentation. The construction of protective and mooring structures affected the bottom relief, the speed and direction of currents, as well as the wave regime of the water area, which in turn affected the overall stability of hydraulic structures. In this regard, it becomes necessary to conduct a detailed study of the hydrodynamic and climatic loads affecting various types of structures, as well as an assessment of their durability and operational characteristics. A key element of such studies is the development of information and mathematical models that allow forecasting the behavior of waves and currents in the water area when external conditions and parameters of structures change [3, 4].

The development of information technologies and numerical modeling methods has made it possible to analyze and predict in more detail the dynamic interaction of water with various hydraulic structures. Modern mathematical models are capable of taking into account complex factors, such as irregular wave processes, wind loads, thermal expansion of ice and other mechanisms that create loads on structural elements [5, 6]. One of the main approaches to wave modeling is the use of models, which allows describing wave loads based on the amplitudes and phase characteristics. It allows taking into account the influence of all the main components of waves on floating structures and anchor systems used to secure them at a given point in the water area. Of particular interest for the Neva Bay are studies of wave and ice loads on pontoons intended for use as berths for small vessels. The advantages of floating structures over stationary ones are due to their ability to adapt to changes in water levels and mobility, which is especially important in coastal waters with high wave amplitudes. However, floating structures require additional calculations to ensure their stability under conditions of time- and space-varying loads. Particular attention should be paid to the mooring systems that hold the pontoons in a given position and limit their horizontal movements. These systems, represented by anchor chains and cables, experience significant loads when the water level changes, when the waves and wind oscillate, and when there is ice cover. The reliability of such systems is determined by the strength of the anchor ties, their resistance to corrosion and wear, and the ability to withstand short-term overloads without damage.

This work provides for the calculation of the anchor fastening system for pontoons. Pontoons can be used for various purposes. They are usually considered as floating berths [7], breakwaters [8, 9], foundations for offshore wind turbines [10], photovoltaic systems [11] and other structures. In this case, the pontoon is considered as a place for small vessels to moor in the harbor near Kotlin Island. At the same time, floating berths for ships have a number of advantages compared to stationary structures. They are less susceptible to fluctuations in water levels, do not depend on the state of the seabed, and are also mobile and easily relocatable structures. Pontoons used as berthing hydraulic structures can have different configurations depending on the size of the water area and mooring vessels. Pontoons can be considered as separate berths, as well as combinations of modules (pontoons) of different shapes and sizes. In addition, pontoons can be secured at a point in the water area using an anchoring system in the form of steel chains or synthetic cables, as well as using piles that limit horizontal movements [12]. The interaction of waves and currents with moored pontoons of various shapes and configurations, an assessment of the influence of their shape, direction of waves and the reaction of anchor ties are presented in works [13–16]. The authors of [17] study the behavior of floating moored structures under the influence of regular waves. The influence of irregular waves on the hydrodynamic reactions of floating objects is shown in studies [11, 18]. Methods of numerical hydrodynamic modeling are considered by the authors in work [19], where the influence of currents caused by tsunamis on pontoons with anchor ties is studied. A moored pontoon is installed in a coastal harbor, with the maximum wave height set by design standards at 0.3 m. Such a wave

is ensured under conditions of constructing protective moles, which is what is proposed in the study. Paper [19] provides an example of performing a destruction analysis in the event that protective moles are not constructed. At the same time, some authors study the dynamic characteristics of pontoons under the influence of irregular and regular waves using model tests [20, 21], comparing the results with numerical calculations.

In addition to the problems associated with the impact of external loads on floating structures, it is necessary to take into account the operation of the mooring system. Floating structures are subject to time-varying loads from waves and wind. Anchor fastening systems hold the structures at a given installation point and limit their movements, taking up loads. At the same time, the connections must avoid sagging, which can lead to sudden jerks and damage to the structure [22].

The working and ultimate indicators of the state of the anchor device of pontoon berths are characterized by a number of possible defects: rupture of anchor chains/ropes, shift of anchors, mechanical and corrosive wear of anchor chains/ropes and fastening elements. At the same time, to ensure a working condition, rupture of anchor connections is not allowed; the ultimate state is characterized by rupture of one element [23].

This research is highly relevant due to the increasing need for reliable coastal infrastructure in areas exposed to intense natural and anthropogenic forces. Pontoons, a key focus of this research, offer unique advantages in such variable conditions. Their mobility, adaptability to water level fluctuations, and ease of installation make them particularly suitable for berthing and protective structures in dynamic coastal environments. Consequently, a detailed study of their anchoring systems is essential to ensure the structures can withstand these conditions while minimizing maintenance and damage over time.

The main goal of the research is to develop a reliable and scientifically validated anchoring system for pontoons, specifically tailored to the conditions of the Neva Bay. This system must ensure the stability and durability of the pontoons under diverse environmental stresses, thereby supporting safe and effective berthing options for small vessels. To achieve this goal, the research is organized around the following tasks:

- 1. Develop a numerical model for wave load calculations and conduct detailed numerical calculations of wave loads and dynamic characteristics of anchor ties using modern modeling approaches to enhance hydraulic engineering applications for pontoons.
- 2. Utilize model data to develop strategic placement plans for floating structures, enabling accurate prediction of their behavior under varying conditions, such as irregular waves and currents.
- 3. Create a tailored information model that reflects the unique hydrodynamic and climatic characteristics of the Neva Bay, ensuring reliable and safe operation of moorings for small vessels.
- 4. Implement advanced methods, such as the spatial radiation source method, to predict wave loads and optimize anchor system parameters in complex water areas like the Neva Bay.
- 5. Perform calculations to establish different external impact scenarios, such as wave heights of 1.1 m and 0.5 m, to identify suitable water areas for placing ship berths within the Neva Bay.
- 6. Design and test the anchor fastening system for pontoons in a protected part of the Neva Bay under maximum wave height conditions, ensuring it holds the structure securely and absorbs loads effectively.
- 7. Define specific operational conditions for the protected part of the Neva Bay to support reliable mooring functionality based on the anchor system testing.
- 8. Assess the suitability of Kupecheskaya harbor as a mooring site for pontoons, focusing on its protection from high waves.
- 9. Develop a generalized design framework for floating structures that can be adapted to other coastal sites, accounting for site-specific hydrodynamic conditions and environmental impacts.

The development of fastening systems is an important task to ensure the reliability and safety of the structures. This problem is solved within the framework of the development of an information model that makes it possible to assess and take into account changes in the natural and climatic characteristics and geometric parameters of the Neva Bay. A forecast of the wave regime of the water area, taking into account the location of protective and berthing structures, allows one to select a location for the mooring of small vessels and conduct further mathematical modeling using the example of a specific structure in a harbor determined in advance by calculations.

2. Methods

In order to solve the set problems of hydrodynamic and climatic loads on hydraulic structures in the protected part of the Neva Bay water area, a comprehensive methodology was used, including the collection of data on the wave regime, during which data on the wave activity of the water area was collected based on observations, model tests and calculations. Spectral wave models can be used to represent irregular waves with two calculated wave heights in the fairway area. Wave load modeling was carried out in software packages capable of taking into account irregular waves. For this purpose, numerical methods of hydrodynamic modeling (finite element method or spatial radiation source method) were selected. Based on the wave spectrum using superposition of harmonic components, wave loads were calculated in six degrees of freedom for each element of the structure. Temperature expansion of the ice cover was determined based on climatic and temperature conditions of the region. The calculations were based on stresses from a solid ice cover formed during its thermal expansion, taking into account its strength and adhesion to the structure. Ice freezing to the structures and its effect during water level fluctuations were taken into account. The wind load was calculated taking into account the length of the object and for several heights of the above-water part. The calculation was performed for the wind speed acting on the surface of the object in the worst position. The wind load was estimated using the flow resistance formula for the calculated section, based on the aerodynamic characteristics and the general projection of the vessel. To analyze the impact of the ice cover on the outer mole, a method for calculating ice loads for a flat ice field interacting with the outer southern mole of the Coastal harbor was used. Based on the strength characteristics of the ice and the contact area of the mole, the maximum load was determined. The calculations were performed taking into account the possibilities of ice destruction and the resistance of the mole material. Verification dynamic calculations of wave loads were made for two variants of wave action in order to take into account different directions and amplitudes of waves. Two scenarios were used to test the stability of the structures: one for typical wave conditions of the water area, the second for extreme ones. Based on the data obtained, the required strength and stability of the piers and pontoons under maximum wave conditions were estimated. Mathematical modeling is carried out in the Anchored Structures PC, according to the methodology proposed by the authors [24]. The software package calculates loads from external influences. An irregular wave is represented as a set of elementary harmonic waves. After setting the wave spectrum, the wave loads from each harmonic of the wave spectrum were calculated (taking into account its direction, magnitude and phase).

Wave load vector on a structure in six degrees of freedom $F_w(t) = (F_{w1}, ... F_{wj}, ... F_{w6})$, time-dependent, is defined in this case as a superposition of the loads of individual components of the wave spectrum [25]:

$$F_{w}(t) = \sum_{i=1}^{N} F_{wi}(\omega_{i}) \sin(w_{i}t + \varphi_{i}), \tag{1}$$

where F_{wi} is vector of amplitudes of loads and moments from the $i^{\,\text{th}}$ harmonic of the wave spectrum; t is time; ω_i is the circular $i^{\,\text{th}}$ harmonic; ϕ_i is the phase of the $i^{\,\text{th}}$ harmonic of the load spectrum; N is the number of harmonics.

Thus, to simulate the dynamic behavior of a structure in waves in the Anchored Structures software package, it is necessary to determine the wave load vector F_w and hydrodynamic parameters of the structure (λ – matrices of added masses and B – matrix of wave resistance coefficients) for each specific frequency of the wave spectrum. To obtain theoretical values of these parameters for different spectrum frequencies, a variation of the widely known method of hydrodynamic features was used – the method of spatial radiation sources. This method is based on obtaining the reflected and incident wave potentials and integrating the resulting liquid pressures over the wetted surface of the structure. Calculation of stresses in the anchor ties was performed by a quasi-static method, the tension and trajectory of the line are a function of the position of the hawse point of the structure. When calculating the anchor ties, their stretching is taken into account, as well as the possibility of laying part of the tie on the bottom of the water area.

To calculate the rigidity characteristics of the anchor ties, an analytical solution of the equations of a freely sagging flexible heavy and stretchable tie was used. This method was developed by the authors of the Anchored Structures software package, was widely tested in the calculations of anchor ties of floating structures and showed high accuracy and reliability of the calculations [24]. The method allows calculating the vertical and horizontal components of the tie tension at an arbitrary position of the hawse point. The

software package constructs the rigidity characteristics of all ties; the general multidimensional piecewise linear rigidity characteristic of the entire retention system is presented as:

$$F_{R}(X_{c}, L_{1}) = \sum_{j=1}^{N} C_{j} \left(T_{j} \left(B_{jx}(X_{c}), B_{jz}(X_{c}) \right) \right), \tag{2}$$

where X_c is vector of displacements of the structure in six degrees of freedom; $B_{jx}\left(X_c\right)$, $B_{jz}\left(X_c\right)$ are operators that allow based on a vector X_c calculate the vertical and horizontal coordinates of the hawse points of an arbitrary j^{th} connection; L_1 is vector of lengths of the first (upper) sections of connections; T_j is an operator that calculates the reaction of each connection based on its stiffness characteristics and the coordinates of the hawse point; $C_j\left(T_j\right)$ is operator that transforms the reaction of the j^{th} link into a reaction vector relative to the center of gravity of the structure; N is number of connections. Thus, the operator of the connection reaction allows us to obtain a reaction relative to the center of gravity of the structure in six degrees of freedom at an arbitrary position of the center of gravity with the ability to control the reaction using the vector L.

3. Results and Discussion

The parking of small vessels is regulated by Russian State Standard GOST R 58736-2019 "Moorings of small vessels. General requirements". According to paragraph 6.1.8 of GOST R 58736-2019: "The creation of wave protection structures is recommended in cases where the normal average annual wave height in an unprotected water area exceeds 0.3 m." At the same time, according to the calculations carried out by the authors, in the considered protected part of the Neva Bay water area, only the Kupecheskaya harbor is suitable for the parking of small vessels. In the Kabotazhnaya harbor, according to the calculations performed, the maximum waves are 0.4–0.6 m. Verification dynamic calculations of wave loads and wave amplitude was 0.7 m, the full wave was 1.4 m. The calculations are made for waves from ships that are sailing along the fairway. These waves are the maximum and spread in the direction of the Kabotazhnaya harbor, since the fairway is in close proximity to the harbor.

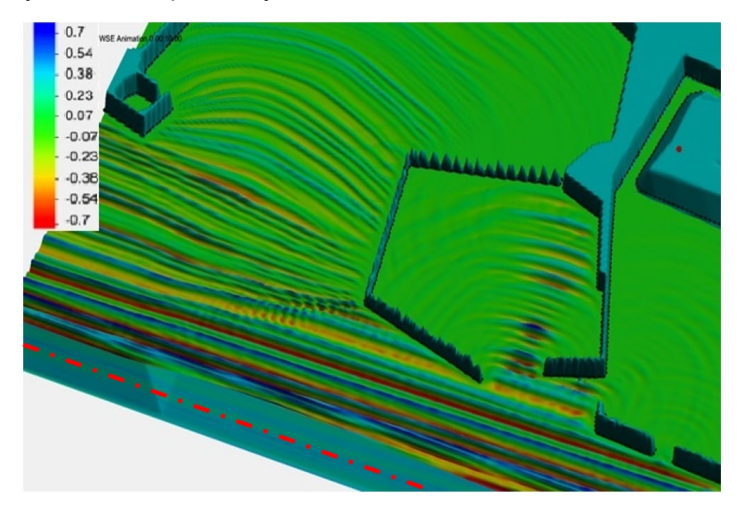


Figure 1. Result of wave height calculation in Kabotazhnaya and Kupecheskaya harbors (option 1).

The wave height in the Fig. 1 consists of two wave amplitudes, since the zero axis is taken as the water level in the Baltic system. The fairway axis is shown in the figure with a dashed line. The color scale corresponds to the wave height (m). For detailed examination, a fragment of the figure in the Harbor behind the protective mole is presented. The wave completely fades toward the shore. The recommended wave height is 0.3 m according to clause 6.1.8 of GOST R 58736-2019.

The wave calculation is performed for the wave direction from the vessel's passage along the fairway. The points of output of the results are presented in Fig. 2, which shows the results of the calculation of the wave height and loads in the Kabotazhnaya and Kupecheskaya harbors. Fig. 2 shows 11 calculation points, in which the wave height in meters (ETA) and the wave load in kN/m are determined for a calculation period of 600 s.

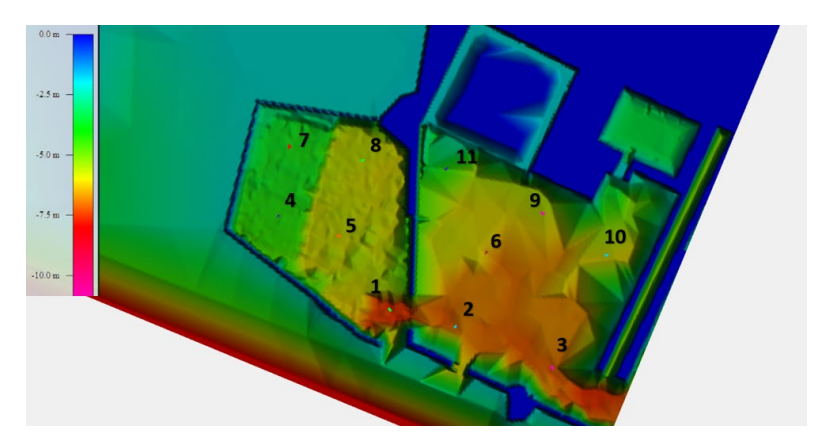


Figure 2. Layout plan of settlement points in Kabotazhnaya and Kupecheskaya harbors.

Table 1 shows the maximum values of wave height and the force of its impact at each calculation point. The given load values do not take into account the streamlining of the object.

Table 1. Maximum values of wave height and force at the moment of time at the calculated points.

No. of calculated point	Maximum wave height, m	Maximum force from wave, kN/m	Time, s
1	0.41	748	280
2	0.4	600	280
3	0.28	600	470
4	0.27	140	520
5	0.28	363	480
6	0.28	470	480
7	0.16	99	490
8	0.22	347	360
9	0.25	371	499
10	0.22	326	360
11	0.4	150	325

A pontoon for mooring small vessels is located in the Kupecheskaya harbor of Kotlin Island. The depth of the water area at the mooring point is 10 m.

A rectangular concrete pontoon in plan is adopted for mooring small vessels. Vessels are moored directly to the pontoon. The characteristics of the pontoons are presented in Table 2.

Table 2. Characteristics of pontoons.

Type of pontoon	Dimensions, L×W×H m	Freeboard height, m	Displacement, t
1	9 × 2.4 × 1.07	0.49	10.1
2	12 × 2.4 × 1.07	0.54	15.0
3	15 × 2.4 × 1.07	0.56	19.7
4	12 × 3.16 × 1.07	0.58	21.3
5	15 × 3.16 × 1.07	0.61	27.9
6	15 × 4.2 × 1.07	0.64	38.8

The pontoon is attached to the bottom of the water area using four 19 m long synthetic ropes on dead anchors. The characteristics of the anchor connections are presented in Table 3.

Table 3. Characteristics of pontoons.

Туре	Quantity	Linear weight, kN/m	Breaking strength, kN
Anchor connections (rope)	4	0.159	1307

Dead reinforced concrete anchor with a vertical holding force (anchor weight) of at least 200 kN - 4 pcs.

Mathematical modeling for the design cases was carried out in the Anchored Structures PC. The software package calculated loads from irregular waves. The Anchored Structures PC allows you to calculate: ballasting, stability; anchoring and positioning systems; wind, current, wave and ice loads; structure dynamics; floating object dynamics during offshore operations; anchor and mooring tie dynamics. After calculating all the necessary hydrodynamic parameters of structures, the program begins directly modeling the dynamics in the frequency domain. Next, a static problem is solved for structures with anchor or mooring tie (the rest are in the initial position). After that, the tie calculations (if any) are performed. Then, the problem is solved in the frequency domain for each harmonic. Next, the static problem is solved taking into account the real force of wave drift in a given wave mode. Then, an iterative solution of the problem is performed in the frequency domain for each harmonic of the real wave spectrum taking into account the viscous quadratic resistance approximated by a linear one for a given oscillation amplitude for each degree of freedom.

Modeling was carried out for two situations: calculating a floating structure for a wave height of 1.1 m, as well as for a wave height of 0.5 m. Accordingly, the impact of waves was modeled: 1) the height of waves with 3 % probability is 1.1 m, the average wave period is 4.7 s and 2) the height of waves with 3 % probability is 0.5 m, the average wave period is 2.8 s.

The calculated directions of wave propagation: 90°, 135°, 180° are shown in Fig. 3.

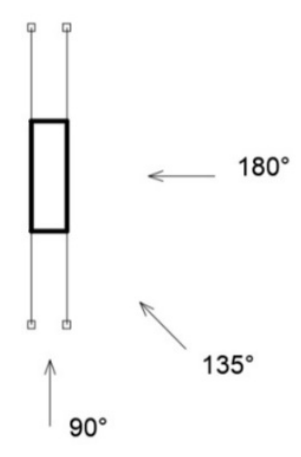


Figure 3. Directions of propagation of excitement.

The model of a floating structure with an anchoring system, defined in the Anchored Structures PC, is shown in Fig. 4.

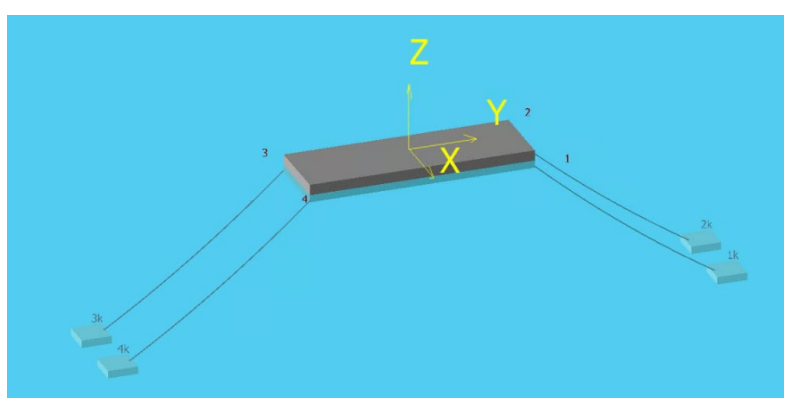


Figure 4. Model of a floating structure. General view.

The modeling task is to calculate the anchoring system for a floating berth structure and the pontoon movements. For this purpose, the calculation of external wave loads on the floating berth was performed in the Anchored Structures software package.

The results of modeling the structure's behavior under the influence of waves from the adopted directions of load propagation are presented in Table 4 (the worst cases for each direction). The results are presented for pontoons with dimensions of $9 \times 2.4 \times 1.07$ (type 1) and $15 \times 4.2 \times 1.07$ (type 6).

Table 4. Security values for pontoon types 1 and 6 (the worst values for each direction are indicated).

Calculation of a	a floatin	g structı	ire for a	wave of 1	.1 m	
Type of pontoon	1	1	1	6	6	6
Direction of excitement	135	180	90	135	180	90
Pontoon displacement, m	1.03	1.7	1.3	4	6.2	5.1
Vertical displacement, m	0.48	0.43	0.35	1.9	1.9	1.3
Roll, degree	2.5	0.5	2.5	9	2	9
Trim, degrees	9.03	13.02	4.5	34.02	50	18.1
Yaw, hail	5.6	1.8	3.4	22	7	13
K₃ anchor ties (worst)	2.9	3.8	5.04	10.2	15	20.01
Tie No.	3	2	4	3	2	4
K₃ mooring ties (worst)	1.46	1.9	3	5.6	7.2	11.8
Tie No.	1	1	1	1	1	1
Horizontal force on anchor, kN	120	101	80	470	400	320
Anchor No.	4	3	3	4	3	3
Calculation of a	a floatin	g structu	ıre for a	wave of 0).5 m	
Type of pontoon	1	1	1	6	6	6
Direction of excitement	135	180	90	135	180	90
Pontoon displacement, m	0.5	1.08	0.42	2	4	1.6
Vertical displacement, m	0.21	0.21	0.12	0.84	0.84	0.84
Roll, degree	0.7	0.7	1	2.8	2.8	4.1
Trim, degrees	4.42	6.23	2.09	17.6	24	8.1
Yaw, hail	4.5	5.5	2.6	18	22	10.4
K₃ anchor ties (worst)	7.7	5.8	60.3	30.8	23.2	240
Tie No.	1	1	4	1	1	4
K₃ mooring ties (worst)	3.1	2.4	5.5	12.4	9.6	22
Tie No.	1	1	1	1	1	1
Horizontal force on anchor, kN	52	60	8.5	208	240	34
Anchor No.	1	1	4	1	1	4

For comparison and juxtaposition, it is possible to select similar structures and methods, since the structure in question has not previously been calculated using the method in question. Mostofi & Bargi (2012) focused on new analysis concepts for floating piers' response to ship berthing impact [12]. Both studies highlight that robust anchoring systems are vital to maintain stability in areas exposed to wave loads, but this research specifically modeling wave impacts of 1.1 and 0.5 m for protected harbors like Kupecheskaya. Lamei, Li, & Hayatdavoodi (2023) explored wave-current interactions for floating objects with square and circular waterplane areas, discovering that shape plays a critical role in dynamic stability [13]. This research corroborates these findings by focusing on rectangular pontoons and analyzing their response to wave conditions typical of Neva Bay, suggesting that customized pontoon design can reduce instability in complex hydrodynamic environments. Tajali & Shafieefar (2011, 2008) performed hydrodynamic analyses of multi-body floating piers, focusing on wave actions in complex marine conditions [15]. Their results suggest that multi-body interactions and spatial wave action analysis improve structure resilience. Claus & Lopez (2022) [14] and Zeng & Bi et al. (2023) [22] examined floating structures in renewable energy settings, noting that durable mooring systems and wave-resistant designs are crucial for long-term stability in marine environments. This research supports the relevance of these findings by demonstrating that the Kupecheskaya harbor's sheltered location and tailored pontoon design make it suitable for small vessel parking, mitigating wave impacts and enhancing durability. Chen et al. (2022) [17] and Huang et al. (2023) [20] conducted numerical simulations to predict wave dissipation and dynamic responses for floating structures under long-period waves, noting that such modeling can anticipate wave impacts effectively. In the current research, similar numerical simulations were conducted with the Anchored Structures software, offering tailored insights for the Neva Bay's specific wave conditions, which also address dynamic wave behaviors and maximum load conditions. Garibin, Egorov & Butsanets (2023) explored floating berths' practical deployment in yacht marinas, emphasizing site-specific mooring requirements. Similarly, this research verifies the suitability of Kupecheskaya harbor for small vessel parking [23].

4. Conclusions

- 1. The numerical calculation of wave loads and the dynamic characteristics of anchor ties using modern approaches is a significant advancement for hydraulic engineering technologies applied to floating pontoons.
- 2. The data presented enable informed planning for the placement of floating structures and provide a basis for predicting their behavior under irregular waves and currents.
- 3. Introducing a model adapted to the specific conditions of the Neva Bay and detailing wave impact parameters ensures reliable operation of moorings for small vessels, enhancing both the safety and durability of these structures.
- 4. The modeling and calculation methods considered, allow for accurate prediction of wave loads and optimization of anchor system parameters, which is especially crucial for complex water areas like the Neva Bay.
- 5. Calculations performed as part of the Neva Bay information model identified suitable areas for placing ship berths and allowed for two modeling scenarios: one with a wave height of 1.1 m and another with a wave height of 0.5 m.
- 6. The anchor fastening system for a pontoon in a protected part of the Neva Bay was tested under two modeled scenarios, taking into account maximum wave heights; the anchor fastening reliably secures the structure and absorbs the acting loads.
- 7. Operational conditions for the selected protected part of the Neva Bay water area were formulated based on these tests.
- 8. The study confirms that Kupecheskaya harbor is a suitable location for a pontoon due to its protection from high waves.
- 9. The proposed approach to the design of floating structures is adaptable to similar projects, especially those requiring detailed analysis of hydrodynamic conditions specific to the installation site.

References

- Ryabchuk, D.V., Nesterova, E.N., Zhamoida, V.A., Kotilainen, A., Vallius, G., Sukhacheva, L.L., Spiridonov, M.A. Dynamics of Sedimentation Processes in the Neva Bay (the Gulf of Finland) under Influence of Anthropogenic Factors. Proceedings of the Russian State Hydrometeorological University. 2014. 35. Pp. 102–118.
- Rodionov, V.Z. Kompleks zashchitnykh sooruzheniy Sankt-Peterburga ot navodneniy: istoriya i ekologicheskiye problem [Complex of protective structures of St. Petersburg from floods: history and environmental problems]. Regional Ecology. 2016. 4. Pp. 13–23.
- 3. Badenko, V.L., Zotov, D.K., Kozinets, G.L., Kozinets, P.V., Chernov, P.V. Digital models for retrospective analysis of the structure of currents in Neva Bay. Magazine of Civil Engineering. 2023. 124(8). Article no. 12411. DOI: 10.34910/MSE.124.11
- 4. Kozinets, G.L., Badenko, V.L., Zotov, D.K. The influence of anthropogenic load on changes in the morphology of the Neva bay bed in the XIX–XXI centuries. Power Technology and Engineering. 2024. 1. Pp. 43–52.
- Andreeva, S.A., Sharapov, D. Hoek–Brown model for ice breaking simulation. Magazine of Civil Engineering. 2023. 123(7).
 Article no. 12303. DOI: 10.34910/MCE.123.3
- 6. Sharapov, D.A., Sumtsova, A.S. Rockfill Stability to Ice Shearing by the Finite Element Method. Power Technology and Engineering. 2023. 57. Pp. 228–232. DOI: 10.1007/s10749-023-01646-1
- 7. Pryanichnikov, K.N., Sharonova, M.I. Designing moored floating berths for the operating conditions in the Black Sea. Bulletin of VSAWT. 2013. 34. Pp. 68–74.
- 8. Dai, J., Wang, C.M., Utsunomiya, T., Duan, W. Review of recent research and developments on floating breakwaters. Ocean Engineering. 2018. 158. Pp. 132–151. DOI: 10.1016/j.oceaneng.2018.03.083
- Blagovidova, I.L., Tertyshnikova, A.S., Babak, A.S., Balagurak, A.V. A floating breakwater design for the protection of LNG terminal and FLNG. The Hydrotechnika. 2024. 2(75). Pp. 28–33.
- Alkarem, Y.R., Ozbahceci, B.O. A complemental analysis of wave irregularity effect on the hydrodynamic responses of offshore wind turbines with the semi-submersible platform. Applied Ocean Research. 2021. 113. Article no. 102757. DOI: 10.1016/j.apor.2021.102757

- Daniel, H.H., Haryo, D.A., Fandy, A.R. Geometric analysis of pontoon and mooring line towards hydrodynamic response. E3S Web of Conferences. 2024. 499. Article no. 01015. DOI: 10.1051/e3sconf/202449901015
- 12. Mostofi, A., Bargi, K. New concept in analysis of floating piers for ship berthing impact. Marine Structures. 2012. 25(1). Pp. 58–70. DOI: 10.1016/j.marstruc.2011.12.001
- Lamei, A., Li, S., Hayatdavoodi, M., Riggs, H.R. Wave-Current Interaction With Floating Objects With Square and Circular Waterplane Areas. Proceedings of the ASME 2023 42nd International Conference on Ocean, Offshore and Arctic Engineering. 5. Ocean Engineering. Melbourne, 2023. Article no. V005T06A023. DOI: 10.1115/OMAE2023-105065
- 14. Claus, R., Lopez, M. Key issues in the design of floating photovoltaic structures for the marine environment. Renewable and Sustainable Energy Reviews. 2022. 164. Article no. 112502. DOI: 10.1016/j.rser.2022.112502
- Tajali, Z., Shafieefar, M. Hydrodynamic analysis of multi-body floating piers under wave action. Ocean Engineering. 2011. 38(17–18). Pp. 1925–1933. DOI: 10.1016/j.oceaneng.2011.09.025
- Tajali, Z., Shafieefar, M., Akhyani, M. Hydrodynamic analysis of multi-body floating piers. Proceedings of the ASME 27th International Conference on Offshore Mechanics and Arctic Engineering. 1. Offshore Technology. Estoril, 2008. Pp. 797–804. DOI: 10.1115/omae2008-57849
- 17. Chen, J., Zhang, J., Wang, G., Zhang, Q., Guo, J., Sun, X. Numerical simulation of the wave dissipation performance of floating box-type breakwaters under long-period waves. Ocean Engineering. 2022. 266(4). Article no. 113091. DOI: 10.1016/j.oceaneng.2022.113091
- 18. Barrera, C., Losada, I.J., Guanche, R., Johanning, L. The influence of wave parameter definition over floating wind platform mooring systems under severe sea states. Ocean Engineering. 2019. 172. Pp. 105–126. DOI: 10.1016/j.oceaneng.2018.11.018
- 19. Ozbahceci, B., Celik, H., Girgin, E. and others. Effect of tsunami induced currents on floating pontoons with the mooring lines. Coastal Engineering Proceedings. 2023. 37. Structures.20. DOI: 10.9753/icce.v37.structures.20
- 20. Huang, H., Chen, X., Ji, S., Miao, Y., Chen, X. Experimental and numerical study on dynamic responses of floating bridge under the shielding effect of a floating platform. Marine Structures. 2023. 89. Article no. 103379. DOI: 10.1016/j.marstruc.2023.103379
- 21. Loukogeorgakia, E., Lentsiou, E.N., Aksel, M., Yagci, O. Experimental investigation of the hydroelastic and the structural response of a moored pontoon-type modular floating breakwater with flexible connectors. Coastal Engineering. 2017. 121. Pp. 240–254. DOI: 10.1016/j.coastaleng.2016.09.002
- 22. Zeng, F., Bi, C., Sree, D., Huang, G., Zhang, N., Law, A.W.-K. An Adaptive Barrier-Mooring System for Coastal Floating Solar Farms. Applied Energy. 2023. 348. Article no. 121618. DOI: 10.1016/j.apenergy.2023.121618
- Garibin, P.A., Egorov, S.V., Butsanets, A.A. Some issues of surveying floating berths of yacht marinas. Vestnik Gosudarstvennogo universiteta morskogo i rechnogo flota imeni admirala S.O. Makarova [Bulletin of the Admiral Makarov State University of Maritime and Inland Shipping]. 2023. 15(5). Pp. 783–797. DOI: 10.21821/2309-5180-2023-15-5-783-797
- Bolshev, A.S., Frolov, S.A., Kuteinikov, M.A. Mathematical modeling of offshore floating facilities using "Anchored Structures" Software Package. Research Bulletin of the Russian Maritime Register of Shipping. 2013. 36. Pp. 68–90.
- Bolshev, A.S., Mikhalenko, E.B., Frolov, S.A. Matematicheskoe modelirovanie povedeniya morskih plavuchih sooruzhenij [Mathematical modeling of the behavior of marine floating structures]. Trudy SPBGTU [Works of SPBGTU]. 2007. 502. Pp. 252–274

Information about the authors:

Galina Kozinetc, Doctor of Technical Sciences

E-mail: kozinets gl@spbstu.ru

Vladimir Badenko, Doctor of Technical Sciences ORCID: https://orcid.org/0000-0002-3054-1786

E-mail: vbadenko@gmail.com

Dmitry Sharapov, PhD in Technical Sciences ORCID: https://orcid.org/0000-0001-8650-2375

E-mail: sharapov.dm@gmail.com

Ekaterina Shonina.

ORCID: <u>https://orcid.org/0000-0001-5292-7295</u>

E-mail: shonina ev@spbstu.ru

Received 31.08.2024. Approved after reviewing 26.10.2024. Accepted 28.10.2024.



Magazine of Civil Engineering

ISSN 2712-8172

journal homepage: http://engstroy.spbstu.ru/

Research article

UDC 624.04:531.391.3

DOI: 10.34910/MCE.131.2



Shotcrete based on composite cement using industrial waste

R.S. Fediuk ^{1,2} ^{1,2} R.V. Vavrenyuk ³, S.V. Klyuev ², L.S. Sabitov ⁴, V.P. Meshalkin ^{5,6}, S.V. Fedosov ⁴, T.B. Chistyakova ⁷

- ¹ Far Eastern Federal University, Vladivostok, Russian Federation
- ² Belgorod State Technological University named after V.G. Shukhov, Belgorod, Russian Federation
- ³ branch FGBU "TSNIIP Russian Ministry of Construction" DalNIIS, Vladivostok, Russian Federation
- ⁴ Moscow State University of Civil Engineering (National Research University), Moscow, Russian Federation
- ⁵ Mendeleev Russian University of Chemistry and Technology, Moscow, Russian Federation
- ⁶ A.N. Frumkin Institute of Physical Chemistry and Electrochemistry RAS, Moscow, Russian Federation

Keywords: composite, underground structure, reliability, seismic resistance, strengthening, technology, shotcrete

Abstract. Reinforced shotcrete was developed and studied for strengthening underground structures. The article novelty lies in the fact that for the first time shotcrete was developed using composite cements, including aluminosilicates from enriched ash-to-slag mixtures. Slight slump flow decrease (47 cm) was observed with aluminosilicate content of 35 wt. %. Effect of increasing compressive strength of shotcrete on composite cement was manifested in an increase in content of aluminosilicates to 35 wt. (56% higher) and 62% higher flexural strength. This is confirmed by the high ratios of strength properties on the first day to those at 28 days of age: compressive strength 0.27 (0.23 for clinker compositions without additives), flexural strength 0.30 (0.26 for clinker compositions). Effectiveness of using the developed shotcrete concrete for strengthening load-bearing structures of underground objects was proven with increase in strength by more than 2 times, which is explained by both high strength of the resulting repair composition and monolithic contact zone between old and new concrete layers. Developed shotcrete is capable of providing the necessary degree of strengthening of load-bearing structures of underground objects, and thickness of the repair layer is 6 cm (with proper soil consolidation) allows using of underground structures as protective objects.

Funding: The work was supported by the RSF project No. 21-79-30029 "Development of technologies set for processing waste of hazard classes 3-5 with the production of useful products" and was carried out in the world-class laboratory of the St. Petersburg State Technological Institute

Citation: Fediuk, R.S., Vavrenyuk, S.V., Klyuev, S.V., Sabitov, L.S., Meshalkin, V.P., Fedosov, S.V., Chistyakova, T.B. Shotcrete based on composite cement using industrial waste. Magazine of Civil Engineering Simplified method for estimating the first natural frequency of a symmetric arch truss. Magazine of Civil Engineering. 2024. 17(7). Article no. 13102. DOI: 10.34910/MCE.131.2

1. Introduction

Currently, there is a significant impact of anomalous natural and man-made impacts [1], [2]. Natural disasters claim the lives of tens of thousands of people (for example, the earthquake in Turkey and Syria

in February 2023), and the negative impact of regional and local conflicts leads to a significant increase in losses among the civilian population. [3], [4]. At the same time, they mainly fall on the civilian population, concentrated in large settlements. In recent years, about 40 military clashes have been observed annually [5], [6]. From year to year, the "arms race" significantly increases the losses among civilians [7], [8]. For comparison, during the years of World War I, the share of civilian casualties did not exceed 5%, in World War II, civilians already accounted for half of the losses, and in Korean and Vietnam Wars (84% and 90%) generally scaring from these figures [9], [10]. It should be noted that the maximum losses are experienced by civilians in large cities [11], [12].

Russian cities currently accommodate 3/4 of the population of the state, while every sixth citizen of the country lives in a millionaire city [13]. In addition to defeating the population, a potential adversary considers cities that are industrial, scientific or cultural centers to be the objects of his aggression [14], [15].

The Accounts Chamber of the Russian Federation [16] announced disappointing figures that 95% of domestic civil defense facilities are not able to accommodate sheltered people due to poor technical condition. Therefore, an important scientific and practical task for increasing the defense capability of the state as a whole and preserving the life and health of citizens is the improvement of constructive methods for the complex repair of underground structures, fixing soils and strengthening load-bearing structural elements [17].

In modern design solutions, it is impossible to increase seismic resistance only by increasing the cross-sections, strength, and weight [18]. The design may be stronger, but not necessarily cost effective, because both the weight and the inertial seismic load may increase even further [19]. New effective methods of seismic protection are required [20]. These methods involve changing the mass or stiffness or damping of the system depending on its displacements and velocities [21].

At the same time, urban planning requirements for the bearing capacity for the construction of civil facilities in non-seismic areas are significantly lower [22]. In particular, various modern methods of seismic protection have not yet been fixed in codes [23]. They should use various techniques to reduce inertial forces in the system: changing the mass and rigidity of individual structures or parts of the building, damping the system, creating inertial masses that oscillate in antiphase with the frame, etc. [24].

At the same time, a significant number of existing and under construction building structures do not comply with current seismic standards, and some of them are at an unacceptable level of seismic risk, that is, unreliable, which greatly affects their protective functions [25]. This is due to the fact that seismic zoning in some cases is underestimated, or was underestimated earlier during the construction of buildings. In addition, there is a need for seismic monitoring of underground structures, such as military, or currently especially research facilities, such as accelerator complexes [26].

Strengthening of soils containing an underground protective object (plugging) consists in the formation of an injected volume that can effectively withstand external pressure [27], [28]. The dimensions of this volume are calculated taking into account the current bearing capacity of the structures of the underground structure and the type of injection mortars used [29], [30].

It is advisable to strengthen the bearing structural elements of underground protective objects, basement floors (foundations) of buildings with shotcrete (sprayed concrete) along the reinforcing cage [31], [32]. At the same time, the effective thickness of the sprayed concrete layer reaches 20 cm [33], [34], a further increase in thickness significantly complicates the technological process and reduces the adhesion strength with the strengthened supporting structure [35], [36].

At the same time, the method and degree of amplification are calculated after an individual assessment of each object, taking into account the calculation of the load from the shock wave (explosion force, distance from the source of the explosion to the object, repayment of the impact force, taking into account the resistance of the soil (clay, sandstone, bulk soil), the presence of laid communications, direct interaction "wall - strong rocks" when using bored wells as the main walls of an underground facility.

The bearing structures of underground structures work both in compression and in bending (due to the lateral pressure of the soil) (Fig. 1) [37]. The choice of wall thickness depends on the type of materials used and the design scheme of the structure [38]. A monolithic reinforced concrete wall is the best option in terms of strength, durability and resistance to soil pressure [39]. In particular, a monolithic reinforced concrete wall is more stable, reliable and durable than a prefabricated one made of blocks or bricks [40]. If the supporting structures of the underground structure are built from small-sized block products (in particular, expanded clay concrete), then the masonry must necessarily be reinforced with longitudinal reinforcement and armored belt laid along the upper border of the block masonry (Table 1) [41]. The use of precast concrete blocks for underground structures has a lower limit of concrete grade C10 (C - concrete, 10 - compressive strength 10 MPa) [42].

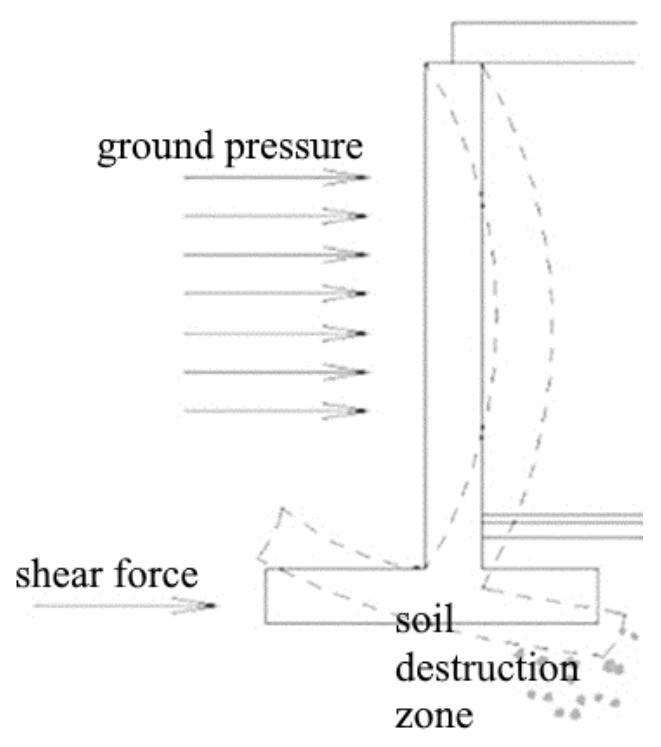


Figure 1. Effects on underground facilities

Table 1. Structural wall dimensions.

Material	Floor he	eight, m	Minimum wall	Providing a degree of		
	No side support	Side support	thickness, cm	protection against overpressure, kPa		
Monolithic concrete of strength grade not less than C12.5	2	2.8	35	25		
Monolithic concrete of strength grade not less than C15	2	2.8	30	30		
Stone and concrete blocks	2	3	34	20		

According to Table 1, the minimum thickness of the wall of underground structures according to the requirements of building codes is 30 cm, which should be taken into account when creating calculation models to assess the effectiveness of underground structures as protective ones [43]. The thickness of the wall will also depend on the class of concrete, soil pressure and the shape of the structure (round, arched, rectangular, etc. [44] To strengthen the load-bearing structures of underground structures, a material is needed that, with a small thickness, is capable of providing a significant increase in the load-bearing ability [45]. This requirement arises from the need to strengthen the walls of underground structures from the inside, which leads to some reduction in the internal area and volume [46].

The purpose of the work is to develop a scientifically based technological solution that ensures the production of composite cement and shotcrete based on it. The tasks to achieve this purpose are:

- 1. Develop shotcrete using composite cements, including aluminosilicates from enriched ash and slag mixes.
- 2. Achieve uniform flowability of shotcrete concrete by varying the dosage of a superplasticizer, which has a high water-reducing ability.
- 3. Increase the compressive strength of shotcrete through the use of composite cement.
- 4. Theoretically and practically prove the effectiveness of using the developed shotcrete for strengthening the load-bearing structures of underground structures.

2. Materials and Methods

2.1. Raw Materials Characterization

Cementation is the consolidation of soils using materials based on Portland cement. At the same time, minimization of cement consumption through the use of composite cements is a modern trend in

environmental safety and resource saving. The basis of composite cement is Portland cement clinker (Spasskcement, Spassk-Dalniy, Russia) (Fig. 2-3). Mixing water does not contain dissolved acids or alkalis that prevent the normal setting or hardening of binders, harmful impurities, decomposing plant substances that can have a harmful effect on concrete hardening. This is achieved by using ordinary drinking water from the tap, which meets all these requirements.



Figure 2. Portland cement clinker appearance.

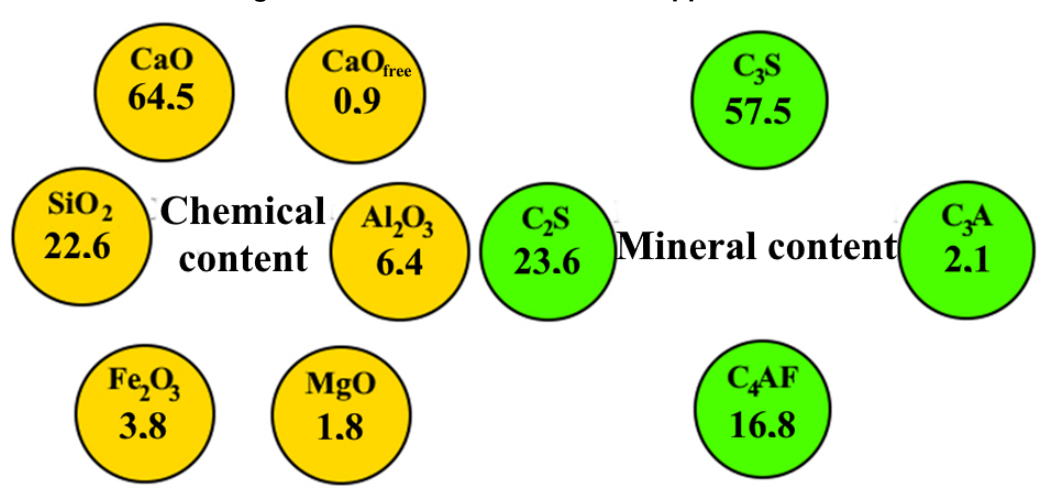


Figure 3. Chemical and mineral content of the Portland cement clinker.

The phase composition of clinker is represented by a crystalline phase in the form of clinker minerals (85%) and an amorphous phase in the form of clinker glass (15%) (Fig. 4).

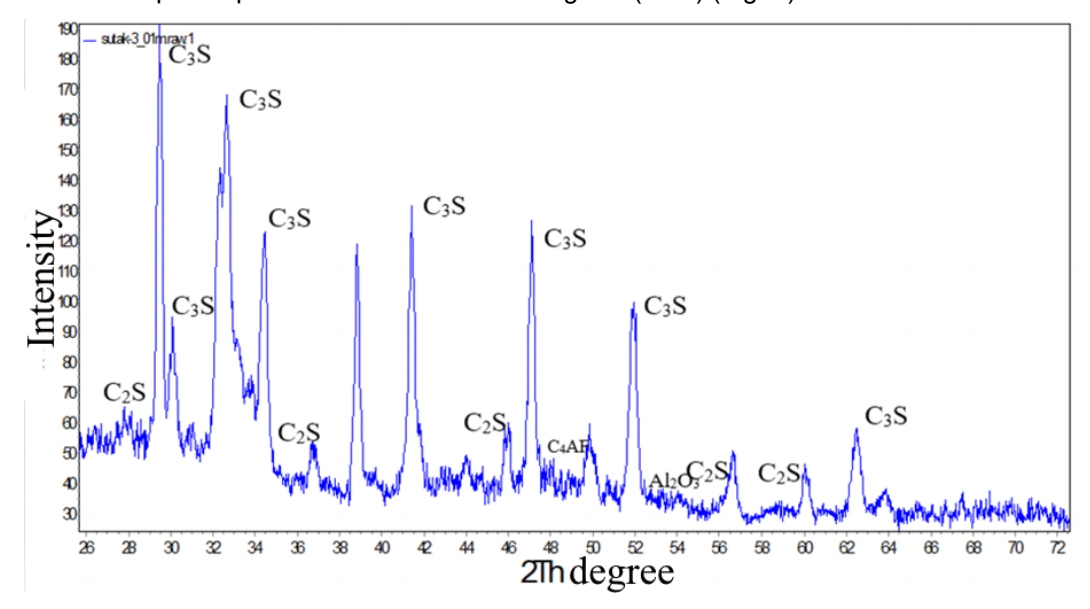


Figure 4. X-ray diffraction pattern of the ground Portland cement clinker.

As a component of the composite cement, an aluminosilicate component (ASC) was used, obtained from ash and slag mixes (ASM) of Primorskaya thermal and power plant (Luchegorsk, Russia) by enrichment by flotation and magnetic separation (Fig. 5).

The setting time was controlled by adding ground gypsum paste (gypsum dihydrate) in an amount of 5% by weight of the clinker.



Figure 5. Aluminosilicate component appearance.

The Volsky polyfractional sand was used to test the composite cement (Table 2).

Table 2. The Volsky polyfractional sand characterization.

SiO ₂ content	≥98%
Humidity	≤0.2%
Loss on ignition	≤0.5%
Content of clay and other impurities	≤0.5%
Residue on the sieve:	
2 mm	0%
1.6 mm	6%
1mm	34%
0.50 mm	67%
0.16 mm	89%
0.08 mm	100%

The fine aggregate was used from screenings of crushed granite (SCG) (Vostokcement, Spassk-Dalniy, Russia) fraction 2.5-5 (Fig. 6).



Figure 6. Screenings of crushed granite.

Both ASC and granite rock can have some radiation background, so it was necessary to study the specific effective activity of these technogenic resources (Table 3).

A skirish , assure	Measurement result (A), Bq/kg				
Activity score	ASM	ASC			
Potassium	392±89	342±68			
Thorium	31.5±19.7	29.5±15.7			
Radium	37.63±6.32	27.23±5.93			
$A_{eff} = A_{Ra} + 1.31A_{Th} + 0.085A_{K}$	80±30	93±20			

It was established that both raw materials belong to the first class of materials (less than 370 Bq/kg) in accordance with the Russian standard GOST 30108-94, and therefore can be effectively used for construction purposes.

According to its technical properties, the manufacturer positions the polycarboxylate superplasticizer Khidetal GP9 alfa B (SKT-standard, Russia) as a chemical modifier for concrete in contact with soil, and recommends a dosage of 0.4 to 1.2% by weight of the binder (Fig. 7).



Figure 7. The superplasticizer characterization.

To accelerate the setting of shotcrete, the dry additive Reolen MS451 (Gidrozo, Moscow, Russia) with a density of 650 kg/m3 and pH = 2.5 was used.

Thus, the materials selected for research are local and often represent waste products.

2.2. Mix design

From the selected components, a line of composite cements (CC) was created, obtained by joint grinding in a vibration mill to a specific surface area of 450 m2/kg (Table 4).

Table 4. The composite cement mixes.

Mix ID	Binder ba	_ Gypsum, % of		
	Clinker	ASC	clinker	
CEM1*	100	_	5	
CEM2	100	-	5	
CC-15**	85	15	5	
CC-25	75	25	5	
CC-35	65	35	5	

^{*} Portland cement clinker, ground together with gypsum up to ≈300 (CEM1) and 450 (CEM2) m²/kg, acted as a control;

From the developed composite cements, a wide range of shotcrete was obtained (Table 5). As a fine aggregate, granite screenings of a fraction of 2.5-5 mm were used. The level of replacement of clinker by the aluminosilicate component ranged from 0 to 35 wt. %. The water-binder (W/B) ratio varied within 0.3-0.4. The ratio "binder: filler" was 1:3.

^{**} the figure means the percentage of the aluminosilicate component

Table 5. The shotcrete mixes.

Mix ID (used	Consumption, kg per 1 m ³								
cement)	Clinker	ASC	Gypsum	Water	SP	Reolen	SCG		
SC1(CEM2)	450	-	22.5	135	-	2.25	1350	0.3	
SC2(CEM2)	450	-	22.5	157.5	-	2.25	1350	0.35	
SC3(CEM2)	450	-	22.5	180	-	2.25	1350	0.4	
SC4(CC-15)	382.5	67.5	19.1	135	1.125	2.25	1350	0.3	
SC5(CC-15)	382.5	67.5	19.1	157.5	1.125	2.25	1350	0.35	
SC6(CC-15)	382.5	67.5	19.1	180	1.125	2.25	1350	0.4	
SC7(CC-25)	337.5	112.5	16.9	135	2.25	2.25	1350	0.3	
SC8(CC-25)	337.5	112.5	16.9	157.5	2.25	2.25	1350	0.35	
SC9(CC-25)	337.5	112.5	16.9	180	2.25	2.25	1350	0.4	
SC10(CC-35)	292.5	157.5	14.6	135	3.375	2.25	1350	0.3	
SC11(CC-35)	292.5	157.5	14.6	157.5	3.375	2.25	1350	0.35	
SC11(CC-35)	292.5	157.5	14.6	180	3.375	2.25	1350	0.4	

2.3. Equipment and methods

2.3.1. Materials morphology

To study the Portland cement mineral composition, a D8 Advance AXS X-ray powder diffractometer (Bruker, Billerick, USA) was used (wavelength λ = 1.5418 Å) using Rietveld refinement. The percentage of oxides and minerals in the Portland cement was determined by the standard method of X-ray fluorescence analysis.

Microstructure of the bottom ash and concrete were studied using a MIRA3 scanning electron microscope (SEM) (Tescan, Brno, Czech Republic), which makes it possible to carry out energy dispersive spectroscopy. The samples used in the SEM analysis of binders were internal fragments of the sample after fracture. When preparing the surface of the SEM samples, polishing was not performed.

Thermal studies (differential thermal analysis DTA and TG thermogravimetry) were carried out by a DTG-60H instrument (Shimadzu, Kyoto, Japan).

2.3.2. Granulometry

The specific surface of bulk raw materials was studied using a PSH-11 device (Khodakov Devices, Moscow, Russia). The granulometry of the particles of the raw materials was evaluated using a laser analyzer Analysette 22 (Fritsch, Idar-Oberstein, Germany).

2.3.3. Fresh properties

The slump of the concrete mix is determined by laying a metal ruler with an edge on the top of the cone and measuring the distance from the lower edge of the ruler to the top of the concrete mixture with an error of up to 0.5 cm. The slump flow of the concrete mix is determined by measuring the diameter of the spread paste with a metal ruler in two mutually perpendicular directions with an error of not more than 0.5 cm.

2.3.4. Physical and mechanical properties

The value of the average density of the samples was calculated by dividing the mass by the volume. The compressive strength was determined according to the standard method of the Russian bltandard GOST 310.4-81 [47] on cubes with an edge of 70 mm. The flexural strength was determined by the three-point method on specimens of prismatic shape $40 \times 40 \times 160$ mm.

2.3.5. Full-scale study of the bearing capacity of the structures

The authors carried out a full-scale study of the bearing capacity of the structures of the underground passage in Vladivostok (Russia) using a non-destructive method using a device for measuring the speed of ultrasound Pulsar 2.2 (Moscow, Russia).

3. Results and Discussion

3.1. Fresh 3roperties

Fresh properties of the developed shotcrete are listed in Table 6.

			•	•	
M	lix ID	Slump, cm	Slump flow, cm	Fresh density, kg/m ³	Density at 28 days age, kg/m³
- 5	SC1	18	47	2455	2368
5	SC2	19	48	2461(+0.2%)	2369(+0.1%)
9	SC3	20	49	2467(+0.6%)	2370(+0.1%)
9	SC4	18	47	2468(+0.6%)	2431(+3.0%)
9	SC5	19	48	2471(+0.8%)	2432(+3.1%)
9	SC6	20	49	2474(+1.0%)	2433(+3.1%)
9	SC7	18	47	2475(+1.0%)	2441 (+3.5%)
5	SC8	19	48	2478(+1.1%)	2442(+3.6%)
5	SC9	20	49	2481(+1.3%)	2443(+3.6%)
S	C10	18	47	2486(+1.5%)	2455(+4.2%)
S	C11	19	48	2492(+1.8%)	2456(+4.3%)
S	C12	20	49	2498(+2.1%)	2457(+4.3%)

Table 6. Fresh properties and dynamics of density development of the concrete mixes.

Achievement of uniform flowability of shotcrete (slump 18-20 cm and slump flow 47-49 cm) was carried out by varying the dosage of the superplasticizer, which has a high water-reducing ability (40%).

An increase in the density of the fresh mix with raise in the content of the aluminosilicate component in the composite cement has been established. This picture is explained by the filling of voids with finely dispersed particles of finely ground CC, which are formed in the process of chemical contraction of the raw mix, resulting from a decrease in volume during hydration. The introduction of the aluminosilicate component in small quantities (up to 25 wt.%) slightly increases the 28-day density of the concrete (by 0.3-0.4%). With an increase in the dosage of ASC (up to 35 percent by weight), an raise in the density of 28-day-old samples was noted, linearly increasing with an increase in the amount of introduced aluminosilicates. This is due to the compaction of the concrete as a result of the pozzolanic reaction and the acceleration of the hydration kinetics of the clinker minerals. In addition, an increase in the volume fraction of the high-density phase of calcium silicate hydrate gel will help reduce the volume of the content of gel submicroporosity.

The beginning of setting is noted no earlier than after 75 minutes, which meets the requirements of Russian standard GOST 31108-2020.

3.2. Compressive and Flexural Strength

The increase in the compressive strength of shotcrete based on CC accelerated with a raise in the content of the aluminosilicate component to 35 wt. %, this was especially pronounced for an early age, for example, at a daily age, the increase in compressive strength compared to the additive-free composition was 56%, and with bending 62%. This is confirmed by the high ratios of the strength values on the first day to the values on the 28th day: for compressive strength, this ratio is 0.27 (0.23 for clinker compositions without additives), for bending strength 0.30 (0.26 for clinker compositions without additives). High early strength makes it possible to effectively use shotcrete for urgent complex repair of underground structures (Table 7).

By day 7, the growth rate of strength properties stabilizes to some extent, however, the tendency to exceed the control composition remains: 20% and 28% for compressive and flexural strength. At the same time, the ratio of flexural and compressive strength at this age (0.14) exceeds the similar characteristic of additive-free compositions, despite the replacement of Portland cement clinker up to 35 wt. %. The ratio of flexural and compressive strengths at different ages can characterize the development of the material's crack resistance. For the rationally developed composition of SC5, it is: on the first day 0.17; on 7 day 0.14; on 28 day 0.15, which in all cases exceeds the values of the control compositions.

As it was found, the strength development of cement materials based on composite cements is carried out more intensively than that of compositions without additives due to the positive effect of the superplasticizer and polymineral components, helping to reduce water demand and intensify the hydration of clinker minerals and heat generation. Compaction of the microstructure leads to a decrease in capillary porosity, and, accordingly, the permeability of the material for liquids and gases. In turn, this leads to an increase in the entire range of performance and durability, including frost resistance.

The differential thermal analysis also confirms the obtained results. Both control sample and composition having 35 wt. % ASC demonstrate similar temperature effects with differences only in hydration

products: at 100-140°C (calcium silicate hydrate CSH and trisulfate alumino-ferrite AFt phases), 180°C (aluminate hydro C4AH19), 600°C (Ca(OH)2), 750 and 780 °C (CaCO3) and 940°C (CSH) (Figure 8).

For modified shotcrete, a decrease in the area of the endothermic effect associated with the evaporation of physically bound adsorption water from hydration products at 100–140°C demonstrates a decrease in the presence of gel-like hydration products due to their crystallization.

The endothermic effect at a temperature of about 600°C corresponds to the dehydration of Ca(OH)2. An increase in the area of this peak on the thermogram of the control sample shows a higher content of portlandite in its composition.

Table 7. Mechanical properties of the developed shotcrete.

Properties	SC1	SC2	SC3	SC4	SC5	SC6	SC7	SC8	SC9	SC10	SC11	SC12
R^1_{com} ., MPa	12.9	14.8 (+15%)	14,0 (+9%)	16.7 (+29%)	18.8 (+46%)	17.9 (+39%)	17.8 (+38%)	19.9 (+54%)	18.8 (+46%)	18.9 (+47%)	20.1 (+56%)	19.0 (+47%)
R_{com}^1/R_{com}^{28}	0.23	0.25	0.24	0.26	0.26	0.26	0.26	0.26	0.26	0.27	0.27	0.27
R_{com}^7 ., MPa	32.7	34.8 (+6%)	33.6 (+3%)	35.0 (+7%)	37.1 (+13%)	36.2 (+11%)	36.1 (+10%)	38.2 (+17%)	37.3 (+14%)	37.2 (+14%)	39.3 (+20%)	38.4 (+17%)
R_{com}^{28} ., MPa	56.9	59.2 (+4%)	58.1 (+2%)	64.2 (+13%)	72.3 (+27%)	68.8 (+21%)	68.5 (+20%)	76.5 (+34%)	72.3 (+27%)	70.0 (+23%)	74.4 (+31%)	70.4 (+24%)
R_{flex}^1 , MPa	2.1	2.3 (+10%)	2.2 (+2%)	2.8 (+33%)	3.2 (+52%)	3.0 (+43%)	3.0 (+43%)	3.4 (+62%)	3.2 (+52%)	3.2 (+52%)	3.4 (+62%)	3.2 (+52%)
R _{flex.} /R _{flex.} , 1 day, MPa	0.16	0.16	0.16	0.17	0.17	0.17	0.17	0.17	0.17	0.17	0.17	0.17
$R_{flex}^1 / R_{flex}^{28}$	0.26	0.30	0.27	0.31	0.30	0.29	0.30	0.30	0.30	0.30	0.30	0.30
R_{flex}^7 , MPa	4.3	4.5 (+2 %)	4.4 (+1%)	4.9 (+14 %)	5.2 (+21%)	5.1 (+19%)	5,1 (+19%)	5.3 (+23%)	5.2 (+21%)	5.2 (+21%)	5.5 (+28%)	5.4 (+26%)
R _{flex} /R _{com.} , 7 days.	0.13	0.13	0.13	0,14	0.14	0.14	0.14	0.14	0.14	0.14	0.14	0.14
R_{flex}^{28} , MPa	8.0	8.3 (+4%)	8.1 (+1%)	9.6 (+20%)	10.8 (+35%)	10,3 (+29%)	10.3 (+29%)	11.5 (+44%)	10.8 (+35%)	10.5 (+31%)	11.2 (+40%)	10.6 (+32%)
R _{flex} /R _{com.} , 28 days.	0.14	0.14	0.14	0.15	0.15	0.15	0.15	0.15	0.15	0.15	0.15	0.15

A high-temperature calcium silicate hydrate endoeffect (940°C) was also revealed in the unmodified SC1 sample, which was more pronounced than in the modified SC2 sample.

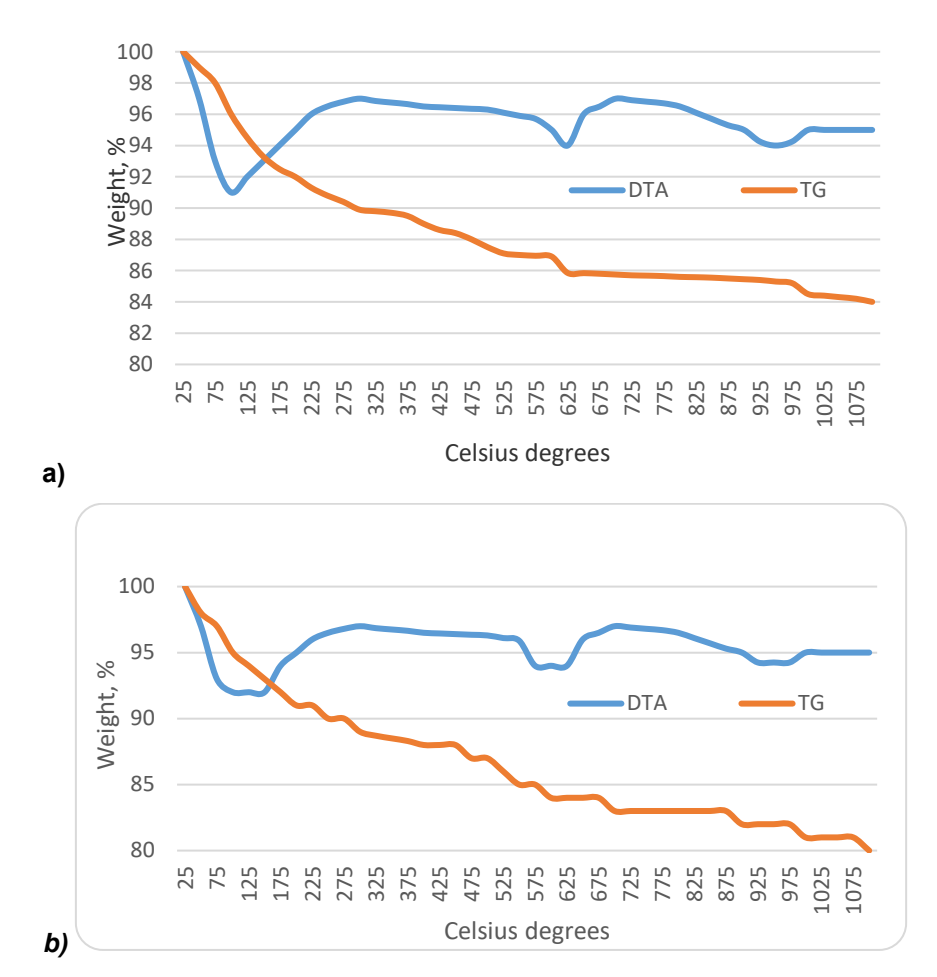


Figure 8. Differential thermal analysis of samples: a) SC11; b) SC1.

3.3. Strengthening of load-bearing structures with developed mixes

The use of the developed materials was carried out with the strengthening of the concrete wall of an underpass with a thickness of 20 cm with a reinforced layer of shotcrete SC5 with a thickness of 6 cm (Fig. 9). A reinforcing mesh was used with a pitch of transverse rods of 300 mm, a pitch of longitudinal networks of 200 mm. Reinforcing anchors for fastening to a reinforced structure were placed every 600 mm. The distance between the reinforcement mesh and the structure was 10 mm, the longitudinal and transverse rods were 10 mm in diameter, and the upper part of the anchor protruded from the reinforcement by 10 mm. Thus, the thickness of the protective concrete layer was 20 mm.



Figure 9. Strengthening a structure with shotcrete.

To ensure reliable joint operation of the reinforced wall, it was necessary to apply the law of affinity of structures when designing shotcrete repair compositions. For this, 15% of concrete scrap by weight of the binder was introduced into the rational composition of SC11. Concrete scrap was taken from exfoliated fragments of reinforced concrete blocks, followed by joint grinding with composite cement components to a specific surface area of 450 m2/kg.

The strengthening results are shown in Table 8. According to these results, the bearing capacity of the wall more than doubled from 15.2 to 37.2 MPa. This is ensured by the fact that the strength of the repair layer of shotcrete SC11 on the 28th day is 74.4 MPa, as well as by compaction and strengthening of the contact zone as a result of applying the provisions of the law of affinity of structures in the design of repair materials, which led to an increase in adhesion of the material by 1.5 times.

	Compressive	Compressive		Wall thickness	Wall thickness
Shotcrete mix	strength before strengthening, MPa	strength after strengthening, MPa	Adhesion to concrete, MPa	before strengthening, cm	after strengthening, cm
SC11	15.2	33.8	2.9	20	26
SC11+15 wt. % concrete		37.2	4.4		

Table 8. Results of strengthening a structure with shotcrete.

An increase in the strength of the interfacial transition zone was achieved by applying the theoretical provisions of the law of affinity of structures, which makes it possible to provide the internal structure of the composite, and, hence, its specified physical and mechanical properties and the durability characteristics of the entire structure. This interfacial transition zone should have similarity, closeness, or rather affinity in terms of basic properties and commonality of geologic origin with the material matrix.

As a result of the complex of studies, the effectiveness of the use of the developed shotcrete for strengthening the bearing structures of underground structures with an increase in strength of more than 2 times was theoretically and practically proved, which is explained both by the high strength of the obtained repair composition and the monolithic contact zone between the old and new layers of concrete. The developed shotcrete is able to provide the necessary degree of strengthening of the supporting structures of underground structures, while the thickness of the repair layer of 6 cm (with proper soil fixation) allows the use of underground structures as dual-use objects.

The results obtained are consistent with other work by independent authors who have published their work on shotcrete in recent years [44–45]. In particular, the advantage of this article is that the adhesion between the old and new concrete layers is increased by one and a half times due to the application of the provisions of the law of structural affinity. At the same time, the physical and mechanical properties and performance characteristics of the developed shotcrete are at the level of (or even exceed) the similar values of these authors [41–43].

4. Conclusions

An important scientific and practical task for increasing the defense capability of the state as a whole and preserving the population is the improvement of constructive methods for the complex repair of underground structures. Reinforced shotcrete was developed and studied to strengthen underground structures, as a result of which the following conclusions were obtained:

- 1. The novelty of the article lies in the fact that for the first time shotcrete was developed using composite cements, including aluminosilicates from enriched ash and slag mixtures.
- 2. Achieving the uniform flowability of shotcrete (slump 18-20 cm, slump flow 47-49 cm) was carried out by varying the dosage of the superplasticizer, which has a high water-reducing ability (40%). An increase in the density of the mixed mixture with a raise in the content of the aluminosilicate component in the composite cement was established. The introduction of the aluminosilicate component in small quantities (up to 25 wt.%) slightly increases the 28-day density of the concrete (0.3-0.4%). With an increase in the dosage of ASC (up to 35 percent by weight), a raise in the density of 28-day-old samples was noted, linearly increasing with an increase in the amount of introduced aluminosilicates.
- 3. The increase in the compressive strength of shotcrete based on CC accelerated with an increase in the content of the aluminosilicate component to 35 wt. %, this was especially evident for an early

- age, for example, at a daily age, the increase in compressive strength compared to the composition without additives was 56%, and with bending 62%. This is also confirmed by the high ratios of the values of strength properties in the first day to those in the grade age: for compressive strength 0.27 (0.23 for clinker compositions without additives), for flexural strength 0.30 (0.26 for additive-free clinker compositions).
- 4. Theoretically and practically proved the effectiveness of the use of the developed shotcrete for strengthening the load-bearing structures of underground structures with an increase in strength by more than 2 times, which is explained both by the high strength of the obtained repair composition and the monolithic contact zone between the old and new layers concrete. The scientific novelty lies in the fact that such an improvement in characteristics is achieved as a result of controlling the structure formation of shotcrete concrete, which leads to high adhesion to the concrete structure being repaired. The developed shotcrete is able to provide the necessary degree of strengthening of the supporting structures of underground structures, while the thickness of the repair layer of 6 cm (with proper soil fixation) allows the use of underground structures as dual-use objects.

References

- Volodchenko A.A. Efficient Silicate Composites of Dense Structure using hollow microspheres and Unconventional Aluminosilicate Raw Materials. Construction Materials and Products. 2023. 6 (2). P. 19 – 34. https://doi.org/10.58224/2618-7183-2023-6-2-19-34
- 2. Fediuk, R., Timokhin, R., Mochalov, A., Otsokov, K., Lashina, I. Performance properties of high-density impermeable cementitious paste. Journal of Materials in Civil Engineering. 2019. 31(4), 04019013 DOI: 10.1061/(ASCE)MT.1943-5533.0002633
- 3. Amran, M., Fediuk, R., Klyuev, S., Qader, D.N. Sustainable development of basalt fiber-reinforced high-strength eco-friendly concrete with a modified composite binder. Case Studies in Construction Materials. 2022. 17. e01550.
- Pavlíková, M., Zemanová, L., Záleská, M., Pokorný, J., Lojka, M., Jankovský, O., Pavlík, Z. Ternary Blended Binder for Production of a Novel Type of Lightweight Repair Mortar. Materials. 2019. 12(6). Pp. 996. DOI:10.3390/ma12060996. URL: https://www.mdpi.com/1996-1944/12/6/996.
- 5. Ahmed, A.A.A., Lesovik, R. V. Thermokinetic Processes of Hydration of Binders Based on Scrap Concrete 2021. Pp. 8–14.
- 6. Usanova, K., Barabanshchikov, Y.G. Cold-bonded fly ash aggregate concrete. Magazine of Civil Engineering. 2020. DOI:10.18720/MCE.95.10.
- Bessmertnyi, V.S., Lesovik, V.S., Krokhin, V.P. The reducing effect of argon in the plasma treatment of high-melting nonmetallic materials (a review). Glass and Ceramics. 2001. 58. Pp. 362–364. DOI:https://doi.org/10.1023/A:1013963916418.
- 8. Fediuk R., Amran M., Klyuev S., Klyuev A. Increasing the performance of a fiber-reinforced concrete for protective facilities. Fibers. 2021. 9(11). 64.
- 9. Klyuev S., Klyuev A., Fediuk R., Ageeva M., Fomina E., Amran M., Murali G. Fresh and mechanical properties of low-cement mortars for 3D printing. Construction and Building Materials. 2022. № 338. P. 127644. DOI:10.1016/j.conbuildmat.2022.127644
- 10. Anuradha, R., Bala Thirumal, R., Naveen John, P. Optimization of Molarity on Workable Self-Compacting Geopolymer Concrete and Strength Study on SCGC by Replacing Flyash with Silica fume and GGBFS. International Journal of Advanced Structures and Geotechnical Engineering ISSN. 2014.
- 11. Motter, C.J., Abdullah, S.A., Wallace, J.W. Reinforced concrete structural walls without special boundary elements. ACI Structural Journal. 2018. DOI:10.14359/51702043.
- 12. Ragavendra, S., Reddy, I.P., Dongre, A. Fibre Reinforced Concrete- A Case Study. 33rd National Convention of Architectural Engineers and National Seminar on "Architectural Engineering Aspect for sustainable building envelopes" ArchEn-BuildEn-2017, Hyderabad, India. 2017.
- 13. Klyuev S., Fediuk R., Ageeva M., Fomina E., Klyuev A., Shorstova E., Sabitov L., Radaykin O., Anciferov S., Kikalishvili D., de Azevedo Afonso R.G., Vatin N. Technogenic fiber wastes for optimizing concrete. Materials. 2022. V. 15(14). P. 5058.
- 14. Aslani, F., Jowkarmeimandi, R. Stress-strain model for concrete under cyclic loading. Magazine of Concrete Research. 2012. 64(8). Pp. 673–685. DOI:10.1680/macr.11.00120.
- 15. Al' Shemali A.A., A.A. Drucker-Prager models for dynamic analysis analysis of granular metamaterials in earthquake engineering. Construction Materials and Products. 2021. 4(2). Pp. 5–11. DOI:10.34031/2618-7183-2021-4-2-5-11. URL: http://bstu-journals.ru/en/archives/10855.
- 16. Eren, N.A., Alzeebaree, R., Çevik, A., Niş, A., Mohammedameen, A., Gülşan, M.E. The effects of recycled tire rubbers and steel fibers on the performance of self-compacting alkali activated concrete. Periodica Polytechnica Civil Engineering. 2021. 65(3). Pp. 890–900. DOI:10.3311/PPci.17601.
- 17. Klyuev S., Fediuk R., Ageeva M., Fomina E., Klyuev A., Shorstova E., Zolotareva S., Shchekina N., Shapovalova A., Sabitov L. Phase formation of mortar using technogenic fibrous materials. Case Studies in Construction Materials. 2022. V. 16. P. e01099
- 18. Klyuev A.V., Kashapov N.F., Klyuev S.V., Lesovik R.V., Ageeva M.S., Fomina E.V., Ayubov N.A. Development of alka-li-activated binders based on technogenic fibrous materials. Construction Materials and Products. 2023. 6 (1). P. 60 73. https://doi.org/10.58224/2618-7183-2023-6-1-60-73
- 19. Scislo, L. High Activity Earthquake Swarm Event Monitoring and Impact Analysis on Underground High Energy Physics Research Facilities. Energies. 2022. 15(10). Pp. 3705. DOI:10.3390/en15103705. URL: https://www.mdpi.com/1996-1073/15/10/3705.
- 20. Kolesnikova, O., Vasilyeva, N., Kolesnikov, A., Zolkin, A. Optimization of raw mix using technogenic waste to produce cement clinker. Mining informational and analytical bulletin. 2022. (10–1). Pp. 103–115. DOI:10.25018/0236_1493_2022_101_0_103. URL: https://elibrary.ru/doi_resolution.asp?doi=10.25018%2F0236_1493_2022_101_0_103.
- 21. Mekhtiyev, A.D., Narkevich, M.Yu., Neshina, Y.G., Kozhas, A.K., Aimagambetova, R.Zh., Aubakirova, B.B., Sarsikeyev, Y.Zh. Fiber optics based system of monitoring load-bearing building structures. Magazine of Civil Engineering. 2023. 123(7). Article no. 12301. DOI: 10.34910/MCE.123

- Smirnova, O.M. Development of classification of rheologically active microfillers for disperse systems with portland cement and super plasticizer. International Journal of Civil Engineering and Technology. 2018. 9(10). Pp. 1966–1973.
- 23. Amran, M., Onaizi, A.M., Fediuk, R., Vatin, N.I., Rashid, R.S.M., Abdelgader, H., Ozbakkaloglu, T. Self-Healing Concrete as a Prospective Construction Material: A Review. Materials, 2022. 15 (9), 3214 DOI: 10.3390/ma15093214
- 24. Khuzin, A., Ibragimov, R. Processes of structure formation and paste matrix hydration with multilayer carbon nanotubes additives. Journal of Building Engineering. 2020. DOI:10.1016/j.jobe.2020.102030.
- Murali, G., Abid, S.R., Amran, M., Fediuk, R., Vatin, N., Karelina, M. Combined effect of multi-walled carbon nanotubes, steel fibre and glass fibre mesh on novel two-stage expanded clay aggregate concrete against impact loading. Crystals, 2021. 11 (7), 720, DOI: 10.3390/cryst11070720
- 26. Salamanova, M., Murtazaev, S.-A., Alashanov, A., Ismailova, Z. Features of Production of Fine Concretes Based on Clinkerless Binders of Alkaline Mixing2019. Pp. 385–388.
- 27. Abdullah M.A.H., Rashid R.S.M., Amran M., Hejazii F., Azreen N.M., Fediuk R., Voo Y.L., Vatin N.I., Idris M.I. Recent Trends in Advanced Radiation Shielding Concrete for Construction of Facilities: Materials and Properties (2022) Polymers, 14 (14),. 2830. DOI: 10.3390/polym14142830
- 28. Klyuev A.V., Kashapov N.F., Klyuev S.V., Zolotareva S.V., Shchekina N.A., Shorstova E.S., Lesovik R.V., Ayubov N.A. Experimental studies of the processes of structure formation of composite mixtures with technogenic mechanoactivated silica component. Construction Materials and Products. 2023. 6 (2). P. 5 18. https://doi.org/10.58224/2618-7183-2023-6-2-5-18
- 29. Kuznetsov D.V., Klyuev S.V., Ryazanov A.N., Sinitsin D.A., Pudovkin A.N., Kobeleva E.V., Nedoseko I.V. Dry mixes on gypsum and mixed bases in the construction of low-rise residential buildings using 3D printing technology. Construction Materials and Products. 2023. 6 (6). 5. DOI: 10.58224/2618-7183-2023-6-6-5
- Nizina T.A., Nizin D.R., Selyaev V.P., Spirin I.P., Stankevich A.S. Big data in predicting the climatic resistance of building materials.
 I. Air temperature and humidity. Construction Materials and Products. 2023. 6. (3). P. 18 30. https://doi.org/10.58224/2618-7183-2023-6-3-18-30
- Ali, M., Abbas, S., Khan, M.I., Anwar Gad, M., Ammad, S., Khan, A. Experimental Validation of Mander's Model for Low Strength Confined Concrete Under Axial Compression. 2020 Second International Sustainability and Resilience Conference: Technology and Innovation in Building Designs(51154). 2020. Pp. 1–6. DOI:10.1109/IEEECONF51154.2020.9319950. URL: https://ieeexplore.ieee.org/document/9319950/.
- 32. Pavlik, Z., Jirickova, M., Cerny, R., Sobczuk, H., Suchorab, Z. Determination of moisture diffusivity using the time domain reflectometry (TDR) method. J. Build. Phys. 2006. 30. Pp. 59–70.
- Zagorodnyuk, L.H., Mestnikov, A.E., Makhortov, D.S., Akhmed, A.A.A. Mixed Binders with the Use of Volcanic Ash2021. Pp. 9– 15.
- 34. Korsun, V., Vatin, N., Korsun, A., Nemova, D. Physical-mechanical properties of the modified fine-grained concrete subjected to thermal effects up to 200°C. Applied Mechanics and Materials. 2014. DOI:10.4028/www.scientific.net/AMM.633-634.1013.
- 35. Volodchenko, A.A., Lesovik, V.S. Effective Composites Employing Fast-Hardening Gypsum Cement Binders for Additive Manufacturing. Proceedings of the International Conference "Actual Issues of Mechanical Engineering" (AIME) on July 27, 2017. 2017. DOI:doi.org/10.2991/AIME-17.2017.23.
- Lukuttsova, N. Water films (nanofilms) in cement concrete deformations. International Journal of Applied Engineering Research.
- 37. Pourjavadi, A., Fakoorpoor, S.M., Khaloo, A., Hosseini, P. Improving the performance of cement-based composites containing superabsorbent polymers by utilization of nano-SiO2 particles. Materials and Design. 2012. DOI:10.1016/j.matdes.2012.05.030.
- 38. Loganina, V.I., Zhegera, Christina Vladimirovna. The effectiveness of use of the composite binder as a dry mix. Case Studies in Construction Materials. 2015. 3. Pp. 137–140. DOI:10.1016/j.cscm.2015.10.004. URL: https://linkinghub.elsevier.com/retrieve/pii/S2214509515300139.
- 39. Dyussembinov, D.S., Awwad, T., Sabitov, Y.Y., Zhumagulova, A.A., Shakhmov, Zh.A., Kaliyeva, Zh., Bazarbayev, D.O. Self-compacting concrete with finely dispersed additives and superplasticizer. Magazine of Civil Engineering. 2023. 123(7). Article no. 12306. DOI: 10.34910/MCE.123.6
- 40. GOST 310.4-81. Cements. Methods of bending and compression strength determination.1981. 25 p.
- 41. Wei Wang, Shaohui Zhang, Yan Wang, Jian Yuan, Ditao Niu. Pore structure characteristics of admixture shotcrete and its quantitative relationship with mechanical properties in high geothermal environment. Journal of Materials Research and Technology. 2023. https://doi.org/10.1016/j.jmrt.2023.10.190
- 42. Fediuk, R.; Yushin, A. Composite binders for concrete with reduced permeability. IOP Conference Series-Materials Science and Engineering. 2016. Volume 116. 012021. DOI 10.1088/1757-899X/116/1/012021
- 43. Zhanming Wu, Yuyin Wang, Yong Mei, Faqi Liu, Changyong Liu. Static behavior of corrugated steel-shotcrete composite arches.Thin-Walled Structures Volume 195, 2024. https://doi.org/10.1016/j.tws.2023.111429
- 44. Wang, X., Islam, Md.M., Zhang Q.MInfluence of materials and nozzle geometry on spray and placement behavior of wet-mix shotcrete. Case Studies in Construction Materials. 2024. Vol. 20. e02852. https://doi.org/10.1016/j.cscm.2024.e02852.
- 45. Malmgren, L., Nordlund, E. Interaction of shotcrete with rock and rock bolts a numerical study. International Journal of Rock Mechanics and Mining Science. 2008. Vol. 45 (4). Pp. 538–553, https://doi.org/10.1016/j.ijrmms.2007.07.024.

Information about the authors:

Roman Fediuk, Doctor of Technical Sciences

ORCID: https://orcid.org/0000-0002-2279-1240

E-mail: roman44@yandex.ru

Svetlana Vavrenyuk, Doctor of Technical Sciences

E-mail: trusanova2014@mail.ru

Sergey Klyuev, Doctor of Technical Sciences

ORCID: <u>https://orcid.org/0000-0002-1995-6139</u>

E-mail: Klyuyev@yandex.ru

Linar Sabitov, Doctor of Technical Sciences

E-mail: sabitov-kgasu@mail.ru

Valery Meshalkin, Doctor of Technical Sciences

E-mail: vpmeshalkin@gmail.com

Sergey Fedosov, Doctor of Technical Sciences

ORCID: <u>https://orcid.org/0000-0001-6117-7529</u>

E-mail: FedosovSV@mgsu.ru

Tamara Chistyakova, Doctor of Technical Sciences

E-mail: nov@technolog.edu.ru

Received 11.11.2023. Approved after reviewing 29.08.2024. Accepted 01.09.2024.

